

# Studies on Monomeric and Dimeric Toluonitriles

Inaugural-Dissertation

zur Erlangung des Doktorgrades  
der Mathematisch-Naturwissenschaftlichen Fakultät  
der Heinrich-Heine-Universität Düsseldorf

vorgelegt von

**Felix Johannes Gmerek**

aus Gladbeck

Düsseldorf, März 2017

aus dem Institut für Physikalische Chemie I  
der Heinrich-Heine-Universität Düsseldorf

Gedruckt mit der Genehmigung der  
Mathematisch-Naturwissenschaftlichen Fakultät der  
Heinrich-Heine-Universität Düsseldorf

Referent: Prof. Dr. Michael Schmitt  
Korreferent: Prof. Dr. Rainer Weinkauff  
Tag der mündlichen Prüfung: 05. April 2017

Ich versichere an Eides Statt, dass die Dissertation von mir selbständig und ohne unzulässige fremde Hilfe unter Beachtung der "Grundsätze zur Sicherung guter wissenschaftlicher Praxis an der Heinrich-Heine-Universität Düsseldorf" erstellt worden ist.

---

Ort, Datum

Unterschrift



# Abstract

One of the most important chemical reaction for all living beings is the photosynthesis. Via this reaction plants produce the complex carbohydrates they need to grow and, more important, they also produce molecular oxygen during this process.

This process is a so called photochemical reaction which means it is triggered by light.

Although the photosynthesis is this important and has been thoroughly studied for a long time it is still not fully understood and leaves opportunities for further studies.

One thing that is still to be investigated is the absorption of light during this reaction.

The molecules which absorb the light belong to the substance class of chlorophylls. There is a variety of different forms of chlorophyll and depending on the fact if they are in bacteria or plants the sidechains are different for each of these forms.

The photosynthesis does not start directly after the absorption of a photon. In fact the excitation energy is transferred from one chlorophyll molecule to another until it hits the so called "special pair" which is a chlorophyll dimer.

The exact mechanism of the excitation of the dimer is not known and is not easily accessible.

To be able to improve the knowledge of energy transfer processes we performed measurements on model systems which are smaller and thus easier to analyse.

The systems that we chose were the dimers of tolunitriles. In this work however, the focus lies on the dimer of 2-tolunitrile.

With the help of single vibronic level fluorescence spectroscopy (SVLF) the structural changes upon electronic excitation of this molecule cluster was determined. With the help of this information we wanted to determine whether one monomer (locally) is excited or both (delocalized).

In order to make it easier to understand the behavior of the dimer, the monomers of 2-tolunitrile and 3-tolunitrile have been investigated.



# Zusammenfassung

Eine der wichtigsten chemischen Reaktionen für Lebewesen ist die Photosynthese.

Durch diese Reaktion ist es Pflanzen und Bakterien möglich, komplexe Kohlenhydrate für ihr Wachstum zu erzeugen. Sie ist ausserdem der Prozess, mit dessen Hilfe molekularer Sauerstoff erzeugt wird.

Die Photosynthese ist eine sogenannte photochemische Reaktion, was bedeutet, dass sie durch Licht gestartet wird.

Obwohl dieser Prozess so wichtig ist und über viele Jahrzehnte erforscht wurde, ist er bis heute noch nicht vollständig verstanden und bietet noch immer Möglichkeiten für weitere Forschungen.

Eine dieser Möglichkeiten ist die Absorption von Licht durch Chlorophyllmoleküle. Diese liegen, je nachdem ob sie in Pflanzen oder Bakterien vorkommen, in unterschiedlichen Formen vor, die sich durch die Art der Seitenketten unterscheiden.

All diese Formen haben jedoch einen gemeinsamen, sehr komplexen und großen Kern, der es schwierig macht, Chlorophyll zu untersuchen.

Es ist ausserdem nicht so, dass die Reaktion der Photosynthese direkt nach Absorption von Licht startet. Viel mehr ist es so, dass die Anregungsenergie von einem Molekül zum nächsten übergeht, bis das sogenannte "spezielle Paar" erreicht wird. Dieses ist ein Chlorophyll-Dimer.

Wie genau diese Dimer angeregt wird ist noch nicht geklärt und ist aufgrund der Komplexität von Chlorophyll auch nicht leicht zugänglich.

Daher haben wir Untersuchungen an einfacheren Modellsystemen durchgeführt, um mehr über diesen Prozess lernen zu können.

Als Modellsystem haben wir die Toluonitril-Dimere ausgewählt und uns aber vorerst auf das 2-Toluonitril-Dimer fokussiert.

Mit Hilfe der dispergierten Fluoreszenzspektroskopie haben wir die Strukturänderungen bei elektronischer Anregung untersucht. Durch diese Ergebnisse wollten wir dem Mechanismus der Anregung erforschen und bestimmen, ob eines der beiden Monomere (lokal) angeregt wird, oder das gesamte Dimer (delokalisiert).

Um das Dimer besser verstehen zu können, wurden zunächst die Monomere von 2-Toluonitril und 3-Toluonitril untersucht.



# Contents

<b>1</b>	<b>Introduction</b>	<b>1</b>
1.1	Photosynthesis . . . . .	1
1.2	Model System . . . . .	4
1.2.1	Monomers . . . . .	4
1.2.2	Cluster . . . . .	6
1.2.3	Dimers . . . . .	7
1.2.4	Water Cluster . . . . .	9
1.2.5	Transition Dipole Moment . . . . .	9
1.3	Davydov splitting . . . . .	11
<b>2</b>	<b>Theory</b>	<b>13</b>
2.1	Methods . . . . .	13
2.1.1	Laser Induced Fluorescence . . . . .	13
2.1.2	Single Vibronic Level Fluorescence . . . . .	14
2.2	Franck-Condon-Principle . . . . .	16
2.3	FCFIT . . . . .	18
2.3.1	The Overlap Integrals . . . . .	18
2.3.2	Calculating The Intensities . . . . .	19
2.3.3	Simulation Of The Spectrum . . . . .	19
2.3.4	The Fit . . . . .	20
2.4	From Measurement To Result . . . . .	20
<b>3</b>	<b>Experimental Set Up</b>	<b>23</b>
3.1	Laser-system . . . . .	24
3.1.1	Nd:YAG-laser . . . . .	24
3.1.2	Dye-laser . . . . .	24
3.2	Vacuum Chamber . . . . .	25
3.2.1	Vacuum Pumps . . . . .	25
3.2.2	Sample Chamber . . . . .	25
3.3	Monochromator . . . . .	26
3.4	Photomultiplier . . . . .	26
3.5	iCCD . . . . .	27

<b>4 Publications</b>	<b>29</b>
4.1 Electronic Spectra of 2- and 3-Tolunitrile in the Gas Phase II: Geometry changes from Franck-Condon Fits of Fluorescence Emission Spectra. . . . .	29
4.2 Franck Condon Spectra of the 2-Tolunitrile Dimer and the Binary 2-TolunitrileWater Cluster in the Gas Phase . . . . .	48
<b>References</b>	<b>81</b>
<b>List of figures</b>	<b>83</b>

# Chapter 1

## Introduction

The interaction of light and matter is of great interest as many processes in nature are activated by light. This is due to the fact that many molecular properties change upon electronic excitation. This leads to various reactions which are not accessible from the ground state of these molecules. These reactions are called photochemical reactions.

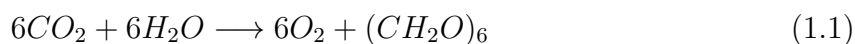
One of the most important photochemical reactions is the photosynthesis which takes place in the chloroplasts of plants.

### 1.1 Photosynthesis

The photosynthesis<sup>[1]</sup> is the process by which plants and some bacteria gain energy in the form of ATP and NADPH from a reaction of  $CO_2$  and  $H_2O$ . This also provides the organisms with complex carbon hydrates which are necessary for their growth.

The production of  $O_2$  is of course another important effect of the photosynthesis.

Usually the equation for the photosynthesis is written like:



but this is only a very general summation of the result. The actual reaction cycle is way more complex<sup>[2]</sup>.

The photosynthesis is composed of two reaction complexes, the light-dependent and the light-independent reactions. Both of these are a series of reactions which are started by the interaction of light and matter.

The light-dependent reactions are composed of four sequential reactions. The first is the photolysis of water in the photosystem II. This means water is cleaved to gain electrons (equation 1.2).



The electrons are then used in the next step to yield more protons.

The third step is once again light driven. Here the energy of the light is converted into chemical energy. This is done by reducing  $NADP^+$  to NADPH (equation 1.3)



In a fourth and final step the protons from the former steps are used to create a proton gradient which is needed to form ATP from ADP.

Both ATP and NADPH are molecules containing high amounts of chemical energy which are used in the light-independent reactions.

These reactions are producing complex carbohydrates from  $CO_2$  and are thus important for plants to be able to grow. Furthermore it is of course important for humans and animals alike that these reactions take place as these are the source of our food.

Although these reactions have been thoroughly studied for a long time there are still some aspects that have not yet been fully understood.

During the photosynthesis light is absorbed by chlorophyll. After that the excitation is passed from one molecule to another until at the end the excitation is passed onto a chlorophyll dimer which then is capable of starting the electron transportation chain described before.

The excitation of the dimer was the starting point for our investigations as well.

Taking one step backwards it is important to have a look at the possible consequences of an interaction of light and matter. First of all, there is a limiting factor which is the necessity of resonance. This means that the light that is shone onto a sample can only be absorbed if it is resonant to a transition in the molecule.

If this is the case the molecule will pass into an excited state from which it will relax to energetically lower states in a very short period of time. This decomposition however can be done in different ways.

The first is the relaxation via fluorescence. This means that the molecule emits a photon and thus falls back into the ground state. A similar process is the phosphorescence. Here the relaxation happens via emittance of a photon but before this happens the excitation is transferred to an electronic state which has a different multiplicity. This process is called inter system crossing.

The second way is by interaction with the surrounding and disposing the excitation energy as heat.

Furthermore the excitation can be redistributed via inner conversion.

The last and by far most interesting way is by energy transfer to another molecule. This means that by going back to the ground state a second molecule of the same sample is excited to the level the first one was excited to originally.

This last process is involved in the photosynthesis as the molecules that absorb the light are not the molecules that transform the light into chemical energy. This means that

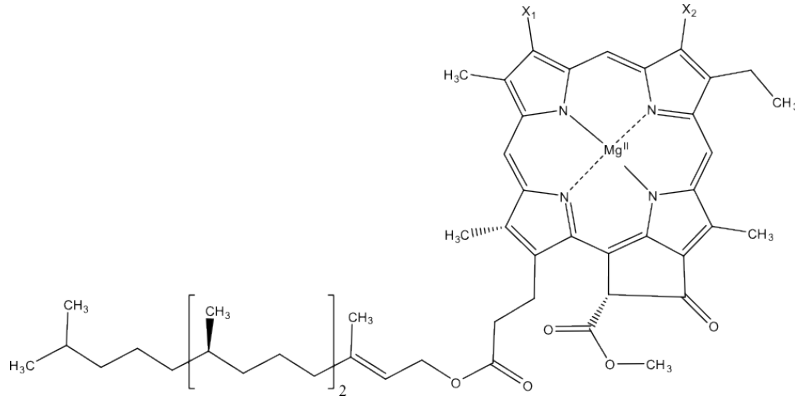


Figure 1.1: Basic structure of different chlorophyll-types. Table 1.1 shows which substituents form which chlorophyll.

there is a cascade of energy transfers following the excitation. At the end of this cascade the exciton moves to a chlorophyll dimer which then passes an electron to promote the reaction.

At this point the question arises how this last excitation happens as the original light absorption happens in a single molecule. But when the exciton hits the dimer there are two possibilities.

Of course the energy can be absorbed by one of the two monomer units but it can also be spread across both monomers. Knowing what happens here is quite interesting as it might help to understand the effectiveness of the reactions and the processes involved.

However, the light absorbing molecules participating in the photosynthesis are chlorophyll (figure 1.1). These are build up from porphyrine and magnesia cations. This means they are very large and present multiple problems for the experiments conducted in this work. First of all the number of degrees of freedom depend on the number of atoms forming a molecule. They can be calculated with the help of formula 1.4.

$$N_{free} = 3N \quad (1.4)$$

In our case only the number of vibrations of a molecule is of interest. These can be calculated by expanding equation 1.4. We then get equation 1.5 for non-linear molecules and equation 1.6 for linear molecules<sup>[3]</sup>.

$$N_{vib} = 3N - 6 \quad (1.5)$$

$$N_{vib} = 3N - 5 \quad (1.6)$$

where N is the number of atoms in the molecule and the numbers 5 and the 6 are the rotational and translational degrees of freedom.

Table 1.1: List of the substituents of different chlorophyll molecules.

type	$X_1$	$X_2$
chlorophyll a	$CH = CH_2$	$CH_3$
chlorophyll b	$CH = CH_2$	$CHO$
chlorophyll d	$CHO$	$CH_3$

## 1.2 Model System

Studying molecules like chlorophyll is far from easy as they are very big and furthermore contain metal ions. Several problems arise from this. First of all molecules of this size are not easily brought into the gas phase and, when using a thermal source, tend to decompose rather than being evaporated. This means the set up used for the experiment is not suited for the measurement of large molecules.

A second problem is the number of vibrations in such a molecule. For a non-linear molecule this number calculates as  $3N - 6$  where  $N$  is the number of atoms in the molecule. For chlorophyll  $N$  has a value of up to 135 depending on which type of chlorophyll is regarded. This leads to a number of vibrations  $N_{vib} \approx 400$ . And for the dimer this number is about twice that high. Considering combination bands and overtones, the number of possible vibrational states and therefore the state density becomes enormous.

For the evaluation of the measurements it is necessary to assign bands from the spectra to normal modes. With 400 base vibrations plus a much higher number of combinational modes and overtones this becomes a nearly impossible task.

The last problem arises from the metal ion in the molecule. This causes problem with the *ab-initio*-calculations required for the evaluation as these are very large and tend to have a lot of interactions with neighbouring atoms.

All this leads to the conclusion that a model system is needed which is easier to analyse. This model needs to be a symmetric dimer with aromatic cores as this is what the chlorophyll dimer is. Furthermore this dimer needs to be constructed in such a way that the afore mentioned problems do not occur.

### 1.2.1 Monomers

To be able to analyse the dimers properly it is important to understand the monomers first. Therefore, we performed measurements on 2-tolunitrile (2-TN) and 3-tolunitrile (3-TN)<sup>[4]</sup>. The 2 samples are constitutional isomers which means, that they consist of the same functional groups and the same core, the bonds are different. In this case the core is a benzene ring with a methyl- and a cyano-group attached to it. In case of 2-TN the cyano-group is located in the ortho-position with respect to the methyl-group while in 3-TN it is in the meta-position. The tolunitriles have been investigated with the help of various methods before, thus giving us a good starting point<sup>[5-13]</sup>.

Alkyl-substituents (like methyl-groups) are electron pushing groups which move electron

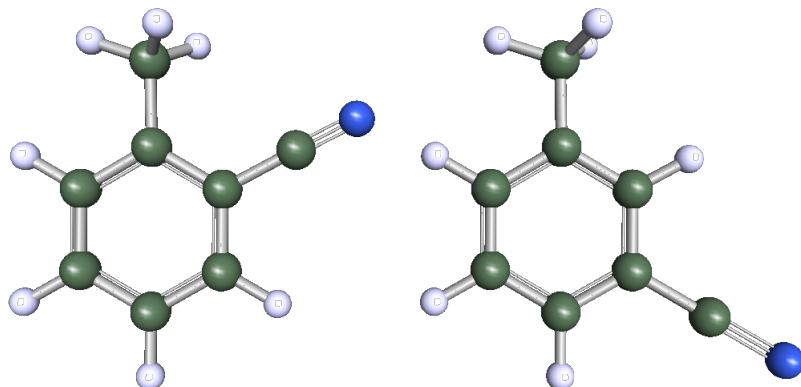


Figure 1.2: Structures of the investigated monomers. On the left side is 2-TN and on the right 3-TN<sup>[4]</sup>

density away from themselves. This effect is called a positive inductive substituent effect (short +I-effect). If new bonds were formed in this process it would be called a positive mesomeric substituent effect (short +M-effect)<sup>[14]</sup>.

The cyano-group has the opposite effect as it draws electron density away from the aromatic core. This is called a negative mesomeric substituent effect (short -M-effect).

These effects do not only shift electron density but by doing so also have a great impact on the electronic properties of the sample. For example the influence on the dipole moment is enormous.

Dipole-moments can either be permanent or induced. Permanent dipole moments occur if there are functional groups in a molecule that either push or pull electron density into a specific direction and if the molecule is not inversion symmetric. If all these forces work in the same direction there will be a permanent dipole moment. If two or more forces point in different directions they might negate each other. Examples for this are water (which has a strong dipole moment) and carbon-dioxide which has no dipole moment.

Having a look at benzene it is obvious that it does not have a dipole moment at all, as it has a center of symmetry and the electron density is spread evenly all over the ring. If now a methyl-substituent is introduced there is a shift in the electron density into one defined direction (away from the methyl-group). The same would happen if a cyano-group is introduced. Although here the sign would be different and the electron density is drawn away from the benzene ring.

If both substituents are introduced there are three possibilities to do so:

- 1) the substituents are in para-position
- 2) the substituents are in meta-position
- 3) the substituents are in ortho-position

In case 1) both effects would be summed as they are working towards the same direction leading to a strong dipole moment. In case 2) it is a bit more difficult as here is an angle between the vectors. This leads to a dipole moment which is tilted with regard to the substituents. In case 3) the substituents are in neighbouring positions and the two forces work nearly in opposing directions. Here it is necessary to know which effect is stronger in order to be able to determine the vector of the dipole moment.

## 1.2.2 Cluster

Our measurements are conducted a molecular beam, i.e. in the gas phase as we usually want to investigate monomers and with our method it is easy to evaporate molecules. If however the intermolecular forces are strong enough it is also possible to investigate clusters of molecules<sup>[15;16]</sup>.

Intermolecular forces are for example dipole-dipole-interactions, van-der-Waals-forces or ionic interactions (Coulomb forces).

These clusters can consist of two or more molecules of the same kind. They are then referred to as dimers, trimers etc..

It is also possible that clusters contain more than one type of molecule. They can for example be build up from either two different gases<sup>[17-19]</sup>, gases and solids or liquids and solids. The last mentioned ones are the biochemically most relevant, especially if the liquid is water<sup>[20]</sup>.

As mentioned before, the number of vibrations in a molecules depends on the number of atoms that are contained (see equation 1.5). For a cluster the number of atoms is the same as the sum of all regarded molecules (for example for a dimer  $N_{cluster} = 2N_{monomer}$ ), yet the number of vibrations is calculated as  $3N - 6$  again, which means there are 6 additional vibrations. These are the intermolecular vibrations, comprised of three lost degrees of freedom of rotation and three of translation of the monomer moieties.

These intermolecular vibrations determine the position of the monomer fragments with regard to each other. These vibrations are caused by what used to be the translational and rotational movements of the monomer subunits of the dimer. For example when both monomers move in the same direction, this is still a translation. But if they move in opposing directions than it is a hindered translation and is thus regarded as a vibration. The intermolecular vibrations are usually found at very low frequencies only about  $100 \text{ cm}^{-1}$  above the 0-0-transition.

### 1.2.3 Dimers

As mentioned before, there are some requirements for our system to be a valid model, to gather information on the chlorophyll dimer. First of all it obviously has to be a dimer, second is has to be symmetric, meaning that there has to be a center of symmetry, and third is has to be aromatic. The last requirement is also given by the fact that our measurements are based on fluorescence. A rather long list of symmetric aromatic dimers

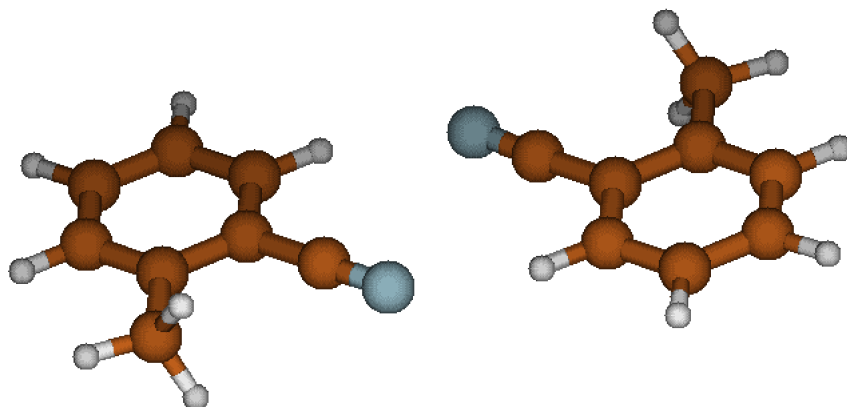


Figure 1.3: Structure of the 2-TN dimer.<sup>[21]</sup>

has already been studied with several methods<sup>[22–32]</sup>. Yet the measurements in this work are suitable to gain further information which may help to deepen the insight on this matter.

Dimers of this type allow the investigation of other interesting phenomena as well. One of these is the interaction and coupling of dipole moments and of transition dipole moments.

The point group of the dimer in the ground state is  $C_{2h}$  and has a center of inversion. As the dimers studied here are centro-symmetric, the overall dipole moment in the ground state has to be zero.

In the excited states this may change depending on what happens when the molecule is excited. Upon absorption of a photon in the dimer it is equally possible to excite each of the monomers but it is also possible that the excitation energy is spread (delocalized) over both monomers. Which of these possibilities is realised depends on whether the excitation is localized or delocalized. This matter will be discussed in more detail later (see section 1.3).

If only one monomer is excited the symmetry of the dimer is disturbed and the overall dipole moment in the excited state is different from zero. If both monomers are excited they change their geometries equally and the symmetry stays the same. The dimer will then still have no dipole moment.

If we have a look at this problem from a more theoretical point of view, the excitation of one monomer is energetically equal to the excitation of the other monomer. This would

lead to a crossing of the two energy surfaces of these excited states. As these are forbidden an energy surface with two minima is formed. Each of these minima can be assigned to the excitation of one monomer with a barrier in the middle.

The barrier however is not very high which leads to rather high tunnelling constants. This means that, as our measurements are relatively slow, we are only able to detect a fluorescence spectrum which is averaged over both minima.

A second energy surface is formed above the first. Due to geometrical reason this surface can be assigned to a geometry which is the same as the one of the ground state. This on the other hand means that here the excitation is spread equally over both monomers.

These two states however have different geometries and thus it is possible to determine which is excited by having a look at the selection rules for this excitation.

The overall geometry of our molecule in the ground state is  $A_g$ . If only one monomer would be excited the  $S_1$  would have a symmetry of  $A'$  for each molecule.

Due to the avoided crossing the symmetry becomes  $B_u$  for the  $S_1$  and  $A_g$  for the  $S_2$ . This means that only the transition  $S_0$  to  $S_1$  is allowed but not the transition to the  $S_2$ .

## 1.2.4 Water Cluster

Clusters of molecules with water are quite interesting as they give information about the intermolecular binding strength. It is however not only possible to create a 1:1-complex (figure 1.4) but to step by step add more water. This means that by investigating

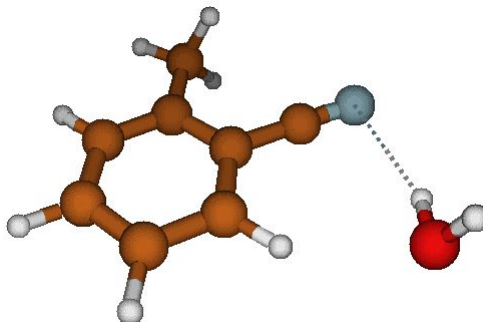


Figure 1.4: Structure of the 2-TN-water cluster.<sup>[21]</sup>

1:1-clusters one can get information about the beginning of the solvation of molecules. Learning something about how a molecule is solved in a certain liquid is very interesting as by knowing this it is possible to gather information about how interaction between a molecule and its surrounding starts and happens.

For the water-cluster of the tolunitriles the restrictions regarding the transitions do not occur as the molecules point group is  $C_1$  leading to all states having a symmetry of A.

## 1.2.5 Transition Dipole Moment

Apart from the permanent electric dipole moment there is a transition dipole moment for each transition that is possible in a molecule. The orientation of this gives information about the interaction of light and the molecule especially about the polarization of the light that is required to excite the molecule.

In case of a dimer the transition dipole moments of both molecules will interact with each other. The result of this interaction will depend on the angle  $\theta$  between the transition dipole moments (see Figure (1.5)).

If the angle  $\theta$  has a value of  $0^\circ \leq \theta < 54.7^\circ$  the interaction is attractive. This means the absorption is shifted to lower wavenumbers. Clusters of this type are called J-aggregates.

In case that  $\theta = 54.7^\circ$  the interaction is 0.

If  $54.7^\circ < \theta \leq 90^\circ$  the interaction will be repulsive which then will result in a shift to higher wavenumbers for the absorption<sup>[33]</sup>. These clusters are called H-aggregates.

Figure 1.6 shows the position of the transition dipole moments in comparison to the parent molecule with only one of the substituents. It can be seen that for 2-TN the vector is turned by about  $90^\circ$  compared to benzonitrile.

The vectors of the transition dipole moments are of great interest as they not only

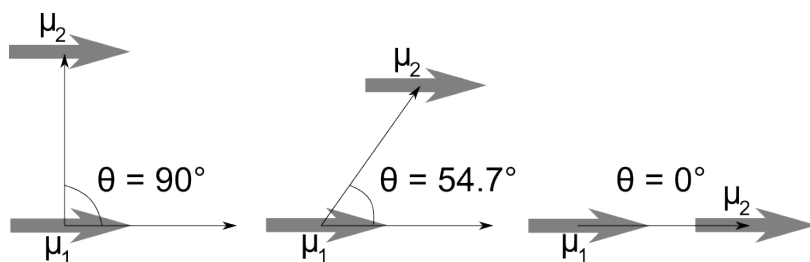


Figure 1.5: Schematic drawing of the angle  $\theta$  between two transition dipole moments. For  $54.7^\circ < \theta \leq 90^\circ$  (left) the transition dipole moments are arranged in a parallel way and form a H-aggregate. For  $0^\circ \leq \theta < 54.7^\circ$  (right) the transition dipole moments are arranged in a head-to-tail way and form a J-aggregate. For  $\theta = 54.7^\circ$  there is no interaction between the transition dipole moments and thus no aggregate is formed.

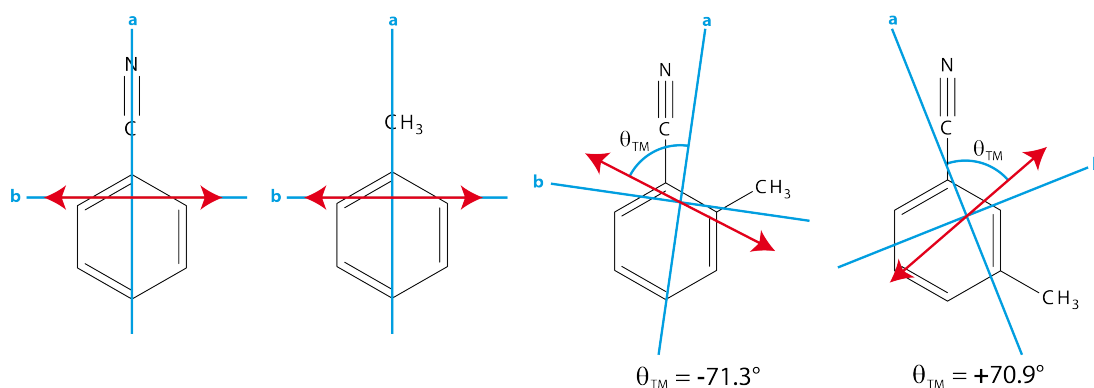


Figure 1.6: Orientation of the transition dipole moments of Benzonitrile, Toluene, 2-TN and 3-TN (from left to right)<sup>[34]</sup>

influence the electronic structure of the monomers but also have an immense impact on the electronic structure of the dimers.

Figure 1.7 shows the dipole vectors of two monomers in the benzonitrile (BN) dimer and for the 2-TN dimer. It is easily seen that in case of the BN dimer the dipole moments are parallel to each other. This leads to an angle  $\theta$  of about  $90^\circ$ .

For the 2-TN dimer the angle  $\theta$  is less than  $54.7^\circ$ .

This leads to the fact that the BN dimer forms a H-aggregate and 2-TN dimer forms a J-aggregate. This now has a great impact on the electronic states as the order of the excited states with regard to their geometry is changed. For the BN dimer the  $A_g$  state is the lowest excited state while for 2-TN dimer it is the  $B_u$  state.

As both have the same geometry in the ground state this changes which states can be excited due to the selection rules.

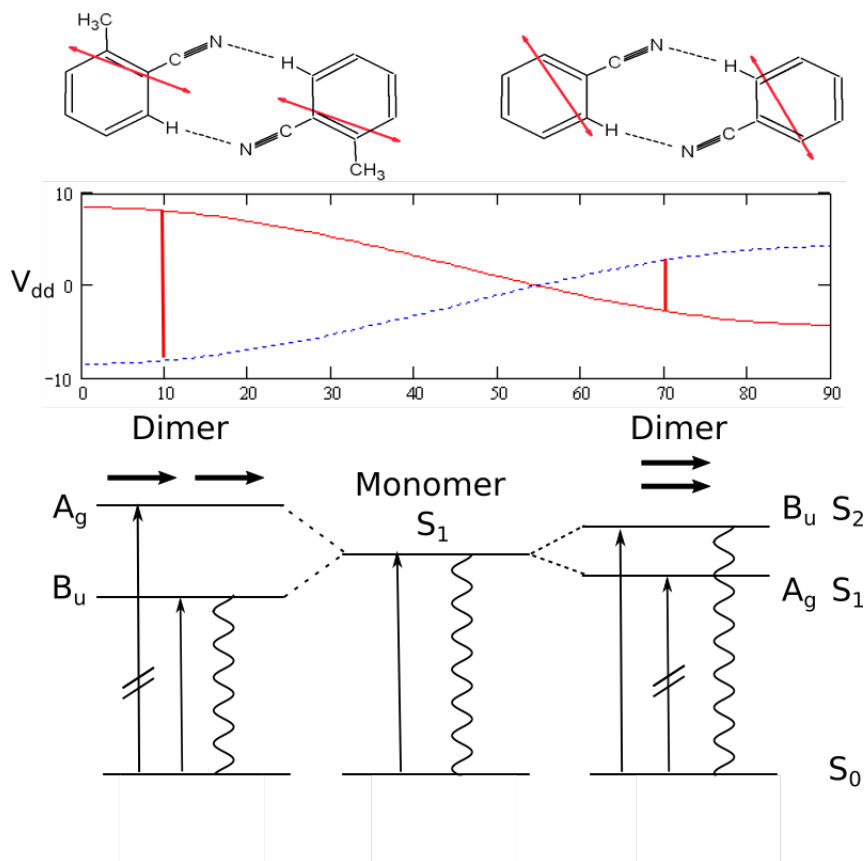


Figure 1.7: The top part of this figure shows the transition dipole moment vectors for the 2-TN dimer and the BN dimer. The middle part shows the energy splitting between the  $S_1$  and the  $S_2$  depending on the angle  $\theta$ . The bottom part shows a scheme of the electronic states and the allowed and forbidden transitions.<sup>[21]</sup>

### 1.3 Davydov splitting

If a molecule is excited it can pass this excitation to another molecule in its vicinity. The energy that is transmitted in this process is called an exciton.

Frenkel was the first to introduce the concept of excitons but it was Davydov<sup>[35]</sup> who described the phenomenon of exciton splitting and treated a wide area of problems in his studies.

Although his studies mainly focused on solid bodies, or crystals to be more precise, his concepts and ideas are valid for the gaseous phase as well.

Davydov investigated and predicted which transitions are allowed upon excitation and which differences appear between free molecules and those located in a crystals lattice. He noticed that these differences would be small and thus the spectra should be dominated by the molecular spectra. This is due to the fact that the light is still absorbed by the chromophores of the molecules and not by the lattice itself. Thus the excitation of lattice vibrations is caused by energy transfer from the molecules to the lattice. The transfer rate however depends on quite a lot of variables and is rather small.

This fact that the spectra are dominated by the molecules spectra again shows to be valid

for clusters in the gaseous phase as will be shown later.

Davydov also investigated and defined if and when an exciton is located or delocated (or "free" as he calls it). He defines this difference by introducing two time variables  $\tau_d$  and  $\tau_t$ .

When a molecule is excited by absorption of light two different things may happen. The first and more obvious is that the molecule reacts and changes its geometry. The time this takes is defined as  $\tau_d$ .

The other thing that can happen is the transfer of the energy to a neighbouring molecule as an exciton. The times for this process is called  $\tau_t$ .

There are now two possibilities:

$$\tau_d < \tau_t \tag{1.7}$$

and

$$\tau_d > \tau_t \tag{1.8}$$

If equation 1.7 is fulfilled the excitation is designated to a specific molecule which leads to a local deformation of the crystal. The exciton is then defined as local.

If equation 1.8 is fulfilled the excitation moves from one molecule to another before the geometry change can take place. The structure of the crystal will not be affected in this case and the exciton is called delocalized.

If we now transfer this definition to our measurements there are some differences.

The largest difference of course will be the number of molecules that are taken into account. Davydov made the assumption that the crystal he described was of unrestricted size and all molecules had that same surrounding. Our sample on the other hand is only a dimer and thus has only two molecules. But as they are isolated, due to the fact that the measurement takes place in the molecular beam, they have the same surrounding as the only neighbour is the other molecule. And as we investigate a heterogeneous dimer this makes both molecules equal to the other.

The other large difference is the fact that we do not have a lattice as is defined by Davydov and thus there are no lattice vibrations. There are however inter-molecular vibrations which basically follow the same restrictions as the lattice vibrations. This means that they do not have a big impact on the recorded spectra though they are still detectable. For the measurements a problem arises from the definition of localised and delocalized excitons as the time for a vibrational movement of our sample  $\tau_v$  is longer than both  $\tau_d$  and  $\tau_t$ . This means that we can never be sure if only one of the two molecules is excited or both.

# Chapter 2

## Theory

The following chapter will contain explanations on the theoretical background of the used methods of measurement as well as of the principles that are needed for the evaluation of the recorded spectra.

### 2.1 Methods

During this work, two different methods of fluorescence spectroscopy have been utilised. The first one is the laser induced fluorescence spectroscopy (LIF) and the second one is the single vibronic level fluorescence spectroscopy (SVLF).

#### 2.1.1 Laser Induced Fluorescence

LIF-spectroscopy is used to obtain excitation spectra of the sample molecules<sup>[36]</sup>. To record these spectra, an excitation laser (see section 3.1) is scanned over a selected spectral range. For every frequency the energy of the resulting photon equals

$$E_{\text{photon}} = h \cdot \nu \quad (2.1)$$

where  $h$  is the planck constant and  $\nu$  is the frequency of the light.

If this energy is equal to the energy gap between the ground state and one of the excited states of the sample (equ.2.2) fluorescence light will be emitted.

$$E_{\text{photon}} = E_{S_1} - E_{S_0} \quad (2.2)$$

This does not only occur if the light is resonant to an electronic state but also if it is resonant to a vibronic transition. For example the transition from  $S_{0,\nu_0}$  to  $S_{1,\nu_1}$ . These later transitions are only visible if the light source has a narrow bandwidth and if there are no effects that would broaden the absorption and emitting bands. These requirements are fulfilled by using a laser and performing the measurements in the gaseous phase in a supersonic jet.

Using a supersonic jet has a second advantage as it cools the sample molecules to a point where they are not only in the electronic but also in the vibrational ground state. This is desirable as it would complicate the evaluation by causing so called hot bands in the spectra. These bands are transitions from vibrational levels of the ground state to vibrational levels of the excited state.

However, not all transitions will be detected but only those which are allowed. Which transitions are allowed depends on the symmetry of the molecules and can be investigated with the help of the group theory.

Furthermore the intensity of the recorded bands depends on the Franck-Condon-Factors (section 2.2).

Usually an excitation spectrum shows up to ten bands. With the help of *ab-initio*-calculations these bands are then assigned to vibrations of the excited state of the molecule. The result of this measurement is the information which vibronic states of the first electronically excited state are accessible from the vibronic ground state of the molecule.

This information is needed for the single vibrational level fluorescence spectroscopy.

### 2.1.2 Single Vibronic Level Fluorescence

For the single vibrational level fluorescence spectroscopy the transitions detected by LIF-spectroscopy are excited one at a time. The emitted fluorescence light then is guided through a monochromator where it is dispersed according to its wavelength. As it is of great importance to have a high resolution the entrance slit is set to  $30\ \mu\text{m}$  and the grating to first order.

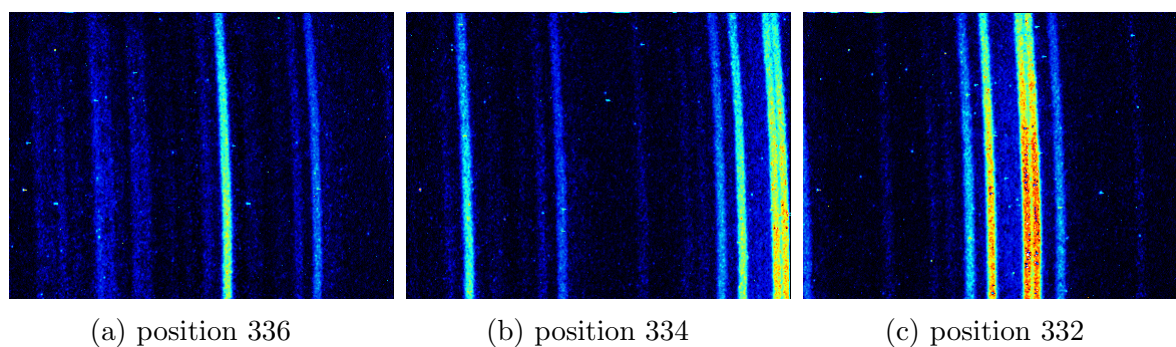


Figure 2.1: Examples for pictures at neighbouring positions of the grating. The intensities are colour coded with red being high intensities and black low.

The fluorescence is detected via an intensified CCD-camera (section 3.5) which allows the detection of a spectral range of about  $600\ \text{cm}^{-1}$  at once on the CCD chip. After every partial spectrum (they will be referred to as picture in the following) the grating is rotated to another position. The positions are usually chosen in a way that two neighbouring pictures overlap by about  $100\text{-}150\ \text{cm}^{-1}$ .

It is necessary that there are at least two bands in this overlap region. If this is not the case, an additional picture has to be taken with a larger overlap.

Due to this overlap it is possible to join all the pictures together to form a spectrum which usually covers a range of 2500 to 3000  $\text{cm}^{-1}$ .

The way this is done makes use of the fact that the relative intensities of bands in the spectra do not change regardless of how different the absolute intensities may be in two different pictures.

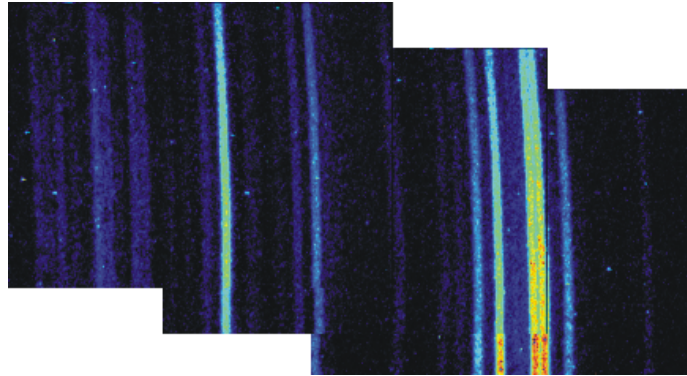


Figure 2.2: Example for the overlapping Bands in neighbouring pictures.

These differences occur as the power output of the laser may fluctuate during the measurement and although every picture is averaged 50 times the differences can be quite significant as can be seen in Figure 2.1. However it still can be seen that there are areas with the same pattern in neighbouring pictures. These are used to stitch the spectrum together. The picture shown in Figure 2.2 is a dispersed image of the fluorescence on the entrance slit of the monochromator. In order to get a spectrum, which depicts intensities vs. wavelength, the color encoded intensities along the lines have to be summed up. This (vertical) summation leads to the spectrum shown in Figure 2.3.

It is to be noted though that these pictures only show the intensities with respect to the horizontal pixel position on the CCD-chip. To get spectral information out of this, it is necessary to perform a calibration for every position of the grating that was used. This is done by setting the laser to a certain wavelength and determining the position of the stray light on the chip. This is repeated until enough positions are measured to perform a fourth order polynomial fit.

As can be seen in figure 2.3 the spectral overlap of the different pictures is quite good and needs only little adjustment. The intensities on the other hand need to be adjusted in a way that does not falsify the measurement.

As has been mentioned before the relative intensities do not change between two pictures. Therefore it is allowed to normalise the spectra. This is done by setting the band with the highest intensity that does not contain the stray light to an intensity of 1. All other values are then given relative to this one.

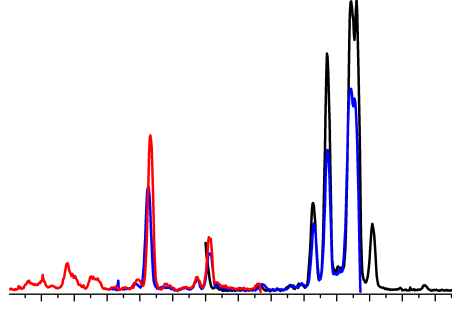


Figure 2.3: Linespectra obtained from the pictures in fig. 2.1. The black line refers to the picture taken at grating position 332, the blue line to the picture taken at grating position 334 and the red line refers to the picture taken at grating position 336.

## 2.2 Franck-Condon-Principle

The intensities of the transitions between two vibronic states  $m$  and  $n$  are proportional to the square of the transition moment  $M_{mn}$ , to the population  $W(T)$  of the initial state, which in case of absorption spectra is determined by the Boltzmann distribution, and to the frequency  $\nu_{mn}$  of the transition for absorption spectra and the fourth power of the frequency  $\nu_{mn}$  for emission spectra, respectively.<sup>1</sup>

$$I_{mn} \propto |M_{mn}|^2 W(T) \nu_{mn} \quad (\text{Absorption}) \quad (2.3)$$

$$I_{mn} \propto |M_{mn}|^2 W(T) \nu_{mn}^3 \quad (\text{Emission}) \quad (2.4)$$

The calculation of spectral intensities of emission and absorption spectra using the Franck-Condon principle is based on two assumptions: (i) the Condon principle, which states, that the electronic transition dipole moment is independent of the nuclear motions, leading to the FC principle. (ii) the BO approximation postulating the independence of nuclear and electronic motions. While the first approximation can easily be extended by expanding the TDM in a Taylor series, in which the first term is the static TDM times the Frank-Condon integral and the second term is the HT contribution, the breakdown of the second assumption poses more problems. The transition dipole moment for a transition between an initial state  $m$  and a final state  $n$  is defined as:

$$M_{mn} = \langle v^m | \mu_{mn}(Q) | v^n \rangle \quad (2.5)$$

---

<sup>1</sup>this refers to energy detecting schemes, while for counting schemes (as for example for the nowadays very common CCD detection in optical multichannel analyzers) the intensity depends on the third power of the frequency  $\nu^3$ .<sup>[37]</sup>

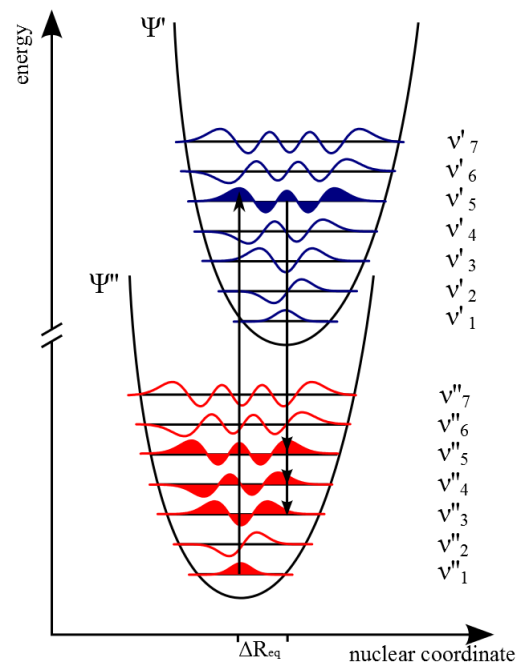


Figure 2.4: Scheme of an energy diagram. Each of the wavefunctions of the vibronic states  $\nu'$  in the electronic state  $\Psi'$  has different values for the overlap with the vibronic states  $\nu''$  in the electronic ground state  $\Psi''$

with

$$\mu_{mn}(Q) = \langle \Psi_m | \mu | \Psi_n \rangle; \quad \mu = \sum_g er_g \quad (2.6)$$

The transition dipole moment  $M_{mn}$  can be expanded in a Taylor series about the equilibrium position at  $Q_0$ . Truncation of the expansion after the second expansion term yields:

$$\begin{aligned} M_{mn} = M_{mn}(Q_0) \langle v^m | v^n \rangle &+ \sum_i \left( \frac{\partial M_{mn}}{\partial Q_i} \right)_{Q_0} \langle v^m | Q_i | v^n \rangle \\ &+ \sum_i \sum_k \left( \frac{\partial^2 M_{mn}}{\partial Q_i \partial Q_k} \right)_{Q_0} \langle v^m | Q_i Q_k | v^n \rangle \end{aligned} \quad (2.7)$$

The first term consisting of the electronic transition moment  $M_{mn}(Q_0)$  at the equilibrium geometry  $Q_0$  and the overlap integral  $\langle v^m | v^n \rangle$  is described by Franck-Condon-Theory, the higher expansion terms are described by Herzberg-Teller theory and will be neglected here.

## 2.3 FCFit

For the evaluation of the measurements we need to have a possibility to assign the bands in the spectra to vibrations of the sample. Therefore we use the programm FCFIT<sup>[38;39]</sup>. This program is able to simulate spectra from given geometries, i.e. from *ab-initio*-calculations.

### 2.3.1 The Overlap Integrals

As mentioned before (see section 2.2) the intensities of transitions in our spectra depend on the overlap integrals of wavefunctions. FCFIT is able to do exactly this<sup>[40]</sup>.

Such an overlap integral can be written in Bra-Ket-form where the final state is written in the Bra and the initial state in the Ket. For an absorption it would look like  $\langle \nu' | \nu'' \rangle$  and for an emission it would be  $\langle \nu'' | \nu' \rangle$ . Both, the Bra and the Ket, are written as quantum strings.

In case of an absorption the usual initial state is the vibrationless electronic ground state, which means the Ket-string consists only of zeros ( $|000\rangle$ ).

The quantum-string of the Bra contains all vibrations that are needed to describe this state. It may look like  $\langle 103|$ . In this case the full integral would look like  $\langle 103|000\rangle$ .

The next step is to calculate the integrals for the transitions where the sum of the quanta in the Bra is reduced by 1 where the minimum for each quantum is 0. This means the integrals  $\langle 003|000\rangle$  and  $\langle 102|000\rangle$  have to be calculated. The values of the integrals are

then stored in hash tables.

After that the sum of quanta is again reduced by one, now leaving us with three integrals to be calculated. The integral  $\langle 003|000\rangle$  leads to  $\langle 002|000\rangle$  and the integral  $\langle 102|000\rangle$  leads to  $\langle 101|000\rangle$  and  $\langle 002|000\rangle$ . The results are then again stored in hash tables.

As can be easily seen, two of the integrals are the same. In this case only one of them is calculated and when the program reaches the second integral, it just takes the value from the hash table and uses this.

The sum of quanta is reduced until both states contain zero quanta.

### 2.3.2 Calculating The Intensities

If these integrals are known, it is possible to calculate the intensities for each transition with formula 2.8.

$$I^{rel}(\nu' \leftarrow \nu'') = \frac{\langle \nu' | \nu'' \rangle^2}{\langle ref \rangle^2} * x_{corr} \quad (2.8)$$

Here  $\langle \nu' | \nu'' \rangle^2$  is the Franck-Condon-factor and  $\langle ref \rangle^2$  is the Franck-Condon-factor for the integral with the highest value. Due to different proportionalities between intensity and energy for absorption and emission it is necessary to include the correction factor  $x_{corr}$ .

For an absorption  $x_{corr}$  is calculated via equation 2.9 and for emission via equation 2.10.

$$x_{corr} = \left( \frac{\tilde{\nu}_{base} + \tilde{\nu}'_i}{\tilde{\nu}_{base} + \tilde{\nu}'_{ref}} \right)^{n_a} \quad (2.9)$$

$$x_{corr} = \left( \frac{\tilde{\nu}_{base} - \tilde{\nu}''_i}{\tilde{\nu}_{base} - \tilde{\nu}''_{ref}} \right)^{n_e} \quad (2.10)$$

In these equations  $\tilde{\nu}'_i$  and  $\tilde{\nu}''_i$  are the frequencies of the vibrations of the initial states while  $\tilde{\nu}_{base}$  is the energy of the electronic state to which  $\nu'_i$  and  $\nu''_i$  belong. The exponents  $n_a$  and  $n_e$  can be 0 if no correction is wanted. If  $x_{corr}$  is used,  $n_a$  has a value of 1, while  $n_e$  can either be 4 if the energy is detected or 3 if the photon count is detected.

Usually the absorption spectrum is just simulated once to assign the transition that are visible in the LIF-spectrum. These then determine the initial states for the simulation of the emission spectra. Here,  $n_e$  is set to 3.

### 2.3.3 Simulation Of The Spectrum

Now that we have the possibility to calculate the intensities for the transitions we can actually simulate a spectrum. However, there are still a few information we need to give

FCFIT as input.

First we need to define the initial states, which are given as quantum strings, as explained before. For each initial state a separate subspectrum will be calculated.

FCFIT will then determine every possible final state. As there is an infinite number of these, thresholds have to be given. These are given in four different ways:

- 1) maximum energy
- 2) maximum single quanta
- 3) maximum excited modes
- 4) maximum quanta sum

Number 1) define up to which energy the final states will be calculated, number 2) defines how many quanta are allowed for a single mode, number 3) defines how many modes can be excited at the same time and number 4) defines how many quanta are allowed at the same time in total.

Now the program is able to calculate the desired spectra.

### 2.3.4 The Fit

FCFIT is not only able to simulate spectra, it is also capable of fitting geometry changes upon excitation based on such spectra.

In order to do so, it needs the above mentioned requirements to be fulfilled and a list of intensities that are assigned to normal modes of the sample. Furthermore the user has to give a list of normal modes along which the program is allowed to change the geometry of the molecule. To improve the result even further, rotational constants can be used as fit parameters.

FCFIT then performs the above described procedure and compares the result with the list that has been given. In the next step the geometry of the molecule is distorted along all of the selected normal modes.

A new spectrum is simulated and is compared to both the list of intensities and the older simulation. This is repeated until there is no improvement between two spectra and the intensities in the list are represented as good as possible.

By comparing the simulated spectrum with the measurements, the user can then try to improve the list again. After that a new fit can be performed.

This has to be repeated until there is no more improvement.

## 2.4 From Measurement To Result

To conclude this chapter I will summarize the procedure of investigation.

The first thing that has to be done are the *ab-initio*-calculations of the molecule. After that a simulation of the absorption spectrum can be done.

Next thing to do is to measure the LIF-spectrum and to compare it to the simulation. Now

the bands in the LIF-spectrum can be assigned to transition, and therefore to vibronic states, of the molecule. These states are then used for the SVLF-spectroscopy. Also simulations are done for these initial states.

The SVLF-spectra are prepared as described in section 2.1.2. With these the list of intensities can be created and the fit can be performed.

After each fit the simulated and measured spectra are compared and the list of intensities is improved.

Finally the geometry that lead to the best result can be extracted from the output of FCFIT.



# Chapter 3

## Experimental Set Up

in the following chapter the experimental set up used for the experiments, described in this thesis will be described in detail. A schematic view of the experiment is shown in figure 3.1).

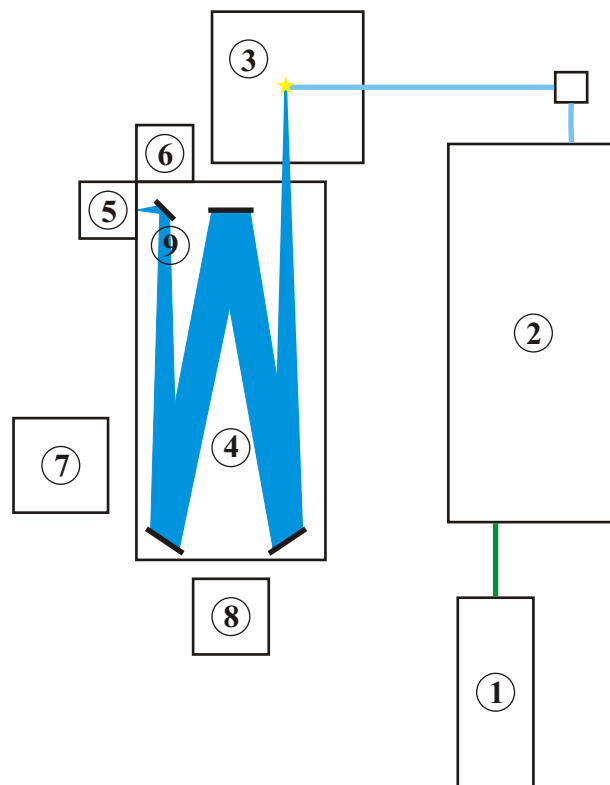


Figure 3.1: Experimental set up. 1) Nd:YAG-laser 2) dye-laser 3) vacuum chamber with sample 4) monochromator 5) photomultiplier 6) iCCD-camera 7) clock 8) computer 9) moveable mirror

In summary our set up consists of a laser system which is used to excite the sample. This sample is prepared in a supersonic-jet. The resulting fluorescence light is then detected after passing through a monochromator. For different experiments two different detectors have been used. LIF was performed, using a photomultiplier, for SVLF we utilized an

image intensified CCD camera.

Laser and valve for the supersonic jet are pulsed with a frequency of 10 Hz.

For timing of all devices, we used a delay generator (Stanford Research Systems Model DG645) is used.

## 3.1 Laser-system

The experiment has some strict requirements for the used light source. One is a very narrow spectral bandwidth and the other is a high intensity. Both of these are fulfilled by a laser.

A problem arises from a third requirement which is a broad spectral range of the laser light. This is needed for the excitation spectra which usually cover several nanometers of wavelength.

All three requirements can not be fulfilled by a single laser. Therefore a combination of two different lasers is used. In this case a Nd:YAG-Laser and a dye-laser.

### 3.1.1 Nd:YAG-laser

The Nd:YAG-laser ( 1) in fig. 3.1) that was used for the measurements is a Quanta-Ray INDI-40-10HG from Spectra-Physics. It generates laser light at three different wavelengths: 1064, 532 and 355 nm. For the measurements in this thesis only the wavelength of 532 nm was used. In this setting the laser has a maximum output of about 200 mJ with a pulse width of 5-8 ns<sup>[41]</sup>.

This means that the Nd:YAG-laser has a high intensity with a narrow bandwidth but it misses the broad spectrum as it only creates three discrete wavelengths. That is why it is used to pump a dye-laser.

### 3.1.2 Dye-laser

The dye-laser ( 2) in fig. 3.1) is used to modify the output of the Nd:YAG-laser. In our set-up a Lambda Physik FL 3002 is used. It has a bandwidth of of  $0.2 \text{ cm}^{-1}$  while being tunable over a wavelength range from 332 to 970 nm. As the measurements are conducted in the ultra-violet range this is not enough. Therefore a crystal is used to generate the second harmonic, thus giving us access to the range from 217 to 348 nm<sup>[42]</sup>.

However it should be mentioned that to use the whole range the dye solution has to be changed.

## 3.2 Vacuum Chamber

The measurements are carried out in the gas phase. This requires a good vacuum which can only be created in special apparatuses. In this chamber the sample is stored during the measurements and the molecular beam is formed. Furthermore it contains a telescope to collect and focus the fluorescence light emitted by the sample.

### 3.2.1 Vacuum Pumps

The vacuum needs to be about  $3 * 10^{-4}$  mbar or better. To get to such a low pressure a combination of two different pumps is used.

The first is a rotary vane pump. On its own this pump reaches a pressure of about  $10^{-2}$  mbar. As this is not nearly enough a second pump is used.

This pump is an oil diffusion pump. It is able to reach very low pressures but it requires a backing pump.

### 3.2.2 Sample Chamber

The sample chamber (see fig. 3.2) is a small metal block with two pipes near the top and a hole in the top side. This hole can be closed with the help of a lid which can be fastened with screws. The sample is placed into this hole. The whole metal block can be heated by several resistors that are fixed around it.

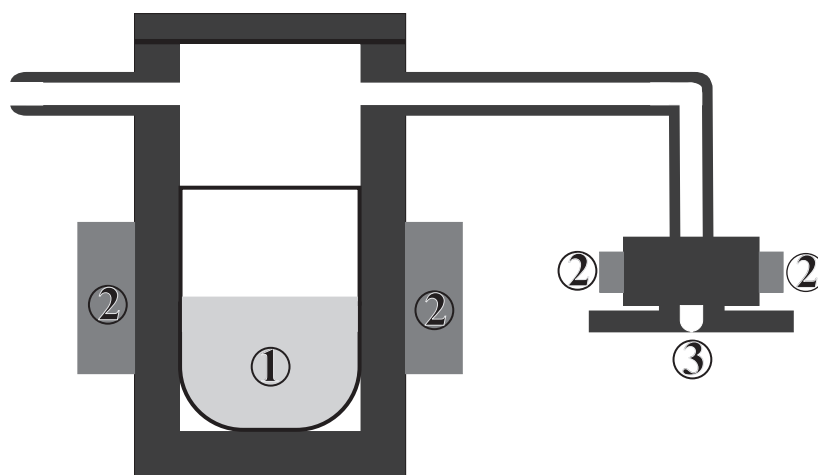


Figure 3.2: Scheme of the sample chamber. 1)sample 2)resistors 3)nozzle

One of the pipes is used to let a carrier gas into the sample chamber. This gas is usually helium but argon can be used too. The second pipe leads to a nozzle which is used to create the supersonic jet. It can be heated the same way as the sample chamber and is usually kept at a temperature about 20 degrees above the chamber's temperature.

The nozzle has an  $500 \mu\text{m}$  orifice and creates a supersonic-jet which contains the sample

and is perpendicular to the excitation laser. The emitted fluorescence light is then collected and focused onto a slit with a telescope.

This telescope is formed by two lenses. The first one is these is a bi-convex lens with a focal length of  $f=5$  cm. This lens is used for collecting and parallelizing the light that is emitted by the sample.

The second lens is placed with an interspacing of 5 cm. It is a bi-convex lens too, but the focal length is  $f=50$  cm. This second lens focuses the light onto the entrance slit of the monochromator. If the focus was not exactly on the entrance slit, it light would also not be focus on the detector, resulting in a loss of resolution.

The combination of the two lenses leads to a magnification of the image, which in this case means a broadening of the detected signal.

### 3.3 Monochromator

The monochromator (4) in fig. 3.1) has an entrance slit, which can be set manually. Depending on the method it is either completely open or set to  $\mu\text{m}$ . The monochromator has a length of 1m and the grating has 2400 lines/mm. The setting of the grating once again depends on the measurement which is conducted. For the measurement of excitation spectra the grating is set to zeroth order and the slit is completely open. For the single vibrational level fluorescence (SVLF) spectra the grating is set to first order and the slit is set to 4  $\mu\text{m}$ .

At the monochromator exit, two different detectors are installed. The first is a photomultiplier (5) in fig. 3.1). It is used for the excitation spectra. The second detector is an intensified CCD-camera (6) in fig. 3.1) and is used for the SVLF-spectra.

Switching between the detectors is possible with the help of a mirror (9) in fig. 3.1) which is mounted on a sleigh on an optical bench.

### 3.4 Photomultiplier

The photomultiplier used in this experiment consists of twelve dynodes which are under high voltage. They are arranged in such a way that when an particle or photon hits the first dynode an electron is emitted. This electron then is accelerated towards the next dynode where it causes several electrons to be emitted. This process repeats at each electrode until the signal caused by a single particle or photon is easily measured. The higher the voltage the stronger the final signal gets.

Furthermore the photomultiplier is cooled to reduce dark current so that the signal to noise ratio gets better.

## 3.5 iCCD

The iCCD-camera used for this experiment is a Flamestar II from LaVision and is UV sensitive.

The light hits a phosphorescent layer which is mounted on a multichannel plate (MCP). This MCP is a two-dimensional array of amplifier tubes which follow a similar principle as the photomultiplier described in section 3.4.

With this device it is possible to determine the position at which the light hit the detector. In combination with the monochromator this means that it is possible to determine the wavelength of the detected light as the grating of the monochromator leads to a spacial separation of the different wavelengths of the light.



# Chapter 4

## Publications

### 4.1 Electronic Spectra of 2- and 3-Tolunitrile in the Gas Phase II: Geometry changes from Franck-Condon Fits of Fluorescence Emission Spectra.

The measurements this publication is based on were performed by Benjamin Stuhlmann and Felix Gmerek, the *ab-initio*-calculations, simulations and Franck-Condon-Fits were made by Felix Gmerek. The rotational constants used for the combined fits were provided by Leonardo Álvarez-Valtierra and the fits of the torsion were performed by Michael Schmitt.

The following section of this chapter has been published in the Journal of Chemical Physics (Gmerek et. al., J. Chem. Phys., 144,2016).

# Electronic Spectra of 2- and 3-Tolunitrile in the Gas Phase II: Geometry changes from Franck-Condon Fits of Fluorescence Emission Spectra.

Felix Gmerek,<sup>a</sup> Benjamin Stuhlmann,<sup>a</sup> Leonardo Álvarez-Valtierra,<sup>b</sup> David W. Pratt<sup>c</sup> and Michael Schmitt<sup>a\*</sup>

<sup>a</sup> *Heinrich-Heine-Universität, Institut für Physikalische Chemie I, D-40225 Düsseldorf, Germany.*

<sup>b</sup> *División de Ciencias e Ingenierías, Universidad de Guanajuato; León, Guanajuato, México 37150*

<sup>c</sup> *Department of Chemistry, University of Vermont; Burlington, VT 05405*

## Highlights

- Fluorescence excitation and single vibronic level fluorescence spectra of 2- and 3-tolunitrile have been recorded in a molecular beam.
- We determined the complete changes of the heavy atom structures in the ground and lowest excited singlet states of o- and m-tolunitrile.
- A combined Franck-Condon/rotational constants fit has been performed.

## Abstract

We determined the changes of the geometries of 2- and 3-tolunitrile upon excitation to the lowest excited singlet states from Franck-Condon fits of the vibronic intensities in several fluorescence emission spectra and of the rotational constant changes upon excitation. These structural changes can be connected to the altered electron distribution in the molecules and are compared to the results of *ab initio* calculations. We show how the torsional barriers of the methyl groups in both components are used as probe of the molecular changes upon electronic excitation.

*Keywords:* Franck-Condon analysis, o- and m-tolunitrile, structure, rotational constants

---

\*corresponding author.

Fax: 49 211 8115195; Tel: 49 0211 81 12100; E-mail: mschmitt@uni-duesseldorf.de

# 1 Introduction

Electronic excitation of aromatic molecules alters a variety of molecular parameters, which can be determined by different spectroscopic techniques. Among the photophysically interesting properties that are strongly altered are the nuclear structure (what is called the geometry of the molecule in the individual electronic state), the electron density and hence the permanent dipole moment of each state and the transition dipole moment, and the barriers to internal motions, which determine the state density of the molecules at a certain energy above the zero-point vibrational level.

2- and 3-Tolunitrile (2-TN and 3-TN) have been studied using rotationally resolved laser induced fluorescence spectroscopy in order to investigate the torsional barriers in both electronic states, as reported in the previous paper I.<sup>1</sup> In the present publication we will use the combined information from the changes of the rotational constants upon electronic excitation and the vibronic intensities in absorption and emission through various absorption bands for a combined Franck-Condon/inertial parameter fit of the geometry change upon electronic excitation.

$S_1 \leftarrow S_0$  fluorescence excitation spectra and  $S_0 \leftarrow S_1$  fluorescence emission spectra of 2-, 3-, and 4-tolunitrile were reported by Fujii *et al.*<sup>2</sup> They determined the torsional barriers of ground and lowest excited singlet states from the low frequency torsional bands in the  $S_0$  and the  $S_1$  states, respectively. The ground state internal rotational parameters of 2-TN have been determined from microwave spectroscopy in the frequency ranges of 22.0-26.0 GHz and 32.0-37.0 GHz<sup>3</sup> and from millimeter wave spectroscopy in the frequency range 50.0 - 75.0GHz.<sup>4</sup> Nakai and Kawai studied the torsional potential of various substituted toluenes, among them 2- and 3-TN.<sup>5</sup> They showed how a  $\pi^*\sigma^*$  hyperconjugation mechanism can be used to explain their different barriers in different electronic states. Later Park *et al.* measured the vibronic emission spectra of the jet-cooled 2-tolunitrile<sup>6</sup> and 3-tolunitrile<sup>7</sup> in a corona-excited supersonic expansion. From a density functional theory (DFT) based analysis of the spectrum, several vibrational modes were assigned in the emission spectrum. The cationic ground state  $D_0$  has been studied using pulsed field ionisation-ZEKE photoelectron spectroscopy by Suzuki *et al.*<sup>8</sup>

Nagao *et al.*<sup>9</sup> investigated oriented 2-, 3- and 4-tolunitrile as guests in  $\alpha$ ,  $\beta$ , and  $\gamma$ -cyclodextrin (CD) using FTIR spectroscopy. They found that the charge distribution of the tolunitriles determines the orientations and depths of inclusion in the CD cavity. Nagabalasubramanian *et al.*<sup>10</sup> calculated the vibrational spectrum of 2-TN using *ab initio* and density functional theory and compared their computational results to FTIR and Raman spectra.

In the present contribution, geometry changes of 2-TN and 3-TN are determined from Franck-Condon (FC) fits of the vibronic band intensities in several fluorescence emission spectra and the changes of the rotational constants upon excitation, which are determined in Paper I of this series.<sup>1</sup>

## 2 Experimental and Computational Details

### 2.1 Experiment

The experimental setup for the dispersed fluorescence (DF) spectroscopy has been described in detail elsewhere<sup>11,12</sup>. In brief, 2- and 3-toluonitrile were evaporated at 293 K and co-expanded through a pulsed nozzle (kept at 328 K to avoid condensation) with a 500  $\mu\text{m}$  orifice (General Valve) into the vacuum chamber using helium as carrier gas. The output of a Nd:YAG (SpectraPhysics INDI) pumped dye laser (Lambda-Physik, FL3002) was frequency doubled and crossed at right angles with the molecular beam. The resulting fluorescence was imaged on the entrance slit of a  $f = 1$  m monochromator (Jobin Yvon, grating 2400 lines/mm blazed at 400 nm in first order). The dispersed fluorescence spectrum was recorded using a gated image intensified UV sensitive CCD camera (Flamestar II, LaVision). One image on the CCD chip spectrally covers approximately  $600\text{ cm}^{-1}$ . Since the whole spectrum is taken on a shot-to-shot basis, the relative intensities in the DF spectra do not vary with the laser power. The relative intensities were afterwards normalized to the strongest band in the spectrum, not including the resonance fluorescence band, which also contains the stray light and is therefore excluded from the FC analysis.

### 2.2 *Ab initio* calculations

Structure optimizations were performed employing Dunning's correlation consistent polarized valence triple zeta basis set (cc-pVTZ) from the TURBOMOLE library.<sup>13,14</sup> The equilibrium geometries of the electronic ground and the lowest excited singlet states were optimized using the approximate coupled cluster singles and doubles model (CC2) employing the resolution-of-the-identity approximation (RI).<sup>15-17</sup> The Hessians and harmonic vibrational frequencies for both electronic states, which are utilized in the FC fit, have been obtained from numerical second derivatives using the NumForce script<sup>18</sup> implemented in the TURBOMOLE program suite.<sup>19</sup> A natural population analysis (NBO)<sup>20</sup> has been performed at the CC2 optimized geometries using the wavefunctions from the CC2 calculations as implemented in the TURBOMOLE package.<sup>19</sup>

### 2.3 Franck-Condon fit of the structural change upon electronic excitation

The change of a molecular geometry upon electronic excitation can be determined from the intensities of absorption or emission bands using the FC principle. According to this principle, the relative intensity of a vibronic band depends on the overlap integral of the vibrational wave functions of both electronic states. The transition dipole moment for a transition between an initial electronic state  $|m, v\rangle$  and a final electronic state  $|n, w\rangle$  is defined as:

$$M_{vw} = \langle v | \mu_{mn}(Q) | w \rangle \quad (1)$$

with the electronic transition dipole moment  $\mu_{mn}(Q)$ :

$$\mu_{mn}(Q) = \langle \Psi_m | \mu | \Psi_n \rangle; \quad \mu = \sum_g e r_g \quad (2)$$

where  $r_g$  is the position vector of the  $g$ th electron. The dependence of the electronic transition dipole moment  $\mu_{mn}$  on the nuclear coordinates can be approximated by expanding  $\mu_{mn}$  in a Taylor series about the equilibrium position at  $Q_0$ . The series is truncated after the first term in the FC approximation.

The fit has been performed using the program FCFIT, which has been developed in our group and described in detail before.<sup>21,22</sup> The program computes the FC integrals of multidimensional, harmonic oscillators mainly based on the recursion formula given in the papers of Doktorov, Malkin, and Man'ko.<sup>23,24</sup> and fits the geometry (in linear combinations of selected normal modes) to the experimentally determined intensities. This is simultaneously done for all emission spectra, which are obtained *via* pumping through different  $S_1$  vibronic modes.

The vibrational modes of the electronically excited state can be expressed in terms of the ground state modes using the following linear orthogonal transformation, first given by Duschinsky<sup>25</sup>:

$$Q' = S Q'' + d \quad (3)$$

Here,  $Q'$  and  $Q''$  are the  $N$ -dimensional vectors of the normal modes of excited and ground state, respectively,  $S$  is a  $N \times N$  rotation matrix (the Duschinsky matrix) and  $d$  is an  $N$ -dimensional vector which describes the linear displacements of the normal coordinates.

The fit of the geometry to the intensities in the vibronic spectra can be greatly improved if independent information about the geometry changes upon electronic excitation is available. This additional information is provided by the change of the rotational constants upon electronic excitation, which can be obtained from rotationally resolved electronic spectroscopy. While geometry fits to the rotational constants are routinely performed using non-linear fits in internal coordinates, the combination of rotational constant changes and vibronic intensities allows for determination of many more geometric parameters.

## 3 Results

### 3.1 *Ab initio* calculations

The structures of 2- and 3-TN in their ground and lowest excited singlet states have been determined from optimizations at the second order coupled cluster (CC2) level of theory using the cc-pVTZ basis set. The atomic numbering used throughout this publication is shown in Figure 1. The Cartesian coordinates of the optimized structures of 2-TN and 3-TN in their  $S_0$  and  $S_1$ -states are given in Tables S1 - S4 the online supplemental material.<sup>26</sup>

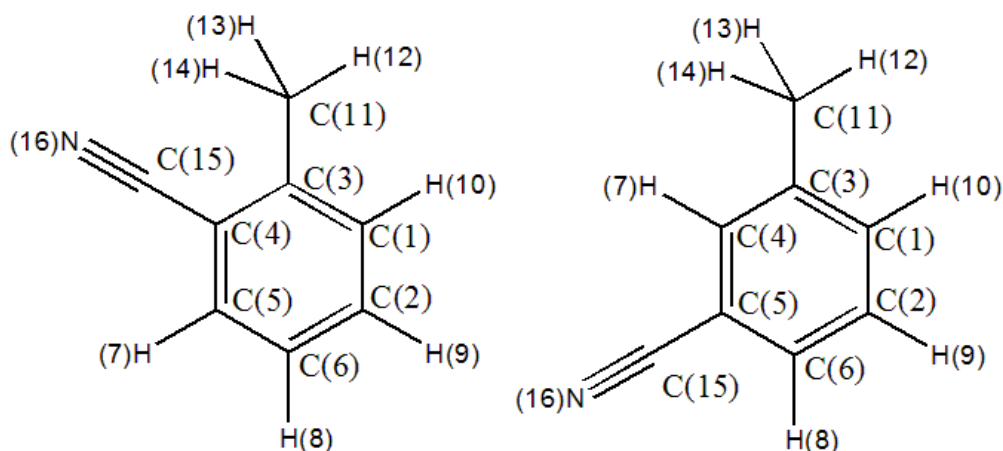


**Figure 1** Structure and atomic numbering of o- and m-tolunitrile.

2- and 3-TN belong to the  $C_s$  symmetry point group in both electronic states, in agreement with experimental inertial defects of  $-2.87 \text{ amu } \text{\AA}^2$  ( $-0.02 \text{ amu } \text{\AA}^2$ ) in 2-TN (3-TN) in the electronic ground state and of  $-3.14 \text{ amu } \text{\AA}^2$  ( $-0.81 \text{ amu } \text{\AA}^2$ ) in 2-TN (3-TN) in the lowest excited state.<sup>1</sup> The inertial defect of 2-TN is approximately the same as a static value of two out-of-plane hydrogens due to the high barrier hindering the torsional motion of the methyl group. For 3-TN much smaller values are reported due to vibrational averaging at the onset of nearly free internal rotation.

Of the 42 normal modes, 27 are symmetric with respect to the mirror plane and 15 are antisymmetric and they transform like  $\Gamma_{vib} = 27A' + 15A''$ . Since both the ground state, as well as the electronically excited state have electronic  $A'$ -symmetry, all vibronic transitions are allowed in absorption and emission. The relevant details about these states are compiled in Table 1 and are compared to the results of the experiments.

The numbering of the 42 normal modes of 2- and 3-TN, their symmetries and their wavenumbers in the electronic ground and excited states are compiled in Tables S4 and S5 of the online supplemental material.<sup>26</sup> The last columns of these Tables show the largest elements of the Duschinsky matrix, which were calculated from the respective Hessians at the equilibrium positions and facilitates the

**Table 1** Rotational constants  $A$ ,  $B$ , and  $C$  are given in MHz, components of the dipole moments  $\mu_a$ ,  $\mu_b$ , and  $\mu_c$  in Debye, the angle of the transition dipole moment  $\theta$  in degrees, vertical ( $\Delta v_{vert.}$ ) and adiabatic excitation energies ( $\Delta v_{adiab.}$ ) in  $\text{cm}^{-1}$ , and oscillator strengths  $f$  are dimensionless. The last four rows give the leading contributions to the transition.

	2-TN				3-TN			
	$S_0$	$S_1$	$S_0(\text{exp.})$	$S_1(\text{exp.})$	$S_0$	$S_1$	$S_0(\text{exp.})$	$S_1(\text{exp.})$
$A$	2944	2917	2892.6	2853.4	3322	3246	3331.8	3256.0
$B$	1505	1459	1500.4	1460.2	1209	1184	1203.0	1177.8
$C$	1002	978	993.5	971.7	891	873	883.9	866.1
$\mu_a$	-3.710	-4.194	-	-	-2.69	-2.89	-	-
$\mu_b$	1.632	1.700	-	-	3.82	4.16	-	-
$\mu_c$	0.000	0.000	-	-	0.00	0.00	-	-
$\theta$	-	-73	-	$\pm 71.3$	-	-71	-	-71
$\Delta v_{vert.}^{\text{emission}}$	-	37272	-	-	-	37473	-	-
$\Delta v_{vert.}^{\text{absorption}}$	-	40332	-	-	-	40420	-	-
$\Delta v_{adiab.}$	-	37603	-	35768.95	-	37726	-	35815.53
$f$	-	0.019	-	-	-	0.012	-	-
HOMO $\rightarrow$ LUMO	-	0.68	-	-	-	0.71	-	-
HOMO-1 $\rightarrow$ LUMO+1	-	0.40	-	-	-	0.47	-	-
HOMO-1 $\rightarrow$ LUMO	-	-0.47	-	-	-	0.38	-	-
HOMO $\rightarrow$ LUMO+1	-	0.36	-	-	-	0.32	-	-

assignments of ground state modes to excited state vibrations. Most of the  $S_1$ -state vibrational modes can be described by a single ground state vibration (diagonal elements of the Duschinsky matrix) and only very few modes are heavily mixed.

## 3.2 Experimental results

### 3.2.1 The fluorescence excitation spectrum of 2-TN

The laser induced fluorescence (LIF) spectrum of 2-TN is shown Figure 2. It is similar to spectra already shown in the literature.<sup>2</sup> Nevertheless, we present it here along with a Franck-Condon simulation of the absorption spectrum (lower trace), since some of the features and assignments in this spectrum are still not fully understood. Furthermore, the vibronic  $S_1$  state assignments are crucial for the Franck-Condon fit of the emission spectra. The inset in the upper trace shows a zoomed part of the spectrum in the region of the torsional transitions that are due to the hindered internal rotation of the methyl group.

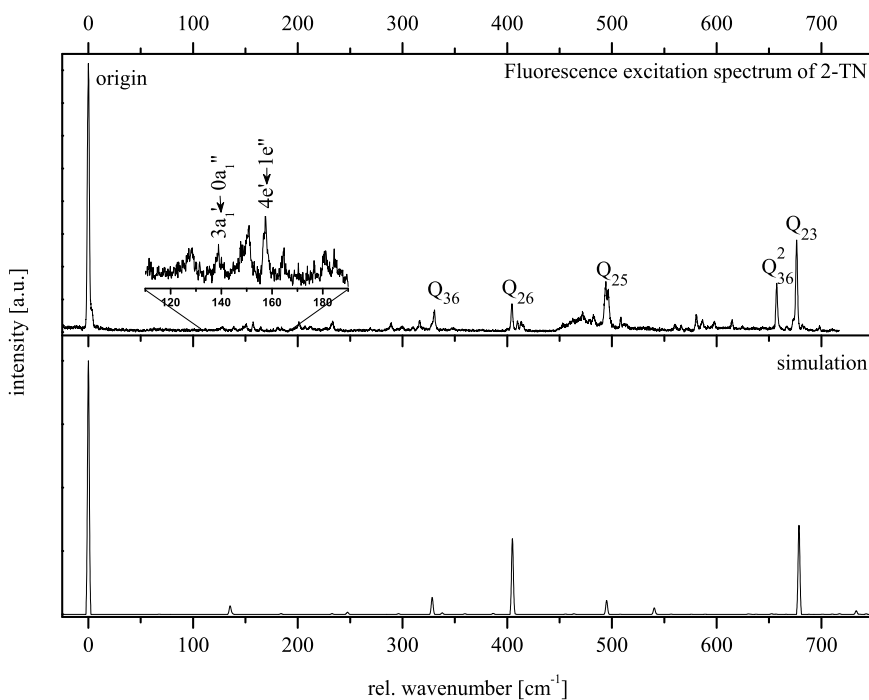


**Figure 2** Fluorescence excitation spectrum of 2-TN along with a Franck-Condon simulation of the absorption spectrum using the *ab initio* parameters.

The agreement between the experimental spectrum and the simulation, calculated using the CC2/cc-pVTZ optimized structures and the Hessians calculated at the stationary points of both electronic states, is fair. In general, deviations between Franck-Condon simulations and absorption spectra

are larger than for emission spectra. The main reason is the larger contributions of Herzberg-Teller effects to the absorption spectra, since the perturbing higher electronic states are energetically closer to the excited state than to the ground state, thus perturbing the absorption spectra more than the emission. Other reasons for deviations between experiment and simulations are common for both types of spectra. These are mainly the non-consideration of anharmonicity in our model, resulting in frequency deviations and the neglect of resonances like Fermi or Darling-Dennison resonances, resulting both in frequency and intensity deviations. Most of the differences between simulation and experiment can be attributed to one of these effects.

The most striking difference, the large intensity of the overtone of the out-of-plane vibration  $Q_{36}$  can be attributed to a Fermi resonance with vibration  $Q_{23}$ , shifting  $Q_{36}^2$  down and  $Q_{23}$  up in energy. In the harmonic approximation,  $Q_{36}^2$  is expected at  $662 \text{ cm}^{-1}$ , right in the middle of the experimental spectrum between the bands at  $658 \text{ cm}^{-1}$  ( $Q_{36}^2$ ) and  $677 \text{ cm}^{-1}$  ( $Q_{23}$ ). But frequency arguments using only the  $S_1$  state, would be a weak basis for reasoning about Fermi resonances in molecules with such a great number of allowed vibrational transitions. We therefore report here a result from the fluorescence emission spectra, which will be presented in detail in section 3.2.2. The emission spectra taken through the vibronic bands at  $658$  and  $677 \text{ cm}^{-1}$  are very similar, showing the strongly mixed character of the underlying excited modes. The strongest emission takes place to the  $Q_{23}$  ground state level, with considerable intensity also in the  $Q_{36}^2$  overtone.

This Fermi doublet of  $Q_{36}^2$  and  $Q_{23}$  is separated by  $19 \text{ cm}^{-1}$  and has an intensity ratio of 1:2, *cf.* Figure 2. Careful experiments showed that neither of the transitions was saturated. Using standard perturbation theory,<sup>27</sup> we adapted the energy distance of unperturbed levels  $\delta = E_{Q_{23}}^0 - E_{Q_{36}^2}^0$ , and the perturbation matrix element  $W_{Q_{23}Q_{36}^2}$  to the measured energy distance of the perturbed levels  $E_{Q_{23}} - E_{Q_{36}^2}$  and to the experimentally observed intensity ratio of 1:2, simultaneously. The energy difference of the perturbed levels can be obtained from  $E = \bar{E}_{ni} \pm \sqrt{4|W_{ni}|^2 + \delta^2}$ , where  $\bar{E}_{ni}$  is the mean of the unperturbed levels. The ratio of the intensities can be adapted through the coefficients of the zero order wave functions:  $a = \left( \frac{\sqrt{4|W_{ni}|^2 + \delta^2} + \delta}{2\sqrt{4|W_{ni}|^2 + \delta^2}} \right)^{\frac{1}{2}}$  and  $b = \left( \frac{\sqrt{4|W_{ni}|^2 + \delta^2} - \delta}{2\sqrt{4|W_{ni}|^2 + \delta^2}} \right)^{\frac{1}{2}}$ , with the intensity ratio given by  $I_n/I_i = a^2/b^2$ . The resulting two mixed wavefunctions are best described by the linear combinations:

$$\psi_{Q_{23}} = 0.817\psi_{Q_{23}}^0 - 0.576\psi_{Q_{36}^2}^0 \quad (4)$$

$$\psi_{Q_{36}^2} = 0.576\psi_{Q_{23}}^0 + 0.817\psi_{Q_{36}^2}^0 \quad (5)$$

using the zero approximation wavefunctions  $\psi_n^0$  and  $\psi_i^0$ . The distance of the unperturbed levels  $\delta = E_{Q_{23}}^0 - E_{Q_{36}^2}^0$  was determined to be  $6.5 \text{ cm}^{-1}$ , the perturbation matrix element  $W_{Q_{23}Q_{36}^2}$  to be  $9.1 \text{ cm}^{-1}$ .

The large number of quite weak transitions around  $100 \text{ cm}^{-1}$  can be traced back to torsional tran-

sitions, which of course cannot be described properly in the harmonic approximation. These torsional transitions in the fluorescence absorption spectrum of 2-TN are very weak. This was attributed before to the weak Franck-Condon factors of the torsional transitions, due to the similar potentials in the  $S_0$  and  $S_1$  states of 2-TN.<sup>2</sup> Table 2 shows the torsional levels of 2-TN and 3-TN in their  $S_0$  and  $S_1$  states that were determined in the present study.

**Table 2** Torsional levels of 2-TN and 3-TN in their electronic ground and lowest excited singlet states, obtained from the LIF and SVLF spectra of this study. Since a and e levels are not linked via allowed transitions, the lowest level (0a<sub>1</sub> and 1e) serve as origins for the torsional ladder within each symmetry.

Level	2-TN		3-TN	
	S <sub>0</sub>	S <sub>1</sub>	S <sub>0</sub>	S <sub>1</sub>
0a <sub>1</sub>	0	0	0	0
1e	0	0	0	0
2e			17	22
3a <sub>1</sub>	130	139	51	58
4e	152	157	80	82
5e	202			
6a <sub>1</sub>			188	183

The bands at 331 cm<sup>-1</sup> (Q<sub>36</sub>), 405 cm<sup>-1</sup> (Q<sub>26</sub>), 494 cm<sup>-1</sup> (Q<sub>25</sub>), and 677 cm<sup>-1</sup> (Q<sub>23</sub>) have been excited in order to obtain the single vibronic level fluorescence (SVLF) spectra, described in section 3.2.2. The assignments of vibronic wavenumber to vibrational modes in the excited state have been performed in an iterative manner. First, based on the result of the *ab initio* calculated vibrational wavenumber, a preliminary assignment was made. This was checked in a second step, through calculation of the Franck-Condon emission spectrum via excitation through this band, which was then compared to the experimental SVLF spectrum. If the agreement was reasonable, the band was included in the list of assignments for the Franck-Condon fit.

Imperfect geometries for one or both states involved in the transition causes errors in the intensities. These can be eliminated by displacing the geometry of one of the electronic states along a selected set of *ab initio* calculated normal modes, in order to better match the geometry changes upon electronic excitation. All emission intensities from the SVLF spectra that were used in the FC fit are compiled in Table S7 of the online supplemental material.<sup>26</sup> In the following paragraphs we describe the fit of the 2-TN SVLF spectra.

### 3.2.2 Single vibronic level fluorescence of 2-TN

We recorded SVLF spectra through the electronic origin 0,0 at 35769 cm<sup>-1</sup> (Figure 3) and through five vibronic bands at 0,0 + 331, 0,0 + 405, 0,0 + 494, 0,0 + 656 and 0,0 + 677 cm<sup>-1</sup>, which are shown in the supplemental figures S1 - S4)<sup>26</sup>. Each experimental spectrum is shown along with a

Franck-Condon simulation using the *ab initio* geometries, and a Franck-Condon fit, with the excited state geometry displaced along selected normal coordinates, given in supplemental Table S10.<sup>26</sup> The assignments of the modes shown in Figure 3 refer to the mode numbering in supplemental Table S5.<sup>26</sup> Below 300 cm<sup>-1</sup> only very weak vibrational activity can be observed. The weak bands that are shown in the zoomed inset of Figure 3 can be assigned to torsional transitions of the methyl group and are included in Table 2. The spectrum is dominated by modes  $Q_{26}$ ,  $Q_{20}$ , and  $Q_{16}$ , which appear as fundamentals, overtones, and in combination with numerous other vibronic bands.

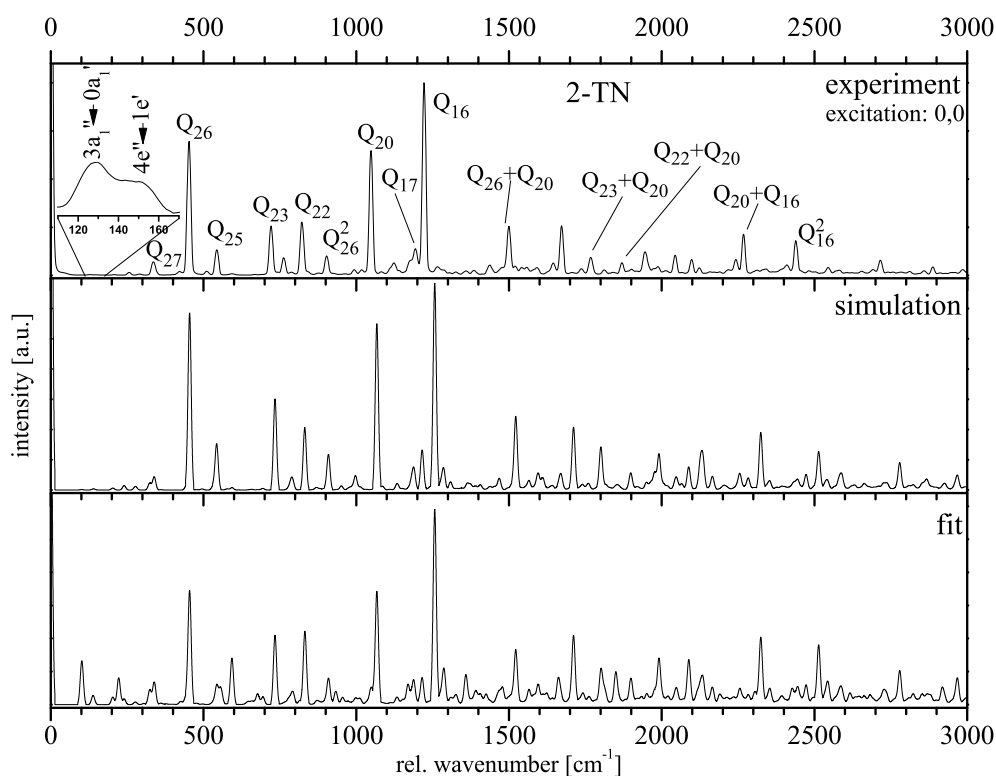


**Figure 3** SVLF spectrum of the electronic origin of 2-TN, along with a simulation of the emission spectrum using the *ab initio* parameters and a FC fit.

### 3.2.3 The fluorescence excitation spectrum of 3-TN

Figure 4 shows the LIF spectrum of 3-TN, along with a Franck-Condon simulation of the absorption spectrum using the *ab initio* parameters. As in the case of 2-TN, the parts of the spectrum with non-harmonic contributions cannot be described by our program, which takes into account only the harmonic Hessians of both states. Therefore the torsional transitions of the methyl group internal rotational are missing. The inset in Figure 4 (shown in the simulation trace with an intensity offset of 0.1) gives a simulation of the torsional bands, using the Hamiltonian described in section 4. Compared

to 2-TN, the torsional bands of 3-TN below  $200\text{ cm}^{-1}$  have a considerably higher intensity due to larger Franck-Condon factors. Most of the torsional transitions have been observed before,<sup>2</sup> with the exception of the  $6a_1' \leftarrow 0a_1''$  transition, cf. Table 2.

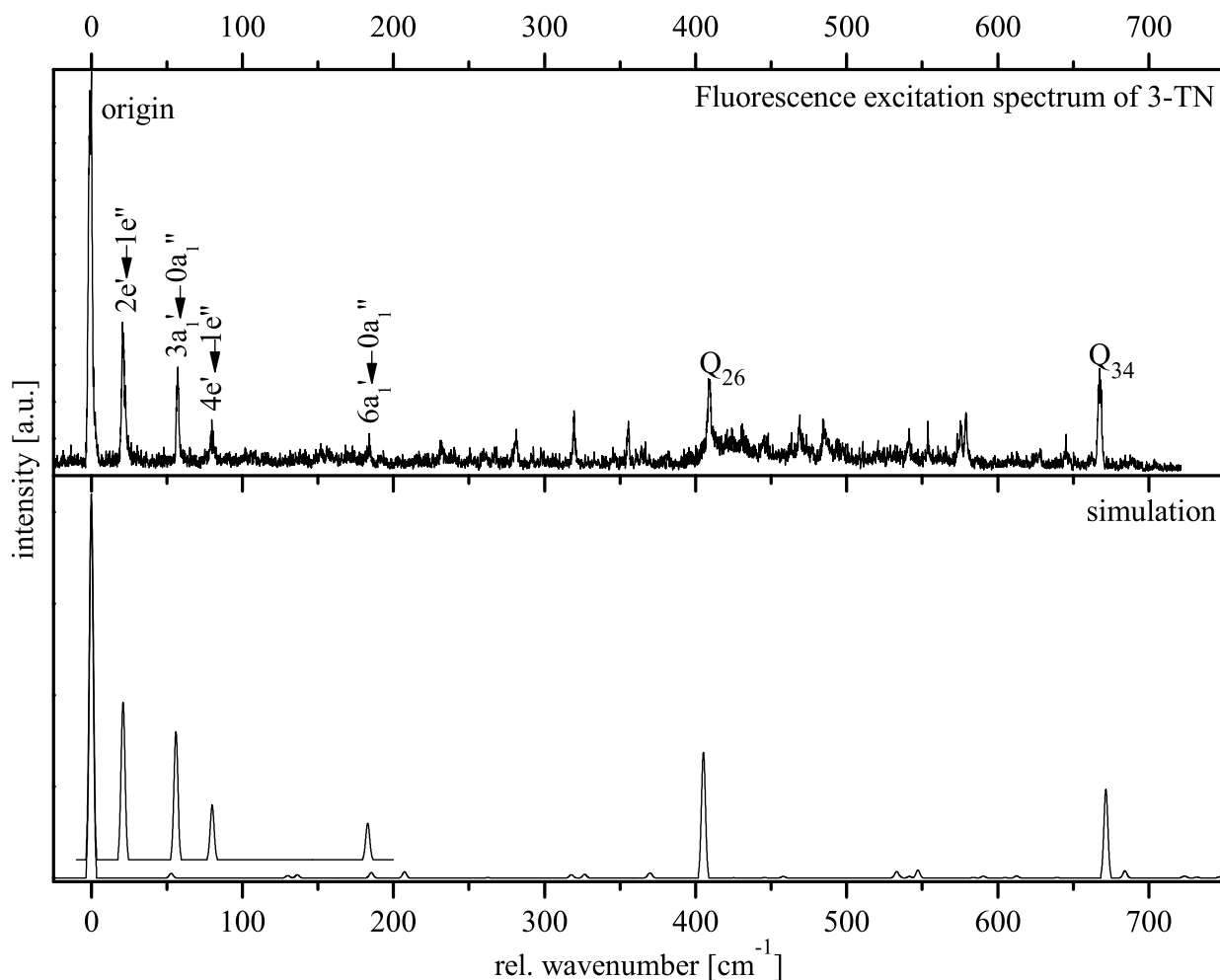


**Figure 4** Fluorescence excitation spectrum of 3-TN along with a Franck-Condon simulation of the absorptions spectrum using the *ab initio* parameters. The spectrum between 0 and  $200\text{ cm}^{-1}$  is additionally fit using the torsional Hamiltonian, described in section 4 and displayed in the lower trace with an intensity offset of 0.1.

The strongest vibronic transitions in the investigated range that are not due to torsional motions are observed at  $409\text{ cm}^{-1}$  and at  $667\text{ cm}^{-1}$ . They are assigned to the vibrational modes  $Q_{26}$  and  $Q_{34}$ , respectively. Their intensities are well reproduced by the Franck-Condon simulation, shown in the lower trace of Figure 4. The vibronic bands at the electronic origin 0,0, at  $0,0 + 79$ ,  $0,0 + 409$  and at  $0,0 + 667\text{ cm}^{-1}$  have been excited in order to obtain SVLF spectra. They will be discussed in section 3.2.4.

### 3.2.4 Single vibronic level fluorescence of 3-TN

The SVLF spectrum obtained via excitation of the vibrationless origin of 3-TN is shown in Figure 5. It is dominated by emission to  $Q_{26}$ ,  $Q_{20}$ , their overtones and their combination bands.

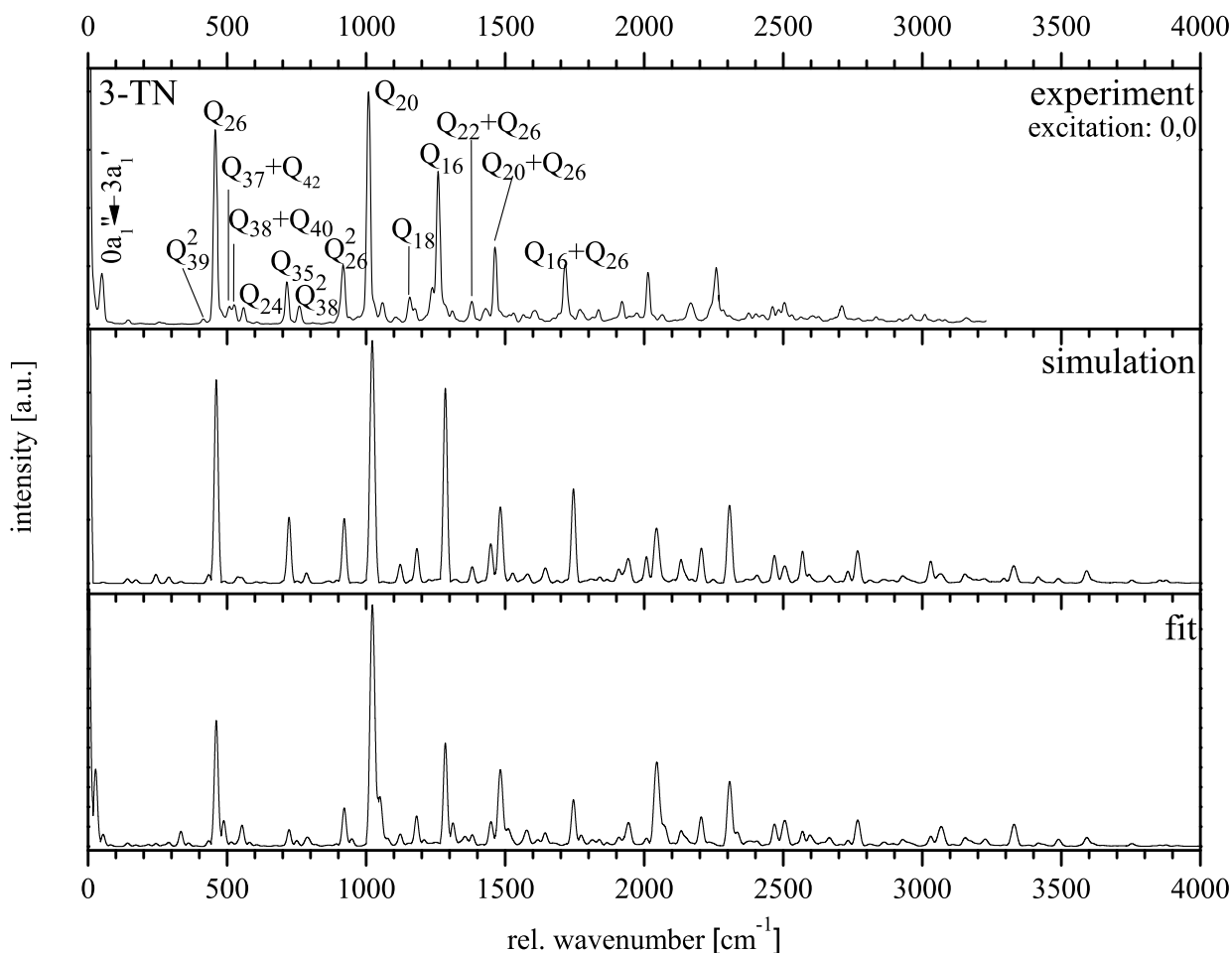


**Figure 5** SVLF spectrum of the electronic origin of 3-TN along with a simulation using the *ab initio* parameters and a FC fit.

Also here, the overall FC fit of the vibronic intensity shows better results than the FC simulation using the *ab initio* geometries for both states. The same holds for the other analyzed bands at 79, 409, and 667  $\text{cm}^{-1}$ , shown in the supplemental Figures S5 - S7.<sup>26</sup> The very good agreement of FC fit and experimental spectrum for the vibration at 79  $\text{cm}^{-1}$  (see supplemental Figure S5<sup>26</sup>) is at first sight surprising, since this band is assigned to the torsional transition  $4e' \leftarrow 1e''$ . Assignment of this band to the third overtone of the mode  $Q_{42}$ , which is the torsion on harmonic approximation leads to a nearly perfect FC fit. Obviously, this band in the  $S_1$  state is sufficiently close to the top of the barrier to be treated in the harmonic approximation. As expected from the assignment of the excited band at

409  $\text{cm}^{-1}$  to mode  $Q_{26}$ , the strongest band in emission is found at 457  $\text{cm}^{-1}$  ( $Q_{26}$ ) in the electronic ground state (supplemental Figure S6<sup>26</sup>). Excitation of  $Q_{34}$  in the excited state at 667  $\text{cm}^{-1}$  results in strongest emission to  $Q_{35}$  in the ground state at 714  $\text{cm}^{-1}$  (Figure S7<sup>26</sup>).

## 4 Discussion

From the combined Franck-Condon/rotational constants fits, the displacements of the excited state geometry with respect to the ground state geometry were determined. These basis for the displacements are selected normal coordinates for each of the conformer from the *ab initio* calculated Hessian. The fit results for the geometry changes of 2-TN and 3-TN upon electronic excitation are depicted in Figure 6. All five (four) SVLF spectra of 2-TN (3-TN) along with the changes of the rotational constants, determined in the second paper of this series have been used for the fit of the geometry changes. In total 82 vibronic intensities (Table S7 of the online supplemental material<sup>26</sup>) and 3 rotational constants changes (supplemental Table S9<sup>26</sup>) were utilized in a fit along twelve normal coordinates for 2-TN and along ten normal coordinates for 3-TN, shown in supplemental Table S10.<sup>26</sup> The reason for the very good agreement between the fitted and the experimental fluorescence emission spectra is indeed the simultaneous use of vibronic band intensities and inertial parameters from the high resolution study. Since the FC analysis is based on the harmonic approximation, distortion in negative and positive direction along a selected normal mode would lead to the same Franck-Condon factor. While this indeterminacy is partially removed by the use of 3N-6 dimensional FC integrals, a much more reliable way to the sign of the distortion is the change of the rotational constants, which are correctly reproduced only with the correct sign of the distortions.

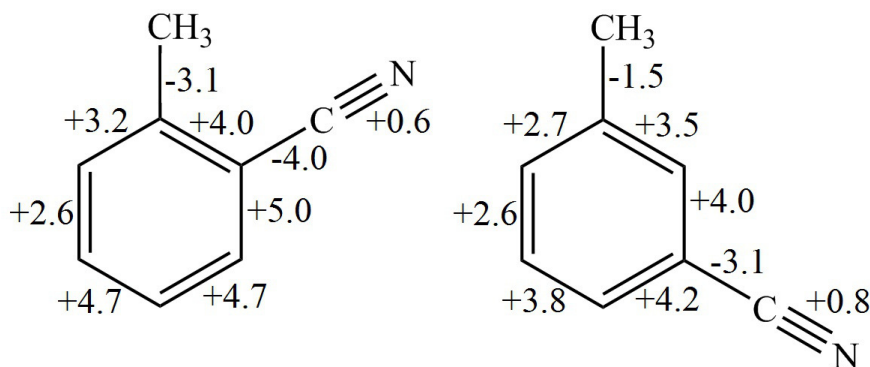


**Figure 6** Geometry changes of 2-TN upon electronic excitation from the FC fit.

In both conformers, the CC bonds between the chromophore and the cyano group, and between the chromophore and the methyl group, decrease upon electronic excitation, while the CN distance of the cyano group increases. The aromatic ring expands upon electronic excitation. In general, these

structural changes can be understood in terms of electron density shifts upon electronic excitation. Excitation from bonding to antibonding orbitals is accompanied by an electron shift from the cyano group to the aromatic ring. The resulting resonance structures are shown in Figure 7. Excitation into antibonding orbitals leads to the observed overall expansion of the aromatic ring, while the bond order of the CN bond decreases, and the CC bond order between the chromophore and the cyano group increases. All these trends are clearly visible in the resonance structures of Figure 7. At the same time, the CC bond length between the chromophore and the methyl group decreases. This effect is considerably larger in 2-TN (-3.1 Å), compared to 3-TN (-1.5 Å). The reason for this different behavior can be rationalized by the resonance structure in the last row of Figure 7. Only substituents in the *ortho* (or *para*) position with respect to the cyano group can stabilize the negative charge at the ring C-atom. This stabilization takes place via three equivalent resonance structures, arising from the three equivalent H-atoms, as shown in Figure 7. Thus, this effect is much larger in 2-TN, compared to 3-TN, since in the *meta*-substituted conformer, only inductive effects can take place. These changes in electronic structure have been quantified by studies of the  $^{14}\text{N}$  quadrupole couplings in benzonitrile and selected molecules.<sup>28</sup>

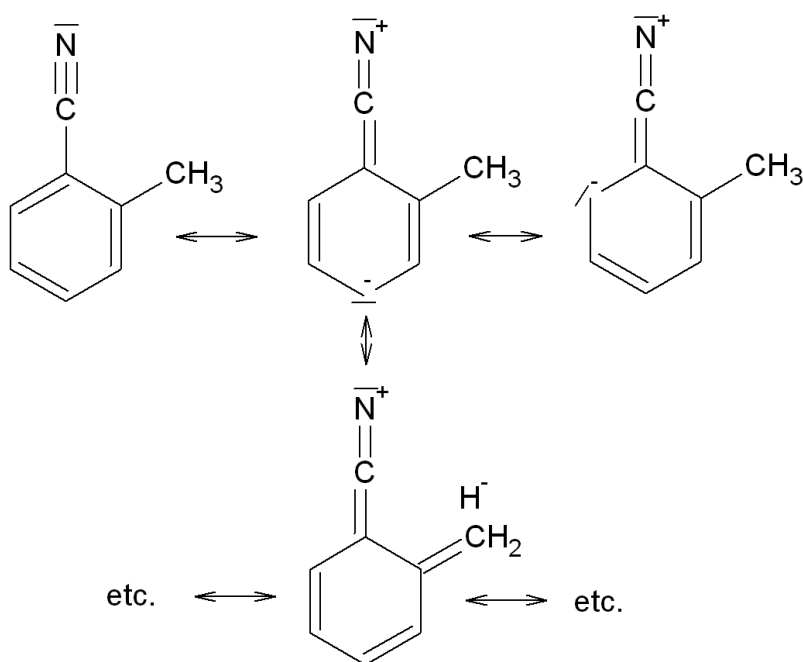


**Figure 7** Resonance structures of 2-TN.

A more subtle view on the geometry changes upon electronic excitation can be made on the basis of a natural population analysis (NPA). The atomic numbering used in the following refers to the numbering of 2-TN in Figure 1. The same arguments hold for structural changes of 3-TN. The main structural effects in the cyano group can be traced back to lone pair (LP) interactions of

the nitrogen atom. The interaction between the nitrogen atom lone pair (in a  $sp^{0.83}$  hybrid) and the unoccupied Rydberg orbital at the neighboring C(15) atom is strongly decreased upon electronic excitation. The resulting bond order reduction of the C(15)N(16) bond leads to the observed bond length increase. LP(N) interaction with the antibonding  $\pi$  bond orbital C(4)C(15)\* also decreases by more than a factor of 2. Thus less electron density is shifted to the antibonding orbital upon electronic excitation, leading to a net increase of bond order and a resulting decrease of the C(4)C(15) bond length. The bond length decrease of the C(3)C(11) bond between the aromatic ring and the methyl group is mainly due to decreased interactions between the bonding  $\pi$  orbital between C(3) and C(11) and the antibonding  $\pi$  orbitals C(3)C(4)\*, C(4)C(5)\*, C(1)C(2)\* and C(1)C(3)\* in the aromatic ring, since their occupancy is increased by  $\pi\pi^*$  excitation.

**Table 3** Experimental and fitted wavenumber of methyl torsional transitions in absorption and emission. The values for the torsional parameters from the fit of 2-TN (3-TN) are:  $F''= 5.57(6) \text{ cm}^{-1}$  ( $5.61(3) \text{ cm}^{-1}$ ),  $V_3''= 180.6(39) \text{ cm}^{-1}$  ( $20.7(12) \text{ cm}^{-1}$ ),  $V_6''= -1.9(164) \text{ cm}^{-1}$  ( $-11.5(41) \text{ cm}^{-1}$ ),  $F'= 5.18(15) \text{ cm}^{-1}$  ( $4.95(6) \text{ cm}^{-1}$ ),  $V_3'= 202.2(53) \text{ cm}^{-1}$  ( $43.3(11) \text{ cm}^{-1}$ ),  $V_6'= -17.6(171) \text{ cm}^{-1}$  ( $-25.6(22) \text{ cm}^{-1}$ )

2-TN			3-TN		
Transition	Exp.	Fit	Transition	Exp.	Fit
$0a'_1 \leftarrow 0a''_1$	0	0	$0a'_1 \leftarrow 0a''_1$	0	0
$1e' \leftarrow 1e''$	-0.098	-0.098	$1e' \leftarrow 1e''$	-1.457	-1.457
$2e' \leftarrow 1e''$	-	97	$2e' \leftarrow 1e''$	22	21.9
$3a'_1 \leftarrow 0a''_1$	139	139	$3a'_1 \leftarrow 0a''_1$	58	58.2
$4e' \leftarrow 1e''$	157	157	$4e' \leftarrow 1e''$	82	80.7
$5e' \leftarrow 1e''$	-	198	$5e' \leftarrow 1e''$	-	122.7
$6a'_1 \leftarrow 0a''_1$	-	264	$6a'_1 \leftarrow 0a''_1$	183	183.5
$1e' \leftarrow 2e''$	-	-88	$1e' \leftarrow 2e''$	-17	-19.7
$0a'_1 \leftarrow 3a''_1$	-130	-130	$0a'_1 \leftarrow 3a''_1$	-51	-51.2
$1e' \leftarrow 4e''$	-152	-152	$1e' \leftarrow 4e''$	-80	-80.9
$1e' \leftarrow 5e''$	-202	-202	$1e' \leftarrow 5e''$	-	-122.9
$0a'_1 \leftarrow 6a''_1$	-	-254	$0a'_1 \leftarrow 6a''_1$	-188	-186.9

Not only do the geometries of the conformers change in a manner that reflects effects of the electronic excitation, but the barriers to methyl torsion change as well. In a one-dimensional model the torsional motion of the rotating methyl group can be described by the Hamiltonian

$$H_T = Fp^2 + \frac{1}{2} \sum_n V_n (1 - \cos n\alpha) \quad (6)$$

with the angular momentum of the internal rotor defined by

$$p = -i\hbar \frac{d}{d\alpha} \quad (7)$$

and the torsional angle  $\alpha$ . The kinetic energy term  $Fp^2$  is that of a free rotor model with the tor-

sional constant  $F$ , while the second term introduces a barrier consisting of different  $n$ -fold periodic potentials. The torsional constant  $F$  is defined as

$$F = \frac{h}{8\pi^2 I_\alpha} \quad (8)$$

where  $I_\alpha$  is the moment of inertia of the methyl top with respect to the torsional axis.

To compare theory with experiment, the Hamiltonian in Equation 6 was set up in free rotor basis function and diagonalized, yielding the eigenvalues and eigenfunctions of the torsional problem. The values for the torsional constants and torsional barriers in ground and excited states of both conformers and the wavenumbers of the torsional transitions are compiled in Table 3, and compared with the experiment. The fit is excellent. Note that the quite large reduction of the value of the torsional constant  $F$  upon electronic excitation in 2-TN is nicely explained by the resonance structures in Figure 7. The C-H distances in the methyl group increase, leading to an increased moment of inertia ( $I_\alpha$ ) of the top, or decreased torsional constant  $F$ .

Also for the torsional barriers, the combination of results from high resolution rotationally resolved electronic spectroscopy and vibronic spectroscopy improves the accuracy of the results considerably. A one-dimensional fit of the torsional barriers for 2-TN and 3-TN to torsional transitions in both states from the low resolution experiment yielded approximate values for the torsional constants  $F$ , and the  $V_3$  and  $V_6$  barrier terms in each electronic state. These were subsequently refined by a combined fit of the first and second order perturbation coefficients and the AE splitting from the high resolution study. In an iterative manner these results were used for a better prediction of torsional transitions in absorption and emission, which could be located this way. In the end a global fit was performed using all pieces of experimental evidence: the first and second order perturbation coefficients, the AE splitting, the torsional transitions in emission and in absorption to obtain the barriers and torsional constants with a high accuracy.

## Acknowledgments

Computational support and infrastructure was provided by the "Centre for Information and Media Technology" (ZIM) at the Heinrich-Heine-University Düsseldorf (Germany). The financial support of the Deutsche Forschungsgemeinschaft (SCHM 1043/12-1) is gratefully acknowledged.

## References

- [1] *First paper of the series [Please insert citation when known]*.
- [2] M. Fujii, M. Yamauchi, K. Takazawa and M. Ito, *Spectrochim. Acta*, 1994, **50A**, 1421–1433.

- [3] A. I. Jaman, S. Maiti and R. N. Nandi, *J. Mol. Spec.*, 2011, **192**, 148–151.
- [4] A. I. Jaman, P. H. Kumar and P. R. Bangal, *J. Atom. Mol. Opt. Phys.*, 2011, **2011**, 480396–1–480396–8.
- [5] H. Nakai and M. Kawai, *J. Chem. Phys.*, 2000, **113**, 2168–2174.
- [6] C. H. Park, G. W. Lee and S. K. Lee, *Bull. Korean Chem. Soc.*, 2006, **27**, 881–885.
- [7] C. H. Park and S. K. Lee, *Bull. Korean Chem. Soc.*, 2007, **27**, 1377–1380.
- [8] K. Suzuki, S. Ishiuchi, M. Sakai and M. Fujii, *J. Electr. Spect. Rel. Phen.*, 2005, **142**, 215–221.
- [9] A. Nagao, A. Kan-no and M. Takayanagi, *J. Mol. Struct.*, 2009, **929**, 43–47.
- [10] P. Nagabalasubramanian, S. Periandy and S. Mohan, *Spectrochim. Acta*, 2009, **A74**, 1280–1287.
- [11] M. Schmitt, U. Henrichs, H. Müller and K. Kleinermanns, *J. Chem. Phys.*, 1995, **103**, 9918–9928.
- [12] W. Roth, C. Jacoby, A. Westphal and M. Schmitt, *J. Phys. Chem. A*, 1998, **102**, 3048–3059.
- [13] R. Ahlrichs, M. Bär, M. Häser, H. Horn and C. Kölmel, *Chem. Phys. Letters*, 1989, **162**, 165–169.
- [14] J. T. H. Dunning, *J. Chem. Phys.*, 1989, **90**, 1007–1023.
- [15] C. Hättig and F. Weigend, *J. Chem. Phys.*, 2000, **113**, 5154–5161.
- [16] C. Hättig and A. Köhn, *J. Chem. Phys.*, 2002, **117**, 6939–6951.
- [17] C. Hättig, *J. Chem. Phys.*, 2002, **118**, 7751–7761.
- [18] P. Deglmann, F. Furche and R. Ahlrichs, *Chem. Phys. Letters*, 2002, **362**, 511–518.
- [19] *TURBOMOLE V6.3 2012, a development of University of Karlsruhe and Forschungszentrum Karlsruhe GmbH, 1989-2007, TURBOMOLE GmbH, since 2007; available from <http://www.turbomole.com>.*
- [20] A. E. Reed, R. B. Weinstock and F. Weinhold, *J. Chem. Phys.*, 1985, **83**, 735–746.
- [21] D. Spangenberg, P. Imhof and K. Kleinermanns, *Phys. Chem. Chem. Phys.*, 2003, **5**, 2505–2514.
- [22] R. Brause, M. Schmitt, D. Spangenberg and K. Kleinermanns, *Mol. Phys.*, 2004, **102**, 1615–1623.

- [23] E. V. Doktorov, I. A. Malkin and V. I. Man'ko, *J. Mol. Spec.*, 1975, **56**, 1–20.
- [24] E. V. Doktorov, I. A. Malkin and V. I. Man'ko, *J. Mol. Spec.*, 1977, **64**, 302–326.
- [25] F. Duschinsky, *Acta Physicochimica U.R.S.S.*, 1937, **7**, 551–577.
- [26] *See supplemental material at [URL will be inserted by AIP] for optimized geometries, additional spectra, and tables with experimental emission frequencies and intensities.*
- [27] G. Herzberg, *Molecular Spectra and Molecular Structure, II. Infrared and Raman Spectra of Polyatomic Molecules*, van Nostrand Reinhold Company, New York, 1945.
- [28] R. G. Bird, J. L. Neill, V. J. Alstadt, J. W. Young, B. H. Pate and D. W. Pratt\*, *J. Phys. Chem. A*, 2011, **115**, 9392–9398.

## 4.2 Franck Condon Spectra of the 2-Tolunitrile Dimer and the Binary 2-TolunitrileWater Cluster in the Gas Phase

The measurements this publication is based on were performed by Elvedina Pehlivanovic under supervision of Benjamin Stuhlmann and Felix Gmerek, the *ab-initio*-calculations and the simulations and Franck-Condon-Fits for the dimer were made by Felix Gmerek and for the 2-TN-Water-cluster the simulations and FC-fits were done by Elvedina Pehlivanovic.

The following section has been accepted for publication in Journal of Molecular Structure (Gmerek et al., J Mol. Struct., 1143, 2017).

# Franck Condon Spectra of the 2-Tolunitrile Dimer and the Binary 2-Tolunitrile Water Cluster in the Gas Phase

Felix Gmerek, Benjamin Stuhlmann, Elvedina Pehlivanovic, and Michael Schmitt\*

Heinrich-Heine-Universität, Institut für Physikalische Chemie I,  
D-40225 Düsseldorf, Germany

## Abstract

We present fluorescence emission spectra of the 2-tolunitrile dimer and the 2-tolunitrile water cluster through various vibronic bands in the electronically excited state. From the transition dipole moments in the individual monomers, the 2-TN dimer has shown to form J-aggregates, which is why the one-photon allowed transition is the  $S_1$  state in this cluster in contrast to other symmetric dimers, which tend to form H-aggregates. The changes of the molecular structures upon electronic excitation have been determined from a fit of the intensities in various fluorescence emission spectra. The excited state structure of the 2-TN dimer has been found to be asymmetric, in contrast to the ground state structure. Thus, emission takes place from one of the locally excited monomer moieties in the 2-tolunitrile dimer.

*Keywords:* Franck-Condon analysis, 2-tolunitrile dimer, water cluster, structure, excitonic splitting

## 1 Introduction

The 2-tolunitrile (2-TN) dimer belongs to the same class of centrosymmetric homodimers, as the benzonitrile dimer<sup>1-4</sup>, the benzoic acid dimer,<sup>5-7</sup> the 2-cyanophenol dimer,<sup>8</sup> the 3-cyanophenol dimer,<sup>9</sup> the azaindole dimer,<sup>10</sup> and the pyridone dimer.<sup>11,12</sup> The question arises, if the electronic excitation in these homodimers is localized in one of the two equivalent chromophores or if it is delocalized over both chromophores. In a recent comprehensive study, Ottiger *et al.*<sup>13</sup> investigated the exciton (Davydov) splitting in these dimers both experimentally, as well as theoretically using a quenching model that reduces the calculated electronic exciton splitting

by a factor which they showed to be the product of excited-state vibrational displacements in the monomer. Clearly, their results point to a delocalized excitation with weak to intermediate coupling. Kopec *et al.*<sup>14</sup> recently showed that the quenched excitonic splitting can be interpreted as nonadiabatic tunneling splitting related to a lower adiabatic double-minimum potential energy surface (PES), but nonadiabatically coupled to the higher PES. One of the delocalized and symmetry-adapted adiabatically split levels in the double-minimum PES has the symmetry of the  $S_1$  state, the other of the  $S_2$ -state. It has to be noted, that the aforementioned dimers form H-aggregates<sup>15</sup> with nearly parallel (or antiparallel) transition dipole moment orientations. However, recently a symmetric homodimer, which forms J-aggregates<sup>16</sup> in a molecular beam, the m-cyanophenol dimer, has been investigated.<sup>17</sup>

\*corresponding author.

Fax: 49 211 8115195; Tel: 49 0211 81 12100; E-mail: mschmitt@uni-duesseldorf.de

Also covalently bound bichromophoric systems show excitonic splitting, with the possibility that depending on the symmetry of the system, both  $S_1$  and  $S_2$  components are bright states. Zwier, Plusquellic, and co-workers have shown, that for the bichromophore diphenylmethane both the  $S_1$  and  $S_2$  states can be observed and that the  $S_1$  origin can be viewed as a completely delocalized, antisymmetric combination of the zero-order locally excited states of the toluene-like chromophores.<sup>18</sup>

Exciton splitting in symmetric dimers has been discussed starting in the late 50's and early 60's.<sup>19–22</sup> While the concept of excitons was originally introduced by Frenkel in order to describe the excitation of atoms in a lattice of an insulator,<sup>23</sup> interest had rapidly been shifted to molecular excitons. Apart from the electronic exciton splitting, electronic excitation in symmetric dimers has an additional aspect, namely stabilization of the excited state through solvation. Consider electronic excitation of a monomer, which is solvated after excitation by a second (identical) monomer. If the stabilization of the monomer excited state by solvation is large enough the excitation will remain at the initially excited center.

$S_1 \leftarrow S_0$  fluorescence excitation spectra and  $S_0 \leftarrow S_1$  fluorescence emission spectra of 2-, 3, and 4-tolunitrile were reported by Fujii *et al.*<sup>24</sup> They determined the torsional barriers of ground and lowest excited singlet states from the low frequency torsional bands in the  $S_0$  and the  $S_1$  states, respectively. The ground state internal rotational parameters of 2-TN have been determined from microwave spectroscopy in the frequency ranges of 22.0–26.0 GHz and 32.0–37.0 GHz<sup>25</sup> and from millimeter wave spectroscopy in the frequency range 50.0 - 75.0 GHz.<sup>26</sup> Nakai and Kawai studied the torsional potential of various substituted toluenes, among them 2- and 3-tolunitrile (3-TN).<sup>27</sup> They showed how a  $\pi^*\sigma^*$  hyperconjugation mechanism can be used to explain their different barriers in different electronic states. Later Park *et al.* measured the vibronic emission spectra of the jet-cooled 2-tolunitrile<sup>28</sup> and 3-tolunitrile<sup>29</sup> in a corona-excited supersonic expansion. From a density functional theory

(DFT) based analysis of the spectrum, several vibrational modes were assigned in the emission spectrum. The cationic ground state  $D_0$  has been studied using pulsed field ionization–ZEKE photoelectron spectroscopy by Suzuki *et al.*<sup>30</sup>

Recently, Gmerek *et al.*<sup>31</sup> and Ruiz-Santoyo *et al.*<sup>32</sup> performed a combination of rotationally resolved electronic spectroscopy and Franck-Condon fits of the fluorescence emission spectra of 2- and 3-TN monomers and determined the change of the geometry upon electronic excitation via a Franck-Condon fit.

The 1:1 water cluster of 2-TN resembles closely the binary benzonitrile-water cluster, which has been studied by Helm *et al.*<sup>33</sup> using a combination of high resolution ultraviolet (UV) and microwave (MW) spectroscopy and Melandri *et al.*<sup>34</sup> using microwave spectroscopy. It forms a double hydrogen bond between one H-atom of the water moiety and the cyano group and the *ortho* hydrogen atom at the aromatic ring and the water O-atom.

In the present paper we will elucidate the change of the molecular structure of both complexes upon electronic excitation from a fit of the FC spectra and shed light on the question, if the excitation in the symmetric homodimer is localized or delocalized.

## 2 Experimental and Computational Details

### 2.1 Experiment

The experimental setup for the dispersed fluorescence (DF) spectroscopy has been described in detail elsewhere<sup>35,36</sup>. In short, 2-tolunitrile was evaporated at 293 K and co-expanded through a pulsed nozzle (kept at 303 K to avoid condensation) with a 500  $\mu\text{m}$  orifice (General Valve) into the vacuum chamber using helium as carrier gas. The output of a Nd:YAG (SpectraPhysics INDI) pumped dye laser (Lambda-Physik, FL3002) was frequency doubled and crossed at right angles with the molecular beam. The resulting fluorescence was imaged on the entrance slit of a

monochromator (Jobin Yvon,  $f = 1$  m). The dispersed fluorescence spectrum was recorded using a gated image intensified UV sensitive CCD camera (Flamestar II, LaVision). The relative intensities were afterwards normalized to the strongest band in the spectrum, not including the resonance fluorescence band, which also contains the stray light and is therefore excluded from the FC analysis.

## 2.2 *Ab initio* calculations

Structure optimizations were performed employing Dunning’s correlation consistent polarized valence triple zeta basis set (cc-pVTZ) from the TURBOMOLE library.<sup>37,38</sup> The equilibrium geometries of the electronic ground and the lowest excited singlet states were optimized using the approximate coupled cluster singles and doubles model (CC2) employing the resolution-of-the-identity approximation (RI).<sup>39–41</sup> The Hessians and harmonic vibrational frequencies for both electronic states, which are utilized in the FC fit and needed for calculation of the zero-point energy (ZPE), have been obtained from numerical second derivatives using the NumForce script<sup>42</sup> implemented in the TURBOMOLE program suite.<sup>43</sup> For the cluster stabilization energies, the basis set superposition errors (BSSE) have been accounted for, using the counterpoise corrections described by Boys and Bernardi<sup>44</sup> and implemented in the JOBSSE jobscript of turbomole. A natural population analysis (NBO)<sup>45</sup> has been performed at the CC2 optimized geometries using the wavefunctions from the CC2 calculations as implemented in the TURBOMOLE package.<sup>43</sup>

## 2.3 Franck-Condon fits

The change of a molecular geometry upon electronic excitation can be determined from a fit of the intensities of absorption or emission bands using the FC principle. According to this principle, the relative intensities of the vibronic bands depend on the overlap integrals of the vibrational wave functions of both electronic states.

The fit has been performed using the program FCFIT, which has been developed in our group and described in detail before.<sup>46,47</sup> The program computes the FC integrals of multidimensional, harmonic oscillators mainly based on the recursion formula given in the papers of Doktorov, Malkin, and Man’ko.<sup>48,49</sup> and fits the geometry (in linear combinations of selected normal modes) to the experimentally determined intensities. This is simultaneously done for all emission spectra, which are obtained *via* pumping through different  $S_1$  vibronic modes.

The FC factors of the 2-TN monomer<sup>31</sup> are used for calculation of the quenching factor  $\Gamma$  for the excitonic splitting of the dimer. This quenching factor is given by:<sup>13</sup>

$$\Gamma = \exp \left( \sum_i \frac{FCF(i_0^1)}{FCF(0_0^0)} \right) \quad (1)$$

where the sum runs over the  $i$  modes of the monomers. The summands are also referred to as Huang-Rhys factors. The vibronic splitting  $\Delta_{vibron}$  is calculated from the pure electronic splitting  $2V_{AB}$  using the relation:<sup>13</sup>

$$\Delta_{vibron} = 2V_{AB}\Gamma \quad (2)$$

# 3 Results

## 3.1 *Ab initio* calculations

### 3.1.1 Structure, Stabilization and Vibrations

The structures of the 2-TN dimer (Figure 1a) and the 2-TN-H<sub>2</sub>O water cluster (Figure 1b) have been optimized at the CC2/cc-pVTZ level of theory in the electronic ground state and the lowest two excited singlet states, cf. Table 1. The Cartesian coordinates of both clusters in their  $S_0$  and  $S_1$  states are given in the online supporting material. (2-TN)<sub>2</sub> is found to be a planar molecule in the electronic ground state of  $C_{2h}$  symmetry.

Its 90 vibrations transform like  $\Gamma_{ired} = 30a_g + 15b_g + 16a_u + 29b_u$ . Upon electronic excitation the ring geometries change differently, and the molecular symmetry of the dimer reduces to

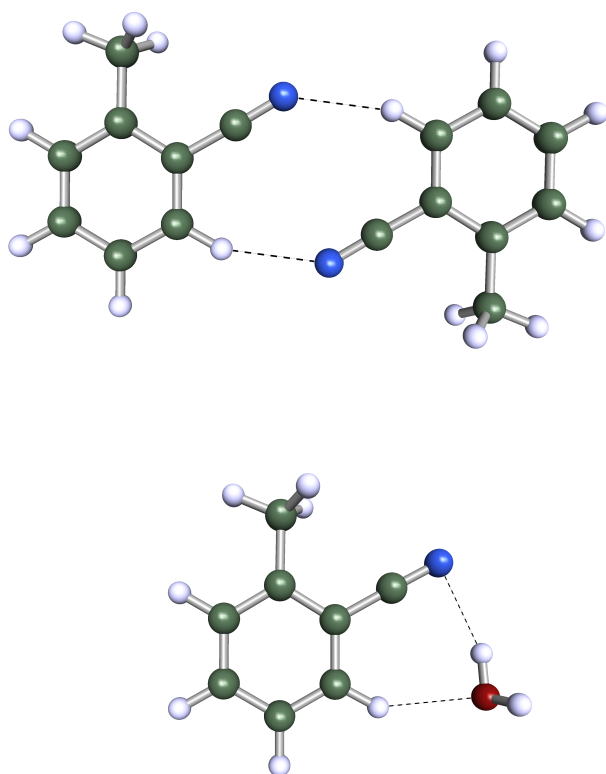


**Figure 1** Structures of  $(2\text{-TN})_2$  and  $2\text{-TN-H}_2\text{O}$  from the optimized CC2/cc-pVTZ geometries.

**Table 1** Rotational constants  $A$ ,  $B$ , and  $C$  are given in MHz, components of the dipole moments  $\mu_a$ ,  $\mu_b$ , and  $\mu_c$  in Debye, the angle of the transition dipole moment with the a-axis  $\theta$  in degrees, the angle of the transition dipole moment with the c-axis  $\phi$  in degrees and the adiabatic excitation energies ( $\nu_0^{\text{adiab.}}$ ) in  $\text{cm}^{-1}$ . The last four rows give the leading contributions to the transition.

	$(2\text{-TN})_2$			$2\text{-TN-H}_2\text{O}$	
	$S_0$	$S_1$	$S_2$	$S_0$	$S_1$
$A$	1002	988	977	1846	1827
$B$	163	164	161	973	959
$C$	141	141	139	641	633
$\mu_a$	0.0	0.70	0.0	3.35	4.05
$\mu_b$	0.0	0.02	0.0	0.66	0.66
$\mu_c$	0.0	0.00	0.0	1.18	1.15
$ \mu $	0.0	0.72	0.0	3.61	4.26
$\theta$	-	-7.0	-	-11.2	-9.2
$\phi$	-	90.0	-	70.9	74.3
$\nu_0^{\text{adiab.}}$	-	37377	38152	-	37.436
$\text{H} \rightarrow \text{L}$	-	-0.75	-	-	0.76
$\text{H-2} \rightarrow \text{L+2}$	-	0.42	-	-	-
$\text{H-1} \rightarrow \text{L+1}$	-	-	-	-	0.43
$\text{H-2} \rightarrow \text{L+1}$	-	-	0.32	-	-
$\text{H-2} \rightarrow \text{L}$	-	0.34	-	-	-
$\text{H-1} \rightarrow \text{L}$	-	-	-0.50	-	-0.35
$\text{H} \rightarrow \text{L+2}$	-	0.27	-	-	-
$\text{H} \rightarrow \text{L+1}$	-	-	-0.47	-	0.27

$C_s$ . The 90 vibrations in  $C_s$  transform like  $59a' + 31a''$ , with the correlation of  $a_g$  and  $b_u$  modes in  $C_{2h}$  to  $a'$  in the  $C_s$  point group. A table with the calculated vibrational ground state frequencies, their symmetries, correlations with the excited state vibrations and largest elements of the Duschinsky matrix is found in the online supporting material (Table S6). The stabilization energy of the dimer in the electronic ground state, including ZPE and BSSE corrections amounts to 24.1 kJ/mol, and to 26.3 kJ/mol in the lowest electronically excited state. The energetically following state has a lower stabilization energy of 20.3 kJ/mol

Figure 1b and Tables S4 and S5 of the online supporting material present the structure of  $2\text{-TN-H}_2\text{O}$ . The cluster belongs to the point group  $C_1$  in both electronic states. As in the benzonitrile-water cluster, the N-atom of the nitrile group acts as proton acceptor towards the water molecule, and the *ortho*-hydrogen atom of the aromatic ring as proton donor, leading to a cyclic structure with

**Table 2** CC2/cc-pVTZ calculated stabilization energies in kJ/mol of the 2-TN dimer and the 2-TN-H<sub>2</sub>O cluster, respectively. Stabilization energies contain zero-point energy and correction of the counter-poise computed BSSE, with the exception of the S<sub>2</sub> state.

	(2-TN) <sub>2</sub>	2-TN-H <sub>2</sub> O
S <sub>0</sub>	24.1	11.5
S <sub>1</sub>	26.3	13.5
S <sub>2</sub>	20.3	-

one hydrogen atom of the water moiety pointing out of the plane. The stabilization energy of the water cluster in the electronic ground state, including ZPE and BSSE corrections amounts to 11.5 kJ/mol, and to 13.5 kJ/mol in the electronically excited state.

### 3.1.2 Excitonic splitting of the 2-TN dimer

In case of a delocalized excitation the electronic origin consists of a one-photon allowed component ( ${}^1B_u \leftarrow {}^1A_g$ ) and one higher (one-photon forbidden) component ( ${}^1A_g \leftarrow {}^1A_g$ ). The lower  $B_u$  and the upper  $A_g$  components emerge from two locally excited harmonic oscillators with one monomer electronically excited and the other in the ground state and *vice versa*, see Figure 2.

We calculated the vertically lowest three excited states in each symmetry of the ground state at CC2 (SCS-CC2) level of theory and found the lowest electronically excited state retaining  $B_u$  symmetry ( $C_{2h}$ ) at 40111 (39258) cm<sup>-1</sup> and the energetically following of  $A_g$  symmetry at 40123 (39264) cm<sup>-1</sup>. Thus, the vertical excitonic splitting for the lowest electronically excited state amounts to 12 (6) cm<sup>-1</sup>. The findings for the other excited states are compiled in Table 3 along vertical excitation energies, and the Cartesian components of the oscillator strengths. The exciton splitting between  $A_g$  and  $B_u$  states increases for the higher electronic states (105 (118) cm<sup>-1</sup> for the splitting between S<sub>3</sub> and S<sub>4</sub> and 521 (216) cm<sup>-1</sup> for the splitting between S<sub>5</sub> and S<sub>6</sub>).

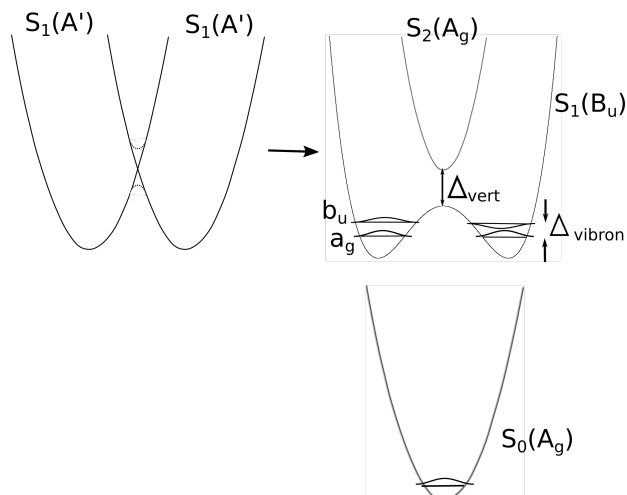


**Figure 2** Schematic drawing of the adiabatic potential energy curves of the lowest three singlet states. The left diagram shows the diabatic (S<sub>1</sub>) states of local excitation of one of the individual monomers. On the right side, the adiabatic (delocalized) S<sub>1</sub> and S<sub>2</sub> states, emerging from the avoided crossing between the diabatic states.

All higher-lying electronically excited states of  $B_g$  symmetry are one-photon forbidden, and those of  $A_u$  symmetry are very weak and z-polarized (out-of-plane).

As described before the pure electronic Davydov splitting  $\Delta_{el} = 2V_{AB}$  is an upper limit to the vibronic splitting  $\Delta_{vibron}$ . The quenching factor  $\Gamma$  (see equation 1), which accounts for the vibronic contribution, has been calculated from the FC factors, that had been determined from the FC analysis of the 2-TN monomer, given in Ref.<sup>31</sup> to be

**Table 3** Electronically excited states of  $C_{2h}$  symmetric (2-TN)<sub>2</sub>. The vertical excitation energy  $\nu_{vert.}$  is given in cm<sup>-1</sup>.

State	Sym.	CC2	SCS-CC2	$f_x$	$f_y$	$f_z$
1	$B_u$	40111	39258	0.2	0.1	0.0
2	$A_g$	40123	39264	0.0	0.0	0.0
3	$A_g$	47943	48052	0.0	0.0	0.0
4	$B_u$	48048	48170	3.3	0.4	0.0
5	$A_g$	55153	56319	0.0	0.0	0.0
6	$B_u$	55674	56535	2.7	3.0	0.0

0.51. Thus, the pure SCS-CC2/cc-pVTZ calculated electronic splitting is reduced to  $3 \text{ cm}^{-1}$ .

Another approach to the size of the excitonic splitting uses Frenkel exciton theory of two dipoles  $\vec{\mu}_1$  and  $\vec{\mu}_2$  at a distance  $R$ .<sup>11,20</sup> The interaction of the two dipoles is given by the dipole-dipole interaction energy  $V_{dd}$ :

$$V_{dd} = \frac{\vec{\mu}_1 \cdot \vec{\mu}_2}{4\pi\epsilon_0 R^3} \cdot (2(\cos\theta)^2 - (\sin\theta)^2 \cos(\phi)) \quad (3)$$

The center of mass (COM) distance  $R$  of the two monomer moieties can be calculated from the inertial parameters of the dimer ( $I_g^{Dimer}$ ) and the monomer ( $I_g^{Monomer}$ ) moieties:

$$R = \sqrt{\frac{\sum_g I_g^{Dimer} - 2\sum_g I_g^{Monomer}}{M}} \quad (4)$$

where  $M$  is the mass of one monomer moiety, and the  $I_g$  are the respective moments of inertia, described by their superscripts, which are calculated from the SCS-CC2/cc-pVTZ calculated rotational constants. For reason of symmetry, the two dipole moments are equal as well as the angle  $\theta$  between the dipole moments and the line connecting the two COM. The angle  $\phi$  describes the dihedral angle between the planes containing the dipole moment vectors. Using the *ab initio* SCS-CC2/cc-pVTZ calculated values of  $1.654 \cdot 10^{-30} \text{ Cm}$  for the transitions dipole  $\vec{\mu}$ ,  $6.627 \cdot 10^{-10} \text{ m}$  for the COM distance  $R$ ,  $90^\circ$  for  $\theta$  and  $0^\circ$  for  $\phi$  one obtains a values of  $\pm 4 \text{ cm}^{-1}$  for  $V_{dd}$  and an excitonic splitting of  $8 \text{ cm}^{-1}$ . For a more detailed discussion of the role of the angle  $\theta$  for the energetic ordering see section 4.

A third approach to the vibronic splitting utilizes the Wentzel-Kramers-Brillouin (WKB) approximation.<sup>50</sup> The vibronic splitting, arising from the semiclassical tunneling through a barrier can be described by:<sup>51</sup>

$$\Delta_{vibron} = \frac{\hbar\omega_f}{\pi} e^{-\theta} \quad (5)$$

where  $\omega_f$  is the classical vibrational frequency in one of the wells that describes the reaction path over the barrier and  $\theta$  is the barrier

penetration integral, which is calculated according to:

$$\theta = \frac{2\pi}{\hbar\omega_i} (V_{eff} - \sqrt{E_0 V_{eff}}) \quad (6)$$

Here,  $\omega_i$  is the imaginary frequency, which describes the motion that leads over the top of the barrier,  $V_{eff}$  is the effective barrier height and  $E_0$  the zero-point energy of the vibration  $\omega_f$ . The effective barrier height is obtained from the vibrational frequencies in the potential well  $\omega_k$  and at the top of the barrier  $\omega_k^*$ :

$$V_{eff} = V_0 + \sum_{k=1}^{F-1} \frac{1}{2} (\hbar\omega_k^* - \hbar\omega_k) \quad (7)$$

For small electronic Davydov splittings  $\Delta_{vert}$ , the barrier height  $V_0$  can be approximated by the difference of the adiabatic excitation energies of  $S_1$  and  $S_2$  state, respectively (cf. Figure 2). The imaginary barrier penetrating vibration  $\omega_i$  and the vibration in the well, which describes the reaction coordinate are excluded from the summation in equation (7). The sum in equation (7) gives the adiabatic contribution of the remaining  $F - 1$  vibrational degrees of freedom to the one-dimensional tunneling motion.

Using the results of normal mode calculations of the  $S_1$  at the minimum structure and at the transition state one obtains for the sum in equation (7) a value of  $956 \text{ cm}^{-1}$ . The value of  $V_0$  is given by the difference of the adiabatic excitation energies of  $S_1$  and  $S_2$  state and amounts to  $775 \text{ cm}^{-1}$ . With a reaction coordinate wavenumber of  $1067 \text{ cm}^{-1}$  and an imaginary vibration of  $1022 \text{ cm}^{-1}$  one obtains a splitting  $\Delta_{vibron}$  of  $3.0 \text{ cm}^{-1}$  in very good agreement with the values obtained from Frenkel theory and from the reduced Davydov splitting.

### 3.1.3 Adiabatic Excitation of the 2-TN dimer

The zero-point energy corrected adiabatic excitation energy for the  $S_1 \leftarrow S_0$  transition to the lowest excited state has been computed at the SCS-CC2/cc-pVTZ level of theory and amounts to  $37377 \text{ cm}^{-1}$ . Adiabatic excitation leads to an excited state, with a reduced symmetry of  $C_s$ . The locally electronically excited state, therefore has

a permanent dipole moment of  $2.4 \cdot 10^{-30}$  Cm (0.72 Debye) compared to the electronic ground state, which for its inversion symmetry has a zero dipole moment. Rotational constants and permanent dipole moment components of this (locally excited) state are compiled in Table 1.

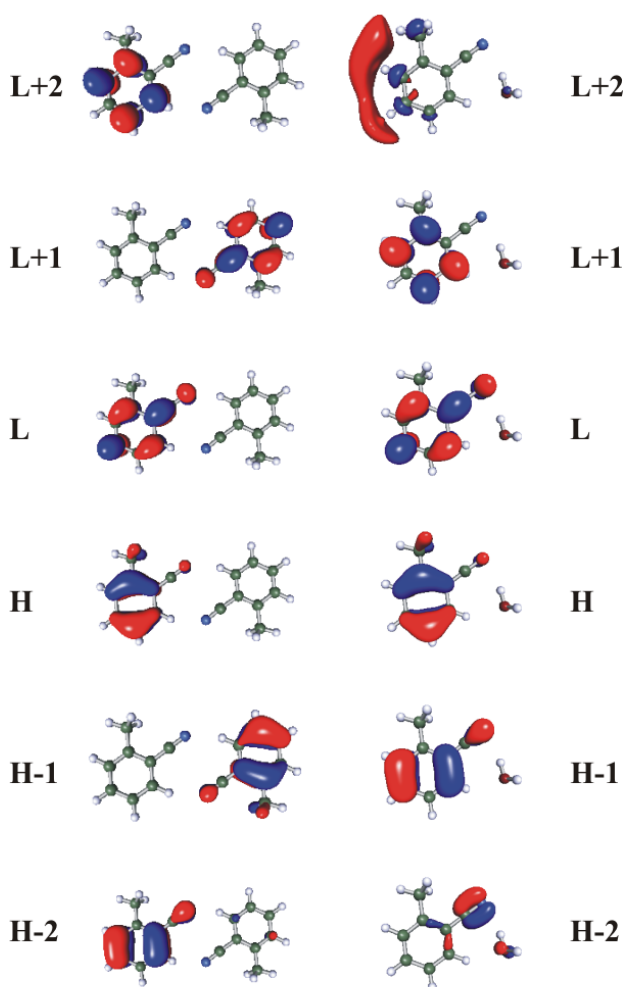


**Figure 3** Frontier orbitals of  $(2\text{-TN})_2$  and  $2\text{-TN-H}_2\text{O}$  from the optimized CC2/cc-pVTZ geometries.

The excitation to the lowest excited singlet state in  $C_s$  symmetry is composed of  $-0.75$  (HOMO  $\rightarrow$  LUMO) +  $0.27$  (HOMO  $\rightarrow$  LUMO+2) +  $0.34$  (HOMO-2  $\rightarrow$  LUMO) +  $0.42$  (HOMO-2  $\rightarrow$  LUMO+2). The respective frontier orbitals are depicted in Figure 5, along with the orbitals of the 2-TN-water cluster for comparison. Notably, in the lower excited state of the dimer

only orbitals are connected, which have non-zero coefficients in the same (excited) monomer moiety.

The adiabatically following state was optimized without symmetry constraints, but has converged to a  $C_{2h}$  symmetric structure, like the  $S_0$  state. Like the  $S_0$  it is of  $A_g$ -symmetry and has consequently no permanent dipole moment, cf. Table 1. The geometry optimization of this state has been performed starting from the optimized  $S_0$  structure as well as from the optimized  $S_1$  structure. Both optimizations converged to a  $C_{2h}$  symmetric state for the  $S_2$ . This excited state connects exclusively orbitals with non-zero coefficients in different monomer moieties, making this transition forbidden:  $0.32$  (HOMO-2  $\rightarrow$  LUMO-1) -  $0.50$  (HOMO-1  $\rightarrow$  LUMO) -  $0.50$  (HOMO  $\rightarrow$  LUMO+1).

The converged  $S_2$  state structure is a true minimum as proven by a normal mode analysis. The vibrational frequencies of the  $S_2$  state are given in the online supporting material. One vibration is found to be very remarkable in the sense, that its wavenumber and its intensity are much higher than expected for a "normal" vibration. Indeed, this vibration is an artifact, due to the fact that the  $S_1$  and the  $S_2$ -states are quasi-degenerate. Inspection of the distortion vectors of this vibration shows, that one of the aromatic rings increases, while the other decreases, thus representing the transition state coordinate which interconnects the two  $S_1$  minima (cf. Figure 2). At the  $S_2$  state minimum  $S_2$  and  $S_1$  are quasi-degenerate and the distortion along this coordinate flips the electronically excited states, causing on one hand side a very steep potential, which leads to the high frequency and secondly a huge change of the dipole moment, which is the reason for the enormous intensity.

The rotational constants of the  $S_1$  and  $S_2$  states are shown in Table 1. The structure at the minimum of  $S_2$  PES has the bond length changes symmetrically distributed over both monomers, while the bond length changes at either of the  $S_1$  minima are localized at one of the monomers. The changes of the bond lengths upon electronic excitation from the ground state are compared in

Figure 4.

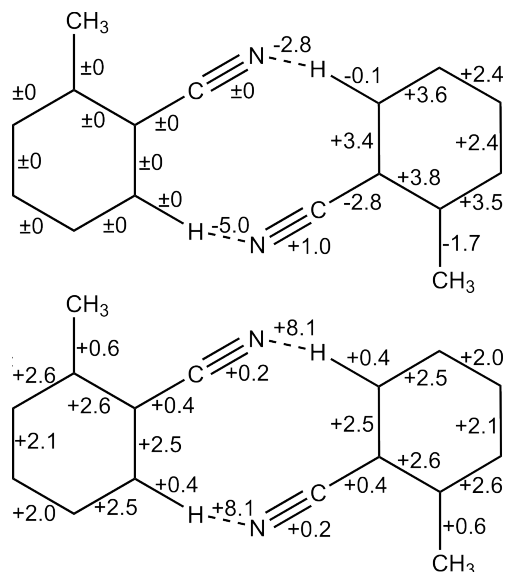


**Figure 4** Changes of the bond lengths of the 2-TN dimer upon excitation to the  $S_1$  (upper structure) and the  $S_2$  state (lower structure), respectively.

In the  $S_1$  state one monomer remains nearly completely in the  $S_0$  state geometry, while the changes of the other monomer moiety upon excitation to the  $S_1$  are close to those of the monomer. Thus, the electronically excited 2-TN monomer is solvated by the second moiety in its lowest excited singlet state. Only very small changes occur, due to inductive effects. Both hydrogen bonds change very asymmetrically. For the excited moiety, in which the CN group is the proton acceptor, the bond length decreases by 5.0 pm, while the other  $CN \cdots H$  bond decreases by 2.8 pm.

In the  $S_2$  state all bond length changes in the two monomer moieties are identical, thus the inversion symmetry of the ground state is retained. Both hydrogen bonds increase symmetrically by 8.1 pm. This increase is reflected in the decrease of binding energy of the cluster in the  $S_2$  state, compared to the binding energy in the  $S_0$  state, cf. Table 2, while the increase in the  $S_1$  state shows up in a reduction of the intermolecular bond lengths.

## 3.2 Experimental Results

### 3.2.1 Fluorescence Excitation Spectra of $(2-TN)_2$ and 2-TN- $H_2O$

Figure 5 shows the fluorescence excitation spectrum of 2-TN entrained into an helium molecular beam, which is recorded to the red of the monomer origin. Several bands appear in the region of  $200 \text{ cm}^{-1}$  to the red of the monomer origin, which show a distinct intensity variation upon variation of the helium backing pressure.

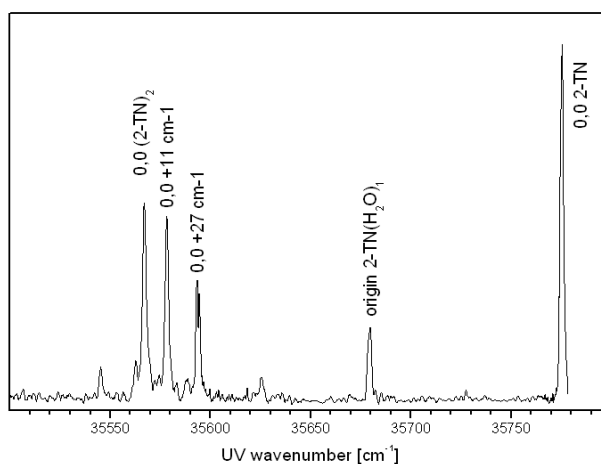


**Figure 5** Fluorescence excitation spectrum of 2-TN,  $(2-TN)_2$  and 2-TN- $H_2O$

An additional band at about  $100 \text{ cm}^{-1}$  to the red of the monomer origin increased, with increasing partial pressure of water vapor, which is seeded into the molecular beam and co-expanded with 2-TN. Therefore, we assigned the band system starting at  $-209 \text{ cm}^{-1}$  to the red of the monomer as belonging to the 2-TN dimer, and the band at  $96 \text{ cm}^{-1}$  to the red of the origin of the monomer as 1:1 water cluster of 2-TN. The water cluster of benzonitrile is found to be  $70 \text{ cm}^{-1}$  red-shifted from the benzonitrile monomer. We tentatively assigned the red-most band at  $35566.8 \text{ cm}^{-1}$  to the electronic origin of the 2-TN dimer and the energetically following bands blue-shifted by  $+11$  and  $+27 \text{ cm}^{-1}$  to vibronic bands of the dimer. From comparison to the results of the normal mode analysis of the excited state of the dimer (cf. Table S6 of the online supporting ma-

terial), both vibrations are of a'' symmetry and can be assigned to the butterfly and the twisting motion of the two monomer moieties.

### 3.2.2 Single vibronic level fluorescence of (2-TN)<sub>2</sub>

The SVLF spectrum of the electronic origin of (2-TN)<sub>2</sub> is shown in Figure 6 along with a FC simulation using the *ab initio* optimized parameters and a FC fit, which was obtained as described in section 4. It shows strong FC activity in modes Q<sub>86</sub> (b<sub>u</sub>) and Q<sub>16</sub> (a<sub>g</sub>) and a rich FC spectrum up to an energy of 2000 cm<sup>-1</sup>. Already the intensities from a FC simulation with the *ab initio* calculated geometries for ground and excited states show a very good agreement with the experimental intensities.

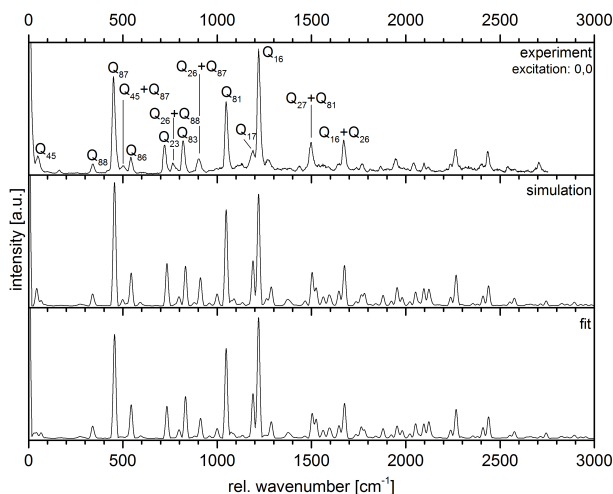


**Figure 6** Fluorescence emission spectrum of the 2-TN dimer upon excitation of the electronic origin at 35566.8 cm<sup>-1</sup>.

Additional SVLF spectra of the vibronic bands at 0,0 + 11 and 0,0 + 27 cm<sup>-1</sup>, along with a Franck-Condon simulation and a FC fit are shown in the online supporting material (Figures S1 and S2). A simultaneous fit of the intensities of all vibronic bands in the three emission spectra (given in Table S7 of the online supporting material) was performed in order to obtain the geometry changes of (2-TN)<sub>2</sub> upon electronic excitation.

The distortion along seven inter- and intramolecular normal modes *Q* serves as a basis for the geometry changes. Their values after fit are shown in Table S8 of the online supporting material.

### 3.2.3 Single vibronic level fluorescence of 2-TN-H<sub>2</sub>O

The SVLF spectrum upon excitation of the electronic origin of 2-TN-H<sub>2</sub>O at 36442.9 cm<sup>-1</sup> is shown in Figure 7 along with a FC simulation using the *ab initio* optimized parameters and a FC fit, which was obtained as described in section 4. As for the 2-TN dimer, the agreement between the experimental and the fitted spectrum is good.

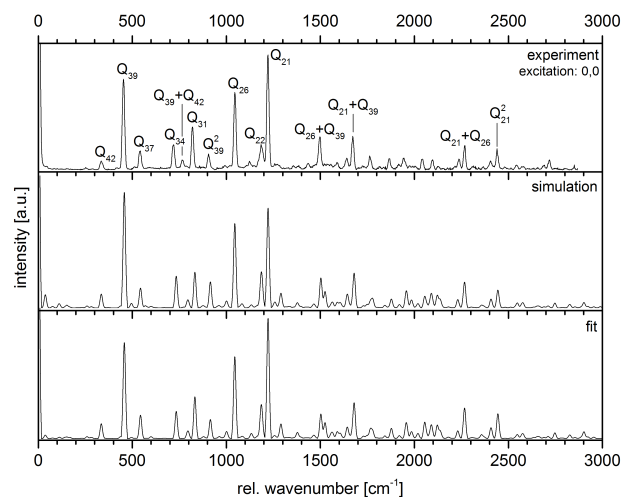


**Figure 7** Fluorescence emission spectrum of 2-TN-H<sub>2</sub>O upon excitation of the electronic origin at 35679.4 cm<sup>-1</sup>.

The distortion along ten inter- and intramolecular normal modes serve as a basis for the geometry changes. Their values after fit are shown in Table S11 of the online supporting material.

## 4 Discussion

In the FC fit of the emission band intensities, we adjust the excited state equilibrium geometry relative to the ground state geometry. The distortion of the excited state structure is performed by adding multiples  $\Delta Q_i$  of the *i*-th column of the

normal coordinate matrix  $\mathbf{L}$  to the *ab initio* calculated Cartesian geometry. A subspace of the distortion parameters  $\Delta Q$  is changed until best agreement between the computed and the observed vibronic intensities is reached.

#### 4.1 The 2-TN dimer

We first discuss the electronic symmetries of the electronic states of 2-TN. As shown above, the  $S_1$  state has  $B_u$  symmetry and is the one-photon allowed state, while the  $S_2$  state is the (forbidden)  $A_g$  symmetric state. Other inversion symmetric dimers (benzonitrile dimer,<sup>3</sup> benzoic acid dimer,<sup>6,7</sup> pyrazine dimer<sup>12</sup>) behave differently and have the  $S_2$ -state as one-photon allowed  $B_u$  state. What is the difference between these dimers and (2-TN)<sub>2</sub>?

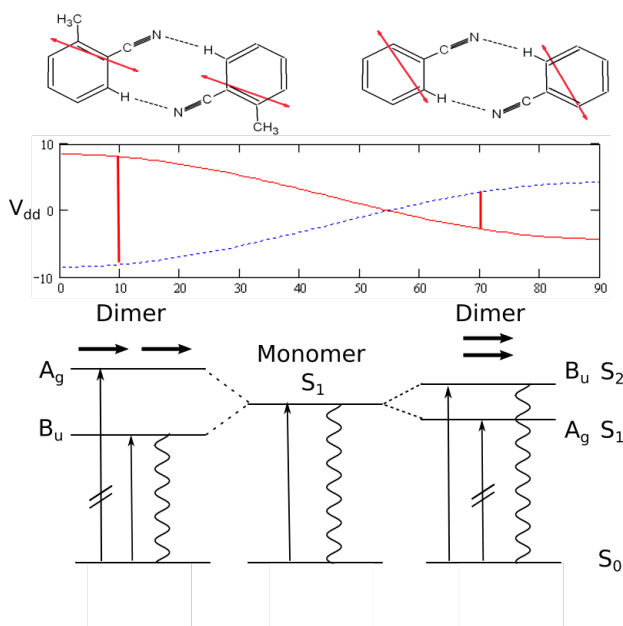


**Figure 8** Schematic drawing of the energetic ordering of the lowest two excited states in an inversion symmetric dimer. The left case refers to J-aggregates like for the 2-TN dimer, the right case to H-aggregates like for the benzonitrile dimer. The dipole-dipole interaction  $V_{dd}$  as function of the angle between the dipoles is shown, and the splitting for the (2-TN)<sub>2</sub> and the (benzonitrile)<sub>2</sub> are marked in the diagram.

Most dimers investigated until now, are singly substituted benzene derivatives, which have their

transition dipole moments along the short ( $b$ ) inertial axes. The resulting two TDMs in these dimers are nearly parallel (H-aggregate) and the lower state is the  $A_g$ . The methyl group in 2-TN rotates the TDM away to a position nearly perpendicular to the bond attaching the methyl group to the benzene ring.<sup>32</sup> The resulting TDMs in the 2-TN dimer are nearly head-tail oriented (J-aggregates) and the lowest excited state of  $B_u$  symmetry is allowed, while the  $S_2$  state ( $A_g$ ) is forbidden. This behaviour has recently also been observed for the m-cyanophenol dimer by Balmer *et al.*<sup>17</sup> The two cases are compared in Figure 8. The dipole-dipole interaction energy,  $V_{dd}$  which is shown as function of the angle  $\theta$  between the dipole moments and the line connecting the two COMs is calculated from equation 4. The angle  $\phi$  between the TDMs has been set to zero in this symmetric dimer, but one has to keep in mind, that upon isotopic substitution in one of the monomer moieties not only the Davydov splitting changes, but also the forbidden second component of the Davydov split bands becomes allowed. This has been shown for the benzonitrile dimer by Balmer *et al.*<sup>4</sup> and the benzoic acid dimer by Ottiger *et al.*<sup>13</sup> Upon <sup>13</sup>C substitution in position 3 of one of the benzene rings in the benzonitrile dimer, Balmer *et al.*<sup>4</sup> showed, that the forbidden  $S_1$  origin appears with nearly 50 % of the intensity of the  $S_2$ , which was attributed to the symmetry reduction from  $C_{2h}$  to  $C_s$ . An interesting system to study would be the singly <sup>13</sup>C substituted benzonitrile dimer in position 1 of the benzene ring. Also for this isotopologue, the  $C_{2h}$  symmetry is broken, but since the substitution position lies on one of the main inertial axes of the monomer, the TDMs in both monomers would remain strictly parallel.

The Franck-Condon fit of the vibronic emission spectra of (2-TN)<sub>2</sub> yields the changes of the bond parameters, shown in Figure 9. Clearly, from the results of the FC fit the excitation is localized on one of the 2-TN chromophores. The bond length changes in one of the chromophores are considerably larger, than in the other, the changes being similar to the changes upon electronic excitation in the 2-TN monomer.<sup>31</sup> Not

only the intramolecular bond length changes differ for both chromophores, but as well the intermolecular  $C\equiv N \cdots H$  bond lengths are substantially different. One hydrogen bond gets considerably stronger, and the bond lengths decreases by 2.0 pm, while the other slightly increases by 0.4 pm.

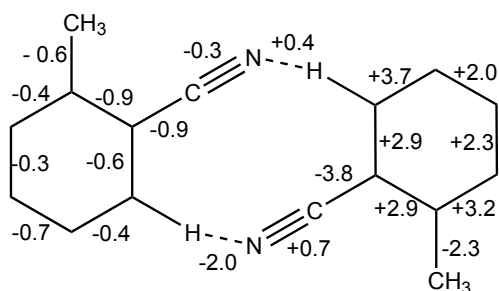


**Figure 9** Geometry changes of the 2-TN dimer from the FC fit.

This can be understood in the light of a natural population analysis (NPA), which has been performed for the monomer.<sup>31</sup> The interaction between the nitrogen atom lone pair (LP(N)) and the unoccupied Rydberg orbital at the neighboring C atom is strongly decreased upon electronic excitation. Therefore, the  $C\equiv N$  bond length increases. LP(N) interaction with the antibonding  $\pi$  orbital between the C atom of the nitrile group and the adjacent C atom also decreases. Thus, less electron density is shifted to the antibonding orbital upon electronic excitation, leading to a net increase of bond order and a resulting decrease of the C–C bond length. In turn, the higher LP(N) electron density in the excited state of 2-TN is responsible for the increase of bond order in the  $C\equiv N \cdots H$  hydrogen bond, which manifests itself in the shortening by 2.0 pm (cf. Fig. 9). The second ( $H \cdots N\equiv C$ ) hydrogen bond increases by 0.4 pm upon electronic excitation.

In the SVLF spectra of the dimer, we observe emission from the  $C_s$  symmetric excited state. This is obvious from the fact, that all observed modes in the emission spectrum belong to the irreducible representation  $a'$  (corresponding to  $a_g$  and  $b_u$  vibrations in the  $C_{2h}$  point group). Thus, emission takes place from the  $C_s$  symmetric adi-

abatically lowest excited state with electronic  $A'$  symmetry.

Additionally, we calculated the emission spectrum from the vibrationless origin of the  $C_{2h}$  symmetric  $S_2$  state and compared it to the emission spectrum from the  $S_1$  state and to the experimental spectrum. Figure 10 shows the results of these calculations. Clearly the emission takes place from the  $S_1$  state minimum, while the simulated emission from the vibrationless  $S_2$  state is completely different from the experimental spectrum.

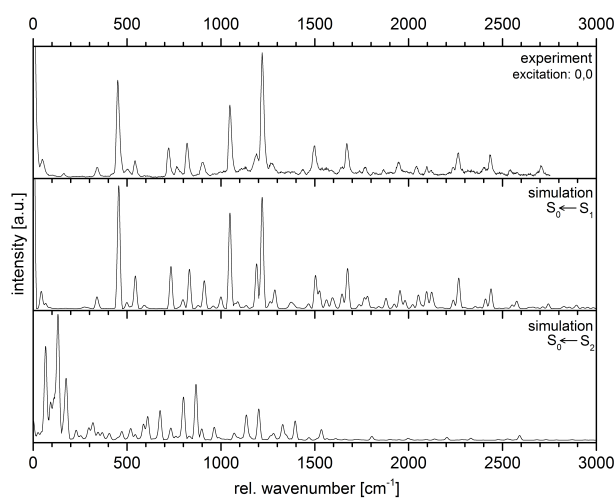


**Figure 10** Comparison of the experimental emission spectrum, obtained by pumping the electronic origin with the simulated  $S_1 \leftarrow S_0$  and the  $S_2 \leftarrow S_0$  spectra.

## 4.2 The 2-TN water cluster

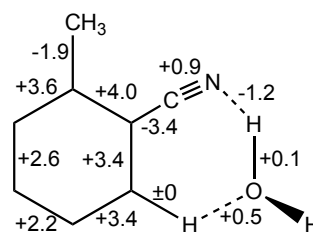


**Figure 11** Geometry changes of 2-TN- $H_2O$  dimer from the FC fit.

For the 2-TN water cluster the situation is

much clearer than for the 2-TN dimer. Since only one chromophore is present, there is no doubt about the site of excitation. The geometry changes upon electronic excitation are localized at the 2-TN chromophore, with the water molecule solvating the excited state after excitation.

Figure 11 summarizes the geometry changes upon electronic excitation of the 2-TN-water cluster. The  $C\equiv N \cdots H$  hydrogen bond length decreases, indicating the increase in bond strength upon electronic excitation of the chromophore. The second ( $H \cdots O-H$ ) hydrogen bond increases by 0.5 pm upon electronic excitation. The geometry changes in the chromophore are very similar to those of the uncomplexed monomer<sup>31</sup> and those of the excited moiety in the 2-TN dimer.

## 5 Conclusions

The geometry changes upon electronic excitation in the 2-TN water cluster and in one of the two moieties of the 2-TN dimer are similar to those of the uncomplexed 2-TN monomer. Contrary to the cases of the benzonitrile dimer, benzoic acid dimer, 2-cyanophenol dimer, 3-cyanophenol dimer, azaindole dimer, pyridone dimer, which all form H-aggregates, the 2-TN dimer exhibits a J-aggregate structure. For all of the aforementioned dimers, the optically bright state is thus the  $S_2$  with  $B_u$  symmetry, while the  $A_g$  symmetric  $S_1$  state, exhibiting a double minimum potential is the bright state for the 2-TN dimer, cf. Figure 8.

Even though the asymmetric excitation in one of the 2-TN moieties of the dimer suggests a localized excitation, the current experiment cannot make a distinction between localized and delocalized excitation. Emission spectra from the initially excited 2-TN moiety in the dimer or from the other moiety after excitation hopping will result in the same emission spectrum. Delocalized excitation in the context of the current experiments means that the semiclassical hopping time for excitation transfer between the monomers is shorter than the laser pulse duration of a few ns. This hopping time, which is the inverse of the res-

onance transfer rate can be estimated from the vibronic splitting:

$$\tau = 1/k_{AB} = \frac{h}{4|V_{AB}|} = \frac{1}{2\Delta_{vibron}c} \quad (8)$$

With the calculated value of the vibronic splitting of  $6 \text{ cm}^{-1}$  one obtains a hopping time of 2.7 ps. The value obtained here is shorter than for the H aggregates benzoic acid dimer (18 ps)<sup>7</sup> and benzonitrile dimer (8 ps),<sup>4</sup> but comparable to the J aggregate m-cyanophenol dimer (2.3 ps).<sup>17</sup> However, one has to keep in mind that the dipole approximation used in the derivation of equation (8) is valid only if the distance of the dipoles is large compared to the lengths of the dipoles. This certainly is not the case for the dimers studied here, so the dipole approximation is a poor approximation in these cases and rate constants for resonant transfer rates must be considered with caution.

Furthermore, although not resolved in the current study, the electronic origin of the 2-TN dimer is split into three components due to the hindered internal rotation of the two equivalent methyl rotors.<sup>52</sup> These components arise from a splitting into an  $A_1$ , a  $G$ , an  $E_1$  and an  $E_3$  component with  $A_1 - A_1$  (A-band),  $G - G$  (G-band), and  $(E_1 + E_3) - (E_1 + E_3)$  (E-band) selection rules. These torsional splittings cannot be resolved in the described experiments, but might be topic of a high resolution study on this system. However, the two E components of the origin band result from a geared and anti-geared motion of the two methyl rotors,<sup>52</sup> which might be responsible for a symmetry breaking between the two monomer moieties in the dimer. Apart from their structural equality, this torsional motion would then introduce an in-equivalence of the two monomers. Such an in-equivalence has shown to be the reason for localization of the excitation in dimeric systems.<sup>13</sup>

## Acknowledgments

Computational support and infrastructure was provided by the "Center for Information and Me-

dia Technology” (ZIM) at the Heinrich-Heine-University Düsseldorf (Germany). The financial support of the Deutsche Forschungsgemeinschaft (SCHM 1043/12-3) is gratefully acknowledged. We thank Rainer Weinkauff, Samuel Leutwyler and Horst Köppel for helpful discussions.

## References

- [1] T. Kobayashi, K. Honma, O. Kajimoto and S. Tsuchiya, *J. Chem. Phys.*, 1987, **86**, 1111–1117.
- [2] M. Takayagani and I. Hanazaki, *J. Opt. Soc. Am. B*, 1990, **7**, 1898–1904.
- [3] M. Schmitt, M. Böhm, C. R. S. Siegert, M. van Beek and W. L. Meerts, *J. Mol. Struct.*, 2006, **795**, 234–241.
- [4] F. A. Balmer, P. Ottiger and S. Leutwyler, *J. Phys. Chem. A*, 2014, **118**, 11253–11261.
- [5] K. Remmers, W. L. Meerts and I. Ozier, *J. Chem. Phys.*, 2000, **112**, 10890–10894.
- [6] I. Kalkman, C. Vu, M. Schmitt and W. L. Meerts, *ChemPhysChem*, 2008, **9**, 1788–1797.
- [7] P. Ottiger and S. Leutwyler, *J. Chem. Phys.*, 2012, **137**, 204303–1–204303–.
- [8] S. Kopec, P. Ottiger, S. Leutwyler and H. Köppel, *J. Chem. Phys.*, 2015, **142**, 084308–1–084308–.
- [9] N. Seurre, K. L. Barbu-Debus, F. Lahmani, A. Zehnacker-Rentien and J. Sepiol, *Chem. Phys.*, 2003, **295**, 21–33.
- [10] K. Sakota and H. Sekiya, *J. Phys. Chem. A*, 1995, **109**, 2718–2721.
- [11] A. Müller, F. Talbot and S. Leutwyler, *J. Chem. Phys.*, 2002, **116**, 2836–2847.
- [12] A. Held and D. W. Pratt, *J. Chem. Phys.*, 1992, **96**, 4869–4876.
- [13] P. Ottiger, H. Köppel and S. Leutwyler, *Chem. Sci.*, 2015, **6**, 6059–6068.
- [14] S. Kopec, P. Ottiger, S. Leutwyler and H. Köppel, *J. Chem. Phys.*, 2012, **137**, 184312–1–084308–10.
- [15] G. Scheibe, *Angew. Chem.*, 1937, **50**, 212–219.
- [16] E. E. Jelley, *Nature*, 1937, **139**, 631–632.
- [17] F. A. Balmer, S. Kopec, H. Köppel and S. Leutwyler, *J. Phys. Chem. A*, 2017, **121**, 73–87.
- [18] J. A. Stearns, N. R. Pillsbury, K. O. Douglass, C. W. Miller, T. S. Zwier and D. F. Plusquellic, *J. Chem. Phys.*, 2008, **129**, 224305–1–224305–13.
- [19] D. S. McClure, *Can. J. Chem.*, 1958, **36**, 59–71.
- [20] A. S. Davydov, *Sov. Phys. Usp.*, 1964, **7**, 145.
- [21] T. Förster, in *Modern Quantum Chemistry*, ed. O. Sinanoglu, Academic Press, New York, 1965, ch. III B, pp. 93–137.
- [22] M. Kasha, H. R. Rawls and M. A. El-Bayoumi, *Pure Appl. Chem.*, 1965, **11**, 371–392.
- [23] J. Frenkel, *Phys. Rev.*, 1931, **37**, 1276.
- [24] M. Fujii, M. Yamauchi, K. Takazawa and M. Ito, *Spectrochim. Acta*, 1994, **50A**, 1421–1433.
- [25] A. I. Jaman, S. Maiti and R. N. Nandi, *J. Mol. Spec.*, 2011, **192**, 148–151.
- [26] A. I. Jaman, P. H. Kumar and P. R. Bangal, *J. Atom. Mol. Opt. Phys.*, 2011, **2011**, 480396–1–480396–8.
- [27] H. Nakai and M. Kawai, *J. Chem. Phys.*, 2000, **113**, 2168–2174.
- [28] C. H. Park, G. W. Lee and S. K. Lee, *Bull. Korean Chem. Soc.*, 2006, **27**, 881–885.
- [29] C. H. Park and S. K. Lee, *Bull. Korean Chem. Soc.*, 2007, **27**, 1377–1380.
- [30] K. Suzuki, S. Ishiuchi, M. Sakai and M. Fujii, *J. Electr. Spect. Rel. Phen.*, 2005, **142**, 215–221.
- [31] F. Gmerek, B. Stuhlmann, L. Alvarez-Valtierra, D. W. Pratt and M. Schmitt, *J. Chem. Phys.*, 2016, **144**, 084304.
- [32] J. A. Ruiz-Santoyo, J. Wilke, M. Wilke, J. T. Yi, D. W. Pratt, M. Schmitt and L. Alvarez-Valtierra, *J. Chem. Phys.*, 2016, **144**, 044303.
- [33] R. M. Helm, H. P. Vogel, H. J. Neusser, V. Storm, D. Consalvo and H. Dreizler, *Z. Naturforsch.*, 1997, **52**, 655–664.
- [34] S. Melandri, D. Consalvo, W. Caminati and P. G. Favero, *J. Chem. Phys.*, 1999, **111**, 3874–3879.
- [35] M. Schmitt, U. Henrichs, H. Müller and K. Kleiner-manns, *J. Chem. Phys.*, 1995, **103**, 9918–9928.
- [36] W. Roth, C. Jacoby, A. Westphal and M. Schmitt, *J. Phys. Chem. A*, 1998, **102**, 3048–3059.

- [37] R. Ahlrichs, M. Bär, M. Häser, H. Horn and C. Kölmel, *Chem. Phys. Letters*, 1989, **162**, 165–169.
- [38] J. T. H. Dunning, *J. Chem. Phys.*, 1989, **90**, 1007–1023.
- [39] C. Hättig and F. Weigend, *J. Chem. Phys.*, 2000, **113**, 5154–5161.
- [40] C. Hättig and A. Köhn, *J. Chem. Phys.*, 2002, **117**, 6939–6951.
- [41] C. Hättig, *J. Chem. Phys.*, 2002, **118**, 7751–7761.
- [42] P. Deglmann, F. Furche and R. Ahlrichs, *Chem. Phys. Letters*, 2002, **362**, 511–518.
- [43] *TURBOMOLE V6.3 2012, a development of University of Karlsruhe and Forschungszentrum Karlsruhe GmbH, 1989-2007, TURBOMOLE GmbH, since 2007; available from <http://www.turbomole.com>.*
- [44] S. F. Boys and F. Bernardi, *Mol. Phys.*, 1970, **19**, 553–566.
- [45] A. E. Reed, R. B. Weinstock and F. Weinhold, *J. Chem. Phys.*, 1985, **83**, 735–746.
- [46] D. Spangenberg, P. Imhof and K. Kleinermanns, *Phys. Chem. Chem. Phys.*, 2003, **5**, 2505–2514.
- [47] R. Brause, M. Schmitt, D. Spangenberg and K. Kleinermanns, *Mol. Phys.*, 2004, **102**, 1615–1623.
- [48] E. V. Doktorov, I. A. Malkin and V. I. Man'ko, *J. Mol. Spec.*, 1975, **56**, 1–20.
- [49] E. V. Doktorov, I. A. Malkin and V. I. Man'ko, *J. Mol. Spec.*, 1977, **64**, 302–326.
- [50] W. H. Miller, *J. Phys. Chem.*, 1979, **83**, 960–963.
- [51] J. Bicerano, H. F. S. III and W. H. Miller, *J. Am. Chem. Soc.*, 1983, **105**, 2550–2553.
- [52] X.-Q. Tan, D. J. Clouthier, R. H. Judge, D. F. Plusquellic, J. L. Tomer and D. Pratt, *J. Chem. Phys.*, 1991, **95**, 7862–7871.

## Supplementary material

The supporting on-line material contains:

- Tables with the Cartesian coordinates (in bohr) of (2-TN)<sub>2</sub> and 2-TN-H<sub>2</sub>O in their S<sub>0</sub>, S<sub>1</sub>, and S<sub>2</sub> states. (Tables S1 - S5)
- A table with the CC2/cc-pVTZ calculated and experimental wavenumbers of the 90 normal modes of the ground and first electronically excited states of 2-TN dimer along with the respective symmetry labels and the coefficients of the Duschinsky matrix, which are larger than 0.4. (Table S6)
- A table with the Intensities of the observed emission bands of three vibronic bands of (2-TN)<sub>2</sub>. (Table S7)
- A table with the fitted factors of the displacements of (2-TN)<sub>2</sub> upon electronic excitation along seven normal modes from the FC fit. (Table S8)
- A table with the CC2/cc-pVTZ calculated and experimental wavenumbers of the 90 normal modes of the ground and first electronically excited states of 2-TN-water. (Table S9)
- A table with the intensities of the observed emission bands of 2-TN-H<sub>2</sub>O. (Table S10)
- A table with the fitted factors of the displacements of (2-TN)<sub>2</sub> upon electronic excitation along seven normal modes from the FC fit. (Table S8)
- A figure with the fluorescence emission spectrum of the 2-TN dimer upon excitation of the electronic origin at 0,0 + 11 cm<sup>-1</sup>. (Figure S1)
- A figure with the fluorescence emission spectrum of the 2-TN dimer upon excitation of the electronic origin at 0,0 + 27 cm<sup>-1</sup>. (Figure S2)

**Table S1** CC2/cc-pVTZ calculated optimized  $S_0$  cartesian coordinates of (2-TN)<sub>2</sub> (in bohr).

c	-9.47963974	-2.72622001	0.00000000
c	-7.09799361	-3.83200954	0.00000000
c	-4.95857370	-2.31995868	0.00000000
c	-5.23002814	0.30182816	0.00000000
c	-7.61577930	1.45217450	0.00000000
c	-9.72364995	-0.11129755	0.00000000
h	-11.14645571	-3.89472852	0.00000000
h	-6.90281235	-5.85683992	0.00000000
h	-3.08736921	-3.12376119	0.00000000
c	-3.04451534	1.86308693	0.00000000
c	-7.85516947	4.26324178	0.00000000
h	-11.57748837	0.73307265	0.00000000
h	-6.94452340	5.07905389	-1.65126567
h	-9.82730656	4.82424011	0.00000000
h	-6.94452340	5.07905389	1.65126567
n	-1.27000335	3.20608633	0.00000000
c	7.61577930	-1.45217450	0.00000000
h	6.94452340	-5.07905389	1.65126567
c	5.23002814	-0.30182816	0.00000000
c	7.09799361	3.83200954	0.00000000
c	9.47963974	2.72622001	0.00000000
h	11.14645571	3.89472852	0.00000000
h	6.94452340	-5.07905389	-1.65126567
h	11.57748837	-0.73307265	0.00000000
h	3.08736921	3.12376119	0.00000000
c	4.95857370	2.31995868	0.00000000
h	6.90281235	5.85683992	0.00000000
n	1.27000335	-3.20608633	0.00000000
c	7.85516947	-4.26324178	0.00000000
c	9.72364995	0.11129755	0.00000000
c	3.04451534	-1.86308693	0.00000000
h	9.82730656	-4.82424011	0.00000000

**Table S2** CC2/cc-pVTZ calculated optimized S<sub>1</sub> cartesian coordinates of (2-TN)<sub>2</sub> (in bohr).

c	-2.10426762	-0.18838263	-0.16630157
c	0.28301763	-1.28153982	-0.18203164
c	2.41562771	0.23972649	-0.12707675
c	2.12936955	2.85908124	-0.05659941
c	-0.26237110	3.99746017	-0.03990950
c	-2.36216669	2.42443443	-0.09595851
h	-3.76504749	-1.36482525	-0.20849240
h	0.48890788	-3.30463609	-0.23677030
h	4.29140550	-0.55534983	-0.13777131
c	4.30515275	4.43285138	-0.00073732
c	-0.51648308	6.80622057	0.03548096
h	-4.22033005	3.25925969	-0.08419975
h	0.39964036	7.67187965	-1.58717482
h	-2.49160235	7.35689871	0.03858953
h	0.37964198	7.58147435	1.71404893
n	6.06607754	5.79310392	0.04687452
c	14.94409023	1.04630183	-0.03077182
h	14.25580878	-2.58935968	1.50967505
c	12.45397236	2.14524395	-0.01523504
c	14.42930597	6.37185344	0.11092071
c	16.88404830	5.31688764	0.09636524
h	18.53347946	6.49871009	0.13805996
h	14.27437719	-2.50036611	-1.77356807
h	18.93825344	1.77566732	0.01182210
h	10.37000622	5.67295135	0.06858435
c	12.22492984	4.83524602	0.05649944
h	14.19125722	8.39161690	0.16438813
n	8.54934092	-0.77355852	-0.11787211
c	15.20961244	-1.72881463	-0.10448697
c	17.10152639	2.65408365	0.02522904
c	10.33496285	0.58496221	-0.07024494
h	17.17687588	-2.30296943	-0.10891575

**Table S3** CC2/cc-pVTZ calculated optimized S<sub>2</sub> cartesian coordinates of (2-TN)<sub>2</sub> (in bohr).

c	-9.65259580	-2.62976018	-0.00478609
c	-7.22391868	-3.72461043	0.00234659
c	-5.04369870	-2.18872490	0.00753762
c	-5.30703493	0.48231972	0.00547626
c	-7.75145978	1.62536700	-0.00163556
c	-9.89468112	0.02525090	-0.00666362
h	-11.31953546	-3.81057501	-0.00878769
h	-7.01044581	-5.75694157	0.00389427
h	-3.17395435	-3.01490282	0.01295944
c	-3.11460434	2.04550462	0.01047682
c	-8.01559325	4.44660389	-0.00358439
h	-11.75329955	0.87965510	-0.01205604
h	-7.09522266	5.27034887	-1.65842913
h	-9.99743218	4.99891050	-0.00954728
h	-7.10484360	5.27170611	1.65590690
n	-1.32200292	3.37063286	0.01437869
c	7.75135563	-1.62539597	-0.00250730
h	7.10430456	-5.27166980	1.65503324
c	5.30701940	-0.48215911	0.00477993
c	7.22426261	3.72460696	0.00107526
c	9.65284855	2.62956656	-0.00616044
h	11.31988121	3.81024853	-0.01035583
h	7.09496339	-5.27034209	-1.65929803
h	11.75325344	-0.88002415	-0.01342989
h	3.17424861	3.01529051	0.01202100
c	5.04390379	2.18890787	0.00657961
h	7.01088206	5.75694763	0.00246122
n	1.32187387	-3.37030846	0.01456328
c	8.01526270	-4.44665162	-0.00438281
c	9.89470900	-0.02546146	-0.00787906
c	3.11449895	-2.04521474	0.01020050
h	9.99705538	-4.99912535	-0.01018749

**Table S4** CC2/cc-pVTZ calculated optimized  $S_0$  cartesian coordinates of 2-TN-H<sub>2</sub>O (in bohr).

c	-1.59561431	-0.32757172	0.05258210
c	0.82117143	-1.33833981	-0.13376535
c	2.89325684	0.25958854	-0.24040746
c	2.51778300	2.86809029	-0.16087690
c	0.09794396	3.92314357	0.02507420
c	-1.94148443	2.27469577	0.13050693
h	-3.21191997	-1.56187806	0.13583237
h	1.09230265	-3.35305682	-0.19711380
h	4.79643836	-0.45208195	-0.38615973
c	4.65608201	4.48712139	-0.27716246
c	-0.24623088	6.72178594	0.10266468
h	-3.82297230	3.04169611	0.27394257
h	0.51437075	7.60315143	-1.59022805
h	-2.23274267	7.20653443	0.25050213
h	0.74442641	7.54100111	1.70538095
n	6.45270148	5.79804769	-0.38132144
o	9.22732104	0.58479702	-0.59710028
h	8.90503078	2.35622974	-0.87431189
h	9.93804585	0.55781634	1.07240944

**Table S5** CC2/cc-pVTZ calculated optimized S<sub>1</sub> cartesian coordinates of 2-TN-H<sub>2</sub>O (in bohr).

c	-1.69074406	-0.39268366	0.05355509
c	0.79093436	-1.36461795	-0.12582362
c	2.93825313	0.24815617	-0.22495186
c	2.61846733	2.92812466	-0.14594033
c	0.10113961	3.94364331	0.02918359
c	-1.99652294	2.26243908	0.12789843
h	-3.29707070	-1.63061612	0.12808312
h	1.09212583	-3.37523901	-0.19280754
h	4.82363932	-0.50630846	-0.36898041
c	4.70402755	4.52905032	-0.24741887
c	-0.24880206	6.70865301	0.09750211
h	-3.85803576	3.07571979	0.26136381
h	0.55844338	7.58011725	-1.58933407
h	-2.22760438	7.22170660	0.23770350
h	0.77799484	7.52757098	1.68849462
n	6.52841524	5.83458604	-0.34483114
o	9.20986486	0.61412417	-0.62144597
h	8.83877604	2.37906162	-0.89061679
h	9.94260841	0.60728319	1.03881433

**Table S6** CC2/cc-pVTZ calculated and experimental wavenumbers of the 90 normal modes of the ground and first electronically excited states of ortho-tolunitrile dimer along with the respective symmetry labels and the coefficients of the Duschinsky matrix, which are larger than 0.4.

Mode	S <sub>0</sub>			S <sub>1</sub>			Duschinsky
	Sym.	Calc.	Obs.	Sym.	Calc.	Obs.	
Q <sub>1</sub> (S <sub>0</sub> )	ag	3244		A'	3263		Q <sub>1</sub> (S <sub>1</sub> ) = +0.76Q <sub>1</sub> (S <sub>0</sub> ) - 0.49Q <sub>63</sub> (S <sub>0</sub> )
Q <sub>2</sub> (S <sub>0</sub> )	ag	3230		A'	3227		Q <sub>4</sub> (S <sub>1</sub> ) = +0.94Q <sub>2</sub> (S <sub>0</sub> )
Q <sub>3</sub> (S <sub>0</sub> )	ag	3221		A'	3224		Q <sub>5</sub> (S <sub>1</sub> ) = -0.92Q <sub>3</sub> (S <sub>0</sub> )
Q <sub>4</sub> (S <sub>0</sub> )	ag	3203		A'	3202		Q <sub>8</sub> (S <sub>1</sub> ) = -0.87Q <sub>4</sub> (S <sub>0</sub> ) - 0.48Q <sub>65</sub> (S <sub>0</sub> )
Q <sub>5</sub> (S <sub>0</sub> )	ag	3167		A'	3167		Q <sub>9</sub> (S <sub>1</sub> ) = +0.98Q <sub>5</sub> (S <sub>0</sub> )
Q <sub>6</sub> (S <sub>0</sub> )	ag	3080		A'	3042		Q <sub>12</sub> (S <sub>1</sub> ) = +0.89Q <sub>6</sub> (S <sub>0</sub> ) - 0.41Q <sub>67</sub> (S <sub>0</sub> )
Q <sub>7</sub> (S <sub>0</sub> )	ag	2122		A'	2035		Q <sub>14</sub> (S <sub>1</sub> ) = -0.97Q <sub>7</sub> (S <sub>0</sub> )
Q <sub>8</sub> (S <sub>0</sub> )	ag	1647		A'	1648		Q <sub>16</sub> (S <sub>1</sub> ) = +0.98Q <sub>8</sub> (S <sub>0</sub> )
Q <sub>9</sub> (S <sub>0</sub> )	ag	1614		A'	1508		Q <sub>21</sub> (S <sub>1</sub> ) = +0.83Q <sub>9</sub> (S <sub>0</sub> ) + 0.45Q <sub>70</sub> (S <sub>0</sub> )
Q <sub>10</sub> (S <sub>0</sub> )	ag	1525		A'	1445		Q <sub>24</sub> (S <sub>1</sub> ) = -0.83Q <sub>10</sub> (S <sub>0</sub> )
Q <sub>11</sub> (S <sub>0</sub> )	ag	1512		A'	1512		Q <sub>20</sub> (S <sub>1</sub> ) = -0.86Q <sub>11</sub> (S <sub>0</sub> ) + 0.49Q <sub>72</sub> (S <sub>0</sub> )
Q <sub>12</sub> (S <sub>0</sub> )	ag	1469		A'	1469		Q <sub>23</sub> (S <sub>1</sub> ) = +0.76Q <sub>12</sub> (S <sub>0</sub> ) - 0.64Q <sub>73</sub> (S <sub>0</sub> )
Q <sub>13</sub> (S <sub>0</sub> )	ag	1435		A'	1437		Q <sub>25</sub> (S <sub>1</sub> ) = -0.94Q <sub>13</sub> (S <sub>0</sub> )
Q <sub>14</sub> (S <sub>0</sub> )	ag	1416		A'	1416		Q <sub>26</sub> (S <sub>1</sub> ) = +0.77Q <sub>14</sub> (S <sub>0</sub> ) - 0.64Q <sub>75</sub> (S <sub>0</sub> )
Q <sub>15</sub> (S <sub>0</sub> )	ag	1317		A'	1318		Q <sub>29</sub> (S <sub>1</sub> ) = +0.89Q <sub>15</sub> (S <sub>0</sub> ) - 0.46Q <sub>76</sub> (S <sub>0</sub> )
Q <sub>16</sub> (S <sub>0</sub> )	ag	1262	1220	A'	1244		Q <sub>32</sub> (S <sub>1</sub> ) = -0.75Q <sub>16</sub> (S <sub>0</sub> ) - 0.63Q <sub>77</sub> (S <sub>0</sub> )
Q <sub>17</sub> (S <sub>0</sub> )	ag	1214	1190	A'	1199		Q <sub>34</sub> (S <sub>1</sub> ) = +0.82Q <sub>17</sub> (S <sub>0</sub> ) + 0.48Q <sub>78</sub> (S <sub>0</sub> )
Q <sub>18</sub> (S <sub>0</sub> )	ag	1199		A'	1177		Q <sub>36</sub> (S <sub>1</sub> ) = +0.93Q <sub>18</sub> (S <sub>0</sub> )
Q <sub>19</sub> (S <sub>0</sub> )	ag	1133		A'	1085		Q <sub>38</sub> (S <sub>1</sub> ) = -0.78Q <sub>19</sub> (S <sub>0</sub> ) - 0.45Q <sub>80</sub> (S <sub>0</sub> )
Q <sub>20</sub> (S <sub>0</sub> )	ag	1068		A'	1069		Q <sub>39</sub> (S <sub>1</sub> ) = +0.91Q <sub>20</sub> (S <sub>0</sub> ) + 0.41Q <sub>81</sub> (S <sub>0</sub> )
Q <sub>21</sub> (S <sub>0</sub> )	ag	1011		A'	1011		Q <sub>40</sub> (S <sub>1</sub> ) = -0.94Q <sub>21</sub> (S <sub>0</sub> )
Q <sub>22</sub> (S <sub>0</sub> )	ag	831		A'	832		Q <sub>43</sub> (S <sub>1</sub> ) = -0.77Q <sub>22</sub> (S <sub>0</sub> ) + 0.64Q <sub>83</sub> (S <sub>0</sub> )
Q <sub>23</sub> (S <sub>0</sub> )	ag	734		A'	734		Q <sub>45</sub> (S <sub>1</sub> ) = -0.73Q <sub>23</sub> (S <sub>0</sub> ) + 0.68Q <sub>84</sub> (S <sub>0</sub> )
Q <sub>24</sub> (S <sub>0</sub> )	ag	595		A'	594		Q <sub>47</sub> (S <sub>1</sub> ) = -0.66Q <sub>24</sub> (S <sub>0</sub> ) - 0.65Q <sub>85</sub> (S <sub>0</sub> )
Q <sub>25</sub> (S <sub>0</sub> )	ag	543		A'	544		Q <sub>49</sub> (S <sub>1</sub> ) = -0.76Q <sub>25</sub> (S <sub>0</sub> ) + 0.63Q <sub>86</sub> (S <sub>0</sub> )
Q <sub>26</sub> (S <sub>0</sub> )	ag	455		A'	407		Q <sub>52</sub> (S <sub>1</sub> ) = +0.73Q <sub>26</sub> (S <sub>0</sub> ) - 0.66Q <sub>87</sub> (S <sub>0</sub> )
Q <sub>27</sub> (S <sub>0</sub> )	ag	339		A'	340		Q <sub>53</sub> (S <sub>1</sub> ) = +0.96Q <sub>27</sub> (S <sub>0</sub> )
Q <sub>28</sub> (S <sub>0</sub> )	ag	162		A'	163		Q <sub>55</sub> (S <sub>1</sub> ) = +1.00Q <sub>28</sub> (S <sub>0</sub> )
Q <sub>29</sub> (S <sub>0</sub> )	ag	66		A'	68		Q <sub>57</sub> (S <sub>1</sub> ) = +1.00Q <sub>29</sub> (S <sub>0</sub> )
Q <sub>30</sub> (S <sub>0</sub> )	ag	44		A'	40		Q <sub>59</sub> (S <sub>1</sub> ) = +0.99Q <sub>30</sub> (S <sub>0</sub> )
Q <sub>31</sub> (S <sub>0</sub> )	bg	3143		A''	3142		Q <sub>60</sub> (S <sub>1</sub> ) = -0.93Q <sub>31</sub> (S <sub>0</sub> )
Q <sub>32</sub> (S <sub>0</sub> )	bg	1503		A''	1504		Q <sub>62</sub> (S <sub>1</sub> ) = -0.91Q <sub>32</sub> (S <sub>0</sub> ) + 0.41Q <sub>47</sub> (S <sub>0</sub> )
Q <sub>33</sub> (S <sub>0</sub> )	bg	1072		A''	1072		Q <sub>64</sub> (S <sub>1</sub> ) = -0.91Q <sub>33</sub> (S <sub>0</sub> ) + 0.42Q <sub>48</sub> (S <sub>0</sub> )
Q <sub>34</sub> (S <sub>0</sub> )	bg	1039		A''	1035		Q <sub>65</sub> (S <sub>1</sub> ) = -0.83Q <sub>34</sub> (S <sub>0</sub> ) - 0.56Q <sub>49</sub> (S <sub>0</sub> )
Q <sub>35</sub> (S <sub>0</sub> )	bg	991		A''	990		Q <sub>67</sub> (S <sub>1</sub> ) = +0.79Q <sub>35</sub> (S <sub>0</sub> ) + 0.61Q <sub>50</sub> (S <sub>0</sub> )
Q <sub>36</sub> (S <sub>0</sub> )	bg	920		A''	768		Q <sub>71</sub> (S <sub>1</sub> ) = -0.77Q <sub>36</sub> (S <sub>0</sub> ) - 0.41Q <sub>50</sub> (S <sub>0</sub> )
Q <sub>37</sub> (S <sub>0</sub> )	bg	802		A''	543		Q <sub>76</sub> (S <sub>1</sub> ) = -0.48Q <sub>37</sub> (S <sub>0</sub> ) + 0.43Q <sub>54</sub> (S <sub>0</sub> )
Q <sub>38</sub> (S <sub>0</sub> )	bg	761		A''	761		Q <sub>72</sub> (S <sub>1</sub> ) = +0.73Q <sub>38</sub> (S <sub>0</sub> ) - 0.68Q <sub>53</sub> (S <sub>0</sub> )
Q <sub>39</sub> (S <sub>0</sub> )	bg	595		A''	595		Q <sub>75</sub> (S <sub>1</sub> ) = +0.67Q <sub>39</sub> (S <sub>0</sub> ) - 0.64Q <sub>54</sub> (S <sub>0</sub> )
Q <sub>40</sub> (S <sub>0</sub> )	bg	480		A''	479		Q <sub>77</sub> (S <sub>1</sub> ) = +0.76Q <sub>40</sub> (S <sub>0</sub> ) + 0.66Q <sub>55</sub> (S <sub>0</sub> )
Q <sub>41</sub> (S <sub>0</sub> )	bg	402		A''	279		Q <sub>81</sub> (S <sub>1</sub> ) = -0.71Q <sub>41</sub> (S <sub>0</sub> ) + 0.61Q <sub>56</sub> (S <sub>0</sub> )
Q <sub>42</sub> (S <sub>0</sub> )	bg	224		A''	222		Q <sub>82</sub> (S <sub>1</sub> ) = -1.00Q <sub>42</sub> (S <sub>0</sub> )
Q <sub>43</sub> (S <sub>0</sub> )	bg	152		A''	132		Q <sub>85</sub> (S <sub>1</sub> ) = +0.69Q <sub>43</sub> (S <sub>0</sub> ) + 0.46Q <sub>59</sub> (S <sub>0</sub> )
Q <sub>44</sub> (S <sub>0</sub> )	bg	131		A''	127		Q <sub>86</sub> (S <sub>1</sub> ) = -0.79Q <sub>44</sub> (S <sub>0</sub> ) - 0.61Q <sub>59</sub> (S <sub>0</sub> )
Q <sub>45</sub> (S <sub>0</sub> )	bg	49	51	A''	44		Q <sub>88</sub> (S <sub>1</sub> ) = +0.98Q <sub>45</sub> (S <sub>0</sub> )
Q <sub>46</sub> (S <sub>0</sub> )	au	3143		A''	3085		Q <sub>61</sub> (S <sub>1</sub> ) = -0.92Q <sub>46</sub> (S <sub>0</sub> )
Q <sub>47</sub> (S <sub>0</sub> )	au	1503		A''	1473		Q <sub>63</sub> (S <sub>1</sub> ) = -0.91Q <sub>47</sub> (S <sub>0</sub> ) - 0.41Q <sub>32</sub> (S <sub>0</sub> )
Q <sub>48</sub> (S <sub>0</sub> )	au	1072		A''	1000		Q <sub>66</sub> (S <sub>1</sub> ) = -0.89Q <sub>48</sub> (S <sub>0</sub> ) - 0.41Q <sub>33</sub> (S <sub>0</sub> )
Q <sub>49</sub> (S <sub>0</sub> )	au	1037		A''	851		Q <sub>69</sub> (S <sub>1</sub> ) = +0.80Q <sub>49</sub> (S <sub>0</sub> ) - 0.54Q <sub>34</sub> (S <sub>0</sub> )
Q <sub>50</sub> (S <sub>0</sub> )	au	991		A''	750		Q <sub>73</sub> (S <sub>1</sub> ) = +0.61Q <sub>50</sub> (S <sub>0</sub> ) - 0.47Q <sub>35</sub> (S <sub>0</sub> ) - 0.47Q <sub>36</sub> (S <sub>0</sub> )
Q <sub>51</sub> (S <sub>0</sub> )	au	919		A''	919		Q <sub>68</sub> (S <sub>1</sub> ) = +0.94Q <sub>51</sub> (S <sub>0</sub> )
Q <sub>52</sub> (S <sub>0</sub> )	au	802		A''	801		Q <sub>70</sub> (S <sub>1</sub> ) = +0.83Q <sub>52</sub> (S <sub>0</sub> ) + 0.55Q <sub>37</sub> (S <sub>0</sub> )
Q <sub>53</sub> (S <sub>0</sub> )	au	761		A''	625		Q <sub>74</sub> (S <sub>1</sub> ) = +0.52Q <sub>53</sub> (S <sub>0</sub> ) + 0.48Q <sub>37</sub> (S <sub>0</sub> ) + 0.48Q <sub>38</sub> (S <sub>0</sub> )
Q <sub>54</sub> (S <sub>0</sub> )	au	596		A''	332		Q <sub>80</sub> (S <sub>1</sub> ) = -0.43Q <sub>54</sub> (S <sub>0</sub> ) - 0.51Q <sub>55</sub> + 0.42Q <sub>40</sub> (S <sub>0</sub> )
Q <sub>55</sub> (S <sub>0</sub> )	au	482		A''	437		Q <sub>78</sub> (S <sub>1</sub> ) = +0.52Q <sub>55</sub> (S <sub>0</sub> ) - 0.47Q <sub>40</sub> (S <sub>0</sub> ) - 0.40Q <sub>54</sub> (S <sub>0</sub> )
Q <sub>56</sub> (S <sub>0</sub> )	au	399		A''	400		Q <sub>79</sub> (S <sub>1</sub> ) = -0.76Q <sub>56</sub> (S <sub>0</sub> ) - 0.65Q <sub>41</sub> (S <sub>0</sub> )
Q <sub>57</sub> (S <sub>0</sub> )	au	224		A''	181		Q <sub>83</sub> (S <sub>1</sub> ) = +0.92Q <sub>57</sub> (S <sub>0</sub> )
Q <sub>58</sub> (S <sub>0</sub> )	au	155		A''	154		Q <sub>84</sub> (S <sub>1</sub> ) = +1.00Q <sub>58</sub> (S <sub>0</sub> )
Q <sub>59</sub> (S <sub>0</sub> )	au	139		A''	95		Q <sub>87</sub> (S <sub>1</sub> ) = -0.54Q <sub>59</sub> (S <sub>0</sub> ) + 0.50Q <sub>44</sub> (S <sub>0</sub> ) - 0.42Q <sub>89</sub> (S <sub>0</sub> ) + 0.41Q <sub>43</sub>
Q <sub>60</sub> (S <sub>0</sub> )	au	29		A''	27	27	Q <sub>89</sub> (S <sub>1</sub> ) = -0.99Q <sub>60</sub> (S <sub>0</sub> )
Q <sub>61</sub> (S <sub>0</sub> )	au	14		A''	13	11	Q <sub>90</sub> (S <sub>1</sub> ) = +0.99Q <sub>61</sub> (S <sub>0</sub> )
Q <sub>62</sub> (S <sub>0</sub> )	bu	3244		A'	3243		Q <sub>2</sub> (S <sub>1</sub> ) = +0.99Q <sub>62</sub> (S <sub>0</sub> )
Q <sub>63</sub> (S <sub>0</sub> )	bu	3230		A'	3238		Q <sub>3</sub> (S <sub>1</sub> ) = +0.80Q <sub>63</sub> (S <sub>0</sub> ) + 0.58Q <sub>1</sub> (S <sub>0</sub> )
Q <sub>64</sub> (S <sub>0</sub> )	bu	3221		A'	3218		Q <sub>6</sub> (S <sub>1</sub> ) = +0.94Q <sub>64</sub> (S <sub>0</sub> )
Q <sub>65</sub> (S <sub>0</sub> )	bu	3203		A'	3217		Q <sub>7</sub> (S <sub>1</sub> ) = -0.80Q <sub>65</sub> (S <sub>0</sub> ) + 0.43Q <sub>4</sub> (S <sub>0</sub> )
Q <sub>66</sub> (S <sub>0</sub> )	bu	3166		A'	3166		Q <sub>10</sub> (S <sub>1</sub> ) = +1.00Q <sub>66</sub> (S <sub>0</sub> )
Q <sub>67</sub> (S <sub>0</sub> )	bu	3080		A'	3080		Q <sub>11</sub> (S <sub>1</sub> ) = +0.90Q <sub>67</sub> (S <sub>0</sub> ) + 0.42Q <sub>6</sub> (S <sub>0</sub> )
Q <sub>68</sub> (S <sub>0</sub> )	bu	2123		A'	2122		Q <sub>13</sub> (S <sub>1</sub> ) = -0.97Q <sub>68</sub> (S <sub>0</sub> )
Q <sub>69</sub> (S <sub>0</sub> )	bu	1647		A'	1574		Q <sub>18</sub> (S <sub>1</sub> ) = -0.95Q <sub>69</sub> (S <sub>0</sub> )
Q <sub>70</sub> (S <sub>0</sub> )	bu	1614		A'	1614		Q <sub>17</sub> (S <sub>1</sub> ) = +0.88Q <sub>70</sub> (S <sub>0</sub> ) - 0.48Q <sub>9</sub> (S <sub>0</sub> )
Q <sub>71</sub> (S <sub>0</sub> )	bu	1525		A'	1526		Q <sub>19</sub> (S <sub>1</sub> ) = +0.93Q <sub>71</sub> (S <sub>0</sub> )
Q <sub>72</sub> (S <sub>0</sub> )	bu	1511		A'	1481		Q <sub>22</sub> (S <sub>1</sub> ) = +0.73Q <sub>72</sub> (S <sub>0</sub> )
Q <sub>73</sub> (S <sub>0</sub> )	bu	1469		A'	1396		Q <sub>27</sub> (S <sub>1</sub> ) = -0.67Q <sub>73</sub> (S <sub>0</sub> ) - 0.56Q <sub>12</sub> (S <sub>0</sub> )
Q <sub>74</sub> (S <sub>0</sub> )	bu	1435		A'	1651		Q <sub>15</sub> (S <sub>1</sub> ) = -0.83Q <sub>74</sub> (S <sub>0</sub> )
Q <sub>75</sub> (S <sub>0</sub> )	bu	1416		A'	1394		Q <sub>28</sub> (S <sub>1</sub> ) = +0.71Q <sub>75</sub> (S <sub>0</sub> ) - 0.59Q <sub>14</sub> (S <sub>0</sub> )
Q <sub>76</sub> (S <sub>0</sub> )	bu	1316		A'	1284		Q <sub>30</sub> (S <sub>1</sub> ) = +0.85Q <sub>76</sub> (S <sub>0</sub> ) + 0.44Q <sub>15</sub> (S <sub>0</sub> )
Q <sub>77</sub> (S <sub>0</sub> )	bu	1262		A'	263		Q <sub>31</sub> (S <sub>1</sub> ) = -0.77Q <sub>77</sub> (S <sub>0</sub> ) + 0.64Q <sub>16</sub> (S <sub>0</sub> )
Q <sub>78</sub> (S <sub>0</sub> )	bu	1215		A'	1215		Q <sub>33</sub> (S <sub>1</sub> ) = +0.86Q <sub>78</sub> (S <sub>0</sub> ) - 0.50Q <sub>17</sub> (S <sub>0</sub> )
Q <sub>79</sub> (S <sub>0</sub> )	bu	1199		A'	1198		Q <sub>35</sub> (S <sub>1</sub> ) = -0.96Q <sub>79</sub> (S <sub>0</sub> )
Q <sub>80</sub> (S <sub>0</sub> )	bu	1133		A'	1133		Q <sub>37</sub> (S <sub>1</sub> ) = +0.87Q <sub>80</sub> (S <sub>0</sub> ) - 0.50Q <sub>19</sub> (S <sub>0</sub> )
Q <sub>81</sub> (S <sub>0</sub> )	bu	1069	1048	A'	987		Q <sub>41</sub> (S <sub>1</sub> ) = -84Q <sub>81</sub> (S <sub>0</sub> )
Q <sub>82</sub> (S <sub>0</sub> )	bu	1011		A'	960		Q <sub>42</sub> (S <sub>1</sub> ) = -0.88Q <sub>82</sub> (S <sub>0</sub> )
Q <sub>83</sub> (S <sub>0</sub> )	bu	832	821	A'	807		Q <sub>44</sub> (S <sub>1</sub> ) = +0.76Q <sub>83</sub> (S <sub>0</sub> ) + 0.63Q <sub>22</sub> (S <sub>0</sub> )
Q <sub>84</sub> (S <sub>0</sub> )	bu	733		A'	680		Q <sub>46</sub> (S <sub>1</sub> ) = +0.72Q <sub>84</sub> (S <sub>0</sub> ) - 0.67Q <sub>23</sub> (S <sub>0</sub> )
Q <sub>85</sub> (S <sub>0</sub> )	bu	594	607	A'	576		Q <sub>48</sub> (S <sub>1</sub> ) = -0.70Q <sub>85</sub> (S <sub>0</sub> ) + 0.47Q <sub>40</sub> (S <sub>0</sub> ) + 0.42Q <sub>24</sub> (S <sub>0</sub> )
Q <sub>86</sub> (S <sub>0</sub> )	bu	544	542	A'	499		Q <sub>50</sub> (S <sub>1</sub> ) = +0.73Q <sub>86</sub> (S <sub>0</sub> ) + 0.61Q <sub>25</sub> (S <sub>0</sub> )
Q <sub>87</sub> (S <sub>0</sub> )	bu	457	450	A'	456		Q <sub>51</sub> (S <sub>1</sub> ) = -0.74Q <sub>87</sub> (S <sub>0</sub> ) - 0.67Q <sub>26</sub> (S <sub>0</sub> )
Q <sub>88</sub> (S <sub>0</sub> )	bu	339	343	A'	329		Q <sub>54</sub> (S <sub>1</sub> ) = -0.95Q <sub>88</sub> (S <sub>0</sub> )
Q <sub>89</sub> (S <sub>0</sub> )	bu	152		A'	145		Q <sub>56</sub> (S <sub>1</sub> ) = -0.81Q <sub>89</sub> (S <sub>0</sub> ) + 0.57Q <sub>43</sub> (S <sub>0</sub> )
Q <sub>90</sub> (S <sub>0</sub> )	bu	54		A'	56		Q <sub>58</sub> (S <sub>1</sub> ) = +0.99Q <sub>90</sub> (S <sub>0</sub> )

**Table S7** Intensities of the observed emission bands of three vibronic bands of (2-TN)<sub>2</sub>. The first line gives the wavenumber of the excited bands, the first column the wavenumbers of the emission bands. The entries of the table represent the intensities, with the most intense band (apart from the excited band whose intensity is biased by stray light.) in each of the emission spectra normalized to 1.

S <sub>0</sub>	0	11	27
51	0.14		
64			0.09
85		0.09	
343	0.08		
348		0.1	
362			0.08
444		0.01	
450	0.78		
469		0.7	
481			0.69
506	0.06		
542	0.13		
553		0.12	
563			0.12
594	0.01		
607	0.01		
721	0.24		
733		0.24	
745			0.16
765	0.09		
775		0.13	
800			0.05
821	0.27		
837		0.26	
846			0.30
904	0.12		
917		0.15	
933			0.10
934		0.08	
1048	0.58		
1064		0.25	
1077			0.34
1111			0.02
1140		0.10	0.04
1157			
1190	0.19		
1203		0.19	
1214			0.24
1220	1.00		
1233		1.00	
1251			1.00
1461			0.03
1500	0.25		
1514		0.24	
1530			0.25

**Table S8** Fitted factors of the displacements of of (2-TN)<sub>2</sub> upon electronic excitation along seven normal modes from the FC fit.

Mode	displacement
$Q_{61}$	$0.013352 \pm 0.13162$
$Q_{60}$	$0.089281 \pm 0.35223$
$Q_{45}$	$0.019211 \pm 0.037853$
$Q_{30}$	$-0.17032 \pm 0.1297$
$Q_{26}$	$-0.01353 \pm 0.031116$
$Q_{23}$	$-0.056396 \pm 0.017771$
$Q_{20}$	$-0.016012 \pm 0.026945$

**Table S9** CC2/cc-pVTZ calculated and experimental wavenumbers of the 90 normal modes of the ground and first electronically excited states of 2-TN-water along with the respective symmetry labels and the coefficients of the Duschinsky matrix, which are larger than 0.4.

Mode	S <sub>0</sub>			S <sub>1</sub>			Duschinsky
	Sym.	Calc.	Obs.	Sym.	Calc.	Obs.	
Q <sub>1</sub> (S <sub>0</sub> )	a	3923		a	3918		Q <sub>1</sub> (S <sub>1</sub> ) = -1.00Q <sub>1</sub> (S <sub>0</sub> )
Q <sub>2</sub> (S <sub>0</sub> )	a	3794		a	3781		Q <sub>2</sub> (S <sub>1</sub> ) = -1.00Q <sub>2</sub> (S <sub>0</sub> )
Q <sub>3</sub> (S <sub>0</sub> )	a	3246		a	3264		Q <sub>3</sub> (S <sub>1</sub> ) = -0.79Q <sub>3</sub> (S <sub>0</sub> ) + 0.52Q <sub>4</sub> (S <sub>0</sub> )
Q <sub>4</sub> (S <sub>0</sub> )	a	3229		a	3237		Q <sub>4</sub> (S <sub>1</sub> ) = -0.81Q <sub>4</sub> (S <sub>0</sub> ) - 0.58Q <sub>3</sub> (S <sub>0</sub> )
Q <sub>5</sub> (S <sub>0</sub> )	a	3219		a	3223		Q <sub>5</sub> (S <sub>1</sub> ) = -0.99Q <sub>5</sub> (S <sub>0</sub> )
Q <sub>6</sub> (S <sub>0</sub> )	a	3204		a	3219		Q <sub>6</sub> (S <sub>1</sub> ) = +0.93Q <sub>6</sub> (S <sub>0</sub> )
Q <sub>7</sub> (S <sub>0</sub> )	a	3168		a	3169		Q <sub>7</sub> (S <sub>1</sub> ) = +0.98Q <sub>7</sub> (S <sub>0</sub> )
Q <sub>8</sub> (S <sub>0</sub> )	a	3142		a	3082		Q <sub>8</sub> (S <sub>1</sub> ) = -1.00Q <sub>8</sub> (S <sub>0</sub> )
Q <sub>9</sub> (S <sub>0</sub> )	a	3082		a	3042		Q <sub>9</sub> (S <sub>1</sub> ) = +0.98Q <sub>9</sub> (S <sub>0</sub> )
Q <sub>10</sub> (S <sub>0</sub> )	a	2121		a	2034		Q <sub>10</sub> (S <sub>1</sub> ) = -1.00Q <sub>10</sub> (S <sub>0</sub> )
Q <sub>11</sub> (S <sub>0</sub> )	a	1658		a	1660		Q <sub>11</sub> (S <sub>1</sub> ) = -1.00Q <sub>11</sub> (S <sub>0</sub> )
Q <sub>12</sub> (S <sub>0</sub> )	a	1648		a	1574		Q <sub>13</sub> (S <sub>1</sub> ) = +0.97Q <sub>12</sub> (S <sub>0</sub> )
Q <sub>13</sub> (S <sub>0</sub> )	a	1616		a	1509		Q <sub>14</sub> (S <sub>1</sub> ) = -0.95Q <sub>13</sub> (S <sub>0</sub> )
Q <sub>14</sub> (S <sub>0</sub> )	a	1525		a	1444		Q <sub>17</sub> (S <sub>1</sub> ) = +0.89Q <sub>14</sub> (S <sub>0</sub> )(S <sub>0</sub> )
Q <sub>15</sub> (S <sub>0</sub> )	a	1512		a	1483		Q <sub>15</sub> (S <sub>1</sub> ) = +0.83Q <sub>15</sub> (S <sub>0</sub> )
Q <sub>16</sub> (S <sub>0</sub> )	a	1504		a	1472		Q <sub>16</sub> (S <sub>1</sub> ) = +1.00Q <sub>16</sub> (S <sub>0</sub> )
Q <sub>17</sub> (S <sub>0</sub> )	a	1469		a	1396		Q <sub>18</sub> (S <sub>1</sub> ) = -0.92Q <sub>17</sub> (S <sub>0</sub> )
Q <sub>18</sub> (S <sub>0</sub> )	a	1437		a	1649		Q <sub>12</sub> (S <sub>1</sub> ) = +0.89Q <sub>18</sub> (S <sub>0</sub> )
Q <sub>19</sub> (S <sub>0</sub> )	a	1417		a	1394		Q <sub>19</sub> (S <sub>1</sub> ) = +0.97Q <sub>19</sub> (S <sub>0</sub> )
Q <sub>20</sub> (S <sub>0</sub> )	a	1315		a	1281		Q <sub>20</sub> (S <sub>1</sub> ) = +0.96Q <sub>20</sub> (S <sub>0</sub> )
Q <sub>21</sub> (S <sub>0</sub> )	a	1262	1222	a	1244		Q <sub>21</sub> (S <sub>1</sub> ) = +0.97Q <sub>21</sub> (S <sub>0</sub> )
Q <sub>22</sub> (S <sub>0</sub> )	a	1216	1185	a	1201		Q <sub>22</sub> (S <sub>1</sub> ) = +0.95Q <sub>22</sub> (S <sub>0</sub> )
Q <sub>23</sub> (S <sub>0</sub> )	a	1199		a	1177		Q <sub>23</sub> (S <sub>1</sub> ) = +0.97Q <sub>23</sub> (S <sub>0</sub> )
Q <sub>24</sub> (S <sub>0</sub> )	a	1133	1106	a	1085		Q <sub>24</sub> (S <sub>1</sub> ) = +0.89Q <sub>24</sub> (S <sub>0</sub> )
Q <sub>25</sub> (S <sub>0</sub> )	a	1073		a	1000		Q <sub>25</sub> (S <sub>1</sub> ) = -0.99Q <sub>25</sub> (S <sub>0</sub> )
Q <sub>26</sub> (S <sub>0</sub> )	a	1068	1045	a	986		Q <sub>26</sub> (S <sub>1</sub> ) = +0.92Q <sub>26</sub> (S <sub>0</sub> )
Q <sub>27</sub> (S <sub>0</sub> )	a	1040		a	858		Q <sub>28</sub> (S <sub>1</sub> ) = -0.96Q <sub>27</sub> (S <sub>0</sub> )
Q <sub>28</sub> (S <sub>0</sub> )	a	1011		a	960		Q <sub>27</sub> (S <sub>1</sub> ) = -0.93Q <sub>28</sub> (S <sub>0</sub> )
Q <sub>29</sub> (S <sub>0</sub> )	a	994		a	752		Q <sub>31</sub> (S <sub>1</sub> ) = +0.70Q <sub>29</sub> (S <sub>0</sub> ) - 0.60Q <sub>30</sub>
Q <sub>30</sub> (S <sub>0</sub> )	a	921		a	772		Q <sub>30</sub> (S <sub>1</sub> ) = -0.75Q <sub>30</sub> (S <sub>0</sub> ) - 0.61Q <sub>29</sub>
Q <sub>31</sub> (S <sub>0</sub> )	a	833	820	a	808		Q <sub>29</sub> (S <sub>1</sub> ) = +0.99Q <sub>31</sub> (S <sub>0</sub> )
Q <sub>32</sub> (S <sub>0</sub> )	a	803		a	543		Q <sub>35</sub> (S <sub>1</sub> ) = -0.59Q <sub>32</sub> (S <sub>0</sub> ) - 0.58Q <sub>36</sub> (S <sub>0</sub> ) + 0.51Q <sub>33</sub> (S <sub>0</sub> )
Q <sub>33</sub> (S <sub>0</sub> )	a	763		a	628		Q <sub>33</sub> (S <sub>1</sub> ) = -0.75Q <sub>33</sub> (S <sub>0</sub> ) - 0.58Q <sub>32</sub> (S <sub>0</sub> )
Q <sub>34</sub> (S <sub>0</sub> )	a	734	720	a	680		Q <sub>32</sub> (S <sub>1</sub> ) = +0.98Q <sub>34</sub> (S <sub>0</sub> )
Q <sub>35</sub> (S <sub>0</sub> )	a	600		a	582		Q <sub>34</sub> (S <sub>1</sub> ) = -0.95Q <sub>35</sub> (S <sub>0</sub> )
Q <sub>36</sub> (S <sub>0</sub> )	a	595		a	441		Q <sub>37</sub> (S <sub>1</sub> ) = -0.55Q <sub>36</sub> (S <sub>0</sub> ) - 0.68Q <sub>38</sub> (S <sub>0</sub> )
Q <sub>37</sub> (S <sub>0</sub> )	a	544	542	a	498		Q <sub>36</sub> (S <sub>1</sub> ) = -0.95Q <sub>37</sub> (S <sub>0</sub> )
Q <sub>38</sub> (S <sub>0</sub> )	a	482		a	337		Q <sub>40</sub> (S <sub>1</sub> ) = +0.69Q <sub>38</sub> (S <sub>0</sub> ) - 0.54Q <sub>36</sub> (S <sub>0</sub> )
Q <sub>39</sub> (S <sub>0</sub> )	a	458	453	a	408		Q <sub>39</sub> (S <sub>1</sub> ) = -0.98Q <sub>39</sub> (S <sub>0</sub> )
Q <sub>40</sub> (S <sub>0</sub> )	a	425		a	452		Q <sub>38</sub> (S <sub>1</sub> ) = -0.99Q <sub>40</sub> (S <sub>0</sub> )
Q <sub>41</sub> (S <sub>0</sub> )	a	399		a	281		Q <sub>42</sub> (S <sub>1</sub> ) = -0.93Q <sub>41</sub> (S <sub>0</sub> )
Q <sub>42</sub> (S <sub>0</sub> )	a	335	335	a	325		Q <sub>41</sub> (S <sub>1</sub> ) = -0.99Q <sub>42</sub> (S <sub>0</sub> )
Q <sub>43</sub> (S <sub>0</sub> )	a	231		a	238		Q <sub>43</sub> (S <sub>1</sub> ) = +0.90Q <sub>43</sub> (S <sub>0</sub> ) + 0.41Q <sub>44</sub> (S <sub>0</sub> )
Q <sub>44</sub> (S <sub>0</sub> )	a	218		a	181		Q <sub>44</sub> (S <sub>1</sub> ) = +0.80Q <sub>44</sub> (S <sub>0</sub> )
Q <sub>45</sub> (S <sub>0</sub> )	a	169	154	a	169		Q <sub>45</sub> (S <sub>1</sub> ) = +0.92Q <sub>45</sub> (S <sub>0</sub> )
Q <sub>46</sub> (S <sub>0</sub> )	a	152		a	154		Q <sub>46</sub> (S <sub>1</sub> ) = +0.98Q <sub>46</sub> (S <sub>0</sub> )
Q <sub>47</sub> (S <sub>0</sub> )	a	141	92	a	131		Q <sub>47</sub> (S <sub>1</sub> ) = +0.79Q <sub>47</sub> (S <sub>0</sub> ) + 0.55Q <sub>48</sub> (S <sub>0</sub> )
Q <sub>48</sub> (S <sub>0</sub> )	a	119		a	89		Q <sub>49</sub> (S <sub>1</sub> ) = -0.73Q <sub>48</sub> (S <sub>0</sub> ) + 0.58Q <sub>47</sub> (S <sub>0</sub> )
Q <sub>49</sub> (S <sub>0</sub> )	a	111		a	114		Q <sub>48</sub> (S <sub>1</sub> ) = +0.99Q <sub>49</sub> (S <sub>0</sub> )
Q <sub>50</sub> (S <sub>0</sub> )	a	78		a	81		Q <sub>50</sub> (S <sub>1</sub> ) = -1.00Q <sub>50</sub> (S <sub>0</sub> )
Q <sub>51</sub> (S <sub>0</sub> )	a	38	42	a	34		Q <sub>51</sub> (S <sub>1</sub> ) = +0.99Q <sub>51</sub> (S <sub>0</sub> )

**Table S10** Intensities of the observed emission bands of 2-TN-H<sub>2</sub>O. The first line gives the wavenumber of the excited bands, the first column the wavenumbers of the emission bands. The entries of the table represent the intensities, with the most intense band (apart from the excited band whose intensity is biased by stray light.) in each of the emission spectra normalized to 1.

S <sub>0</sub>	Int.	S <sub>0</sub>	Int.
42	0.03	1386	0.04
92	0.01	1436	0.06
154	0.01	1499	0.29
252	0.02	1588	0.07
289	0.01	1640	0.10
335	0.08	1672	0.30
418	0.02	1763	0.12
453	0.79	1867	0.10
515	0.03	1976	0.04
542	0.17	1992	0.03
720	0.22	2004	0.03
765	0.09	2044	0.10
820	0.37	2097	0.09
906	0.14	2128	0.03
950	0.02	2216	0.03
993	0.04	2239	0.09
1045	0.67	2268	0.21
1073	0.03	2315	0.04
1106	0.04	2366	0.03
1123	0.08	2405	0.08
1147	0.04	2439	0.19
1185	0.22	2544	0.04
1222	1.00	2692	0.04
1266	0.05	2719	0.09
1358	0.04	2763	0.02

**Table S11** Fitted factors of the displacements of the 2-TN water cluster along the normal modes from the FC fit

Mode	displacement
$Q_{21}$	$0.0083837 \pm 0.002638$
$Q_{24}$	$0.006212 \pm 0.0090191$
$Q_{26}$	$-0.0035196 \pm 0.0029356$
$Q_{31}$	$0.0033854 \pm 0.0021796$
$Q_{34}$	$-0.0062317 \pm 0.0035917$
$Q_{39}$	$-0.0092078 \pm 0.0024931$
$Q_{42}$	$-0.0029472 \pm 0.0072397$
$Q_{47}$	$0.011859 \pm 0.04801$
$Q_{49}$	$0.04938 \pm 0.050309$
$Q_{51}$	$0.035832 \pm 0.050704$

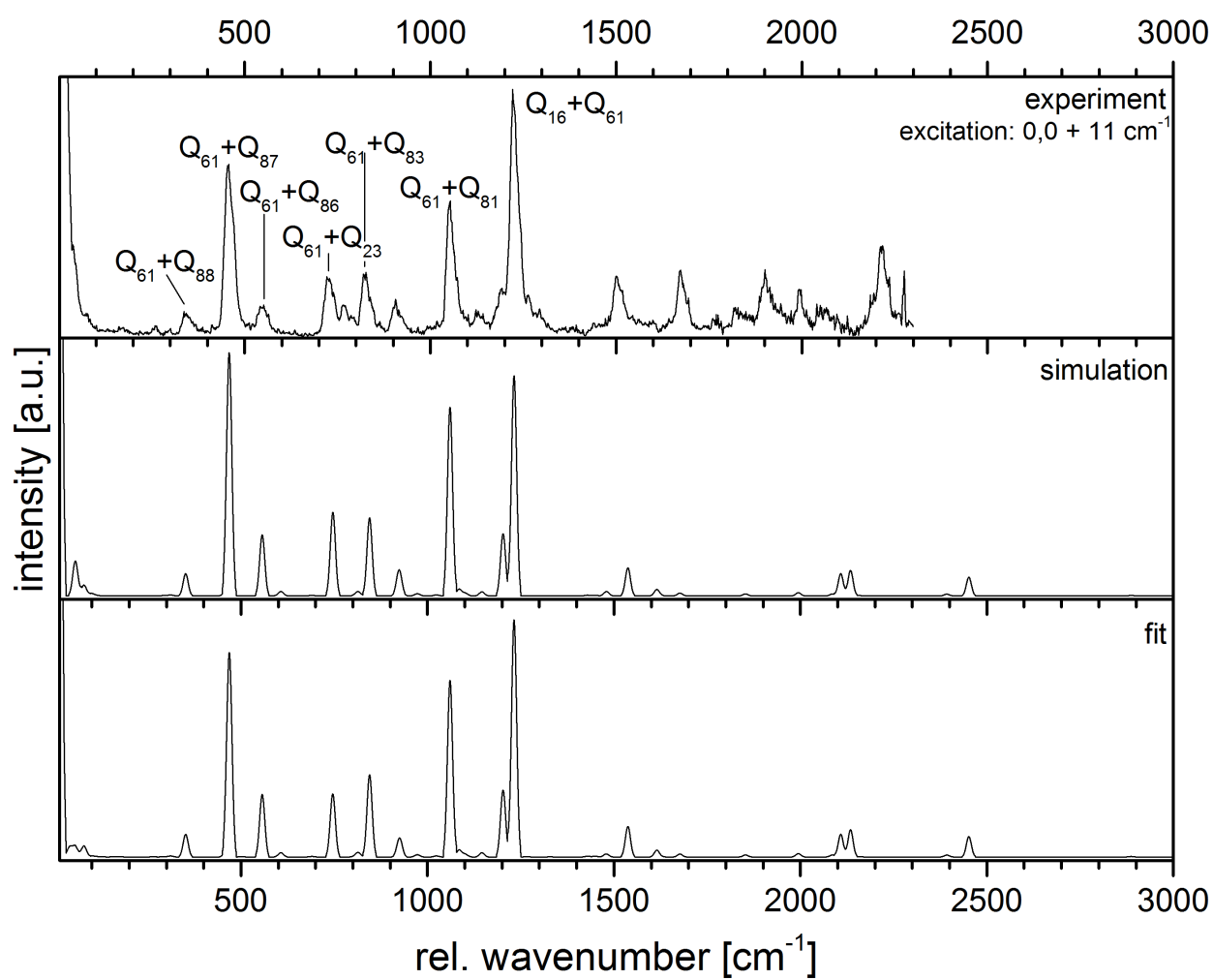


**Figure S1** Fluorescence emission spectrum of the 2-TN dimer upon excitation of the electronic origin at  $0,0 + 11 \text{ cm}^{-1}$ .

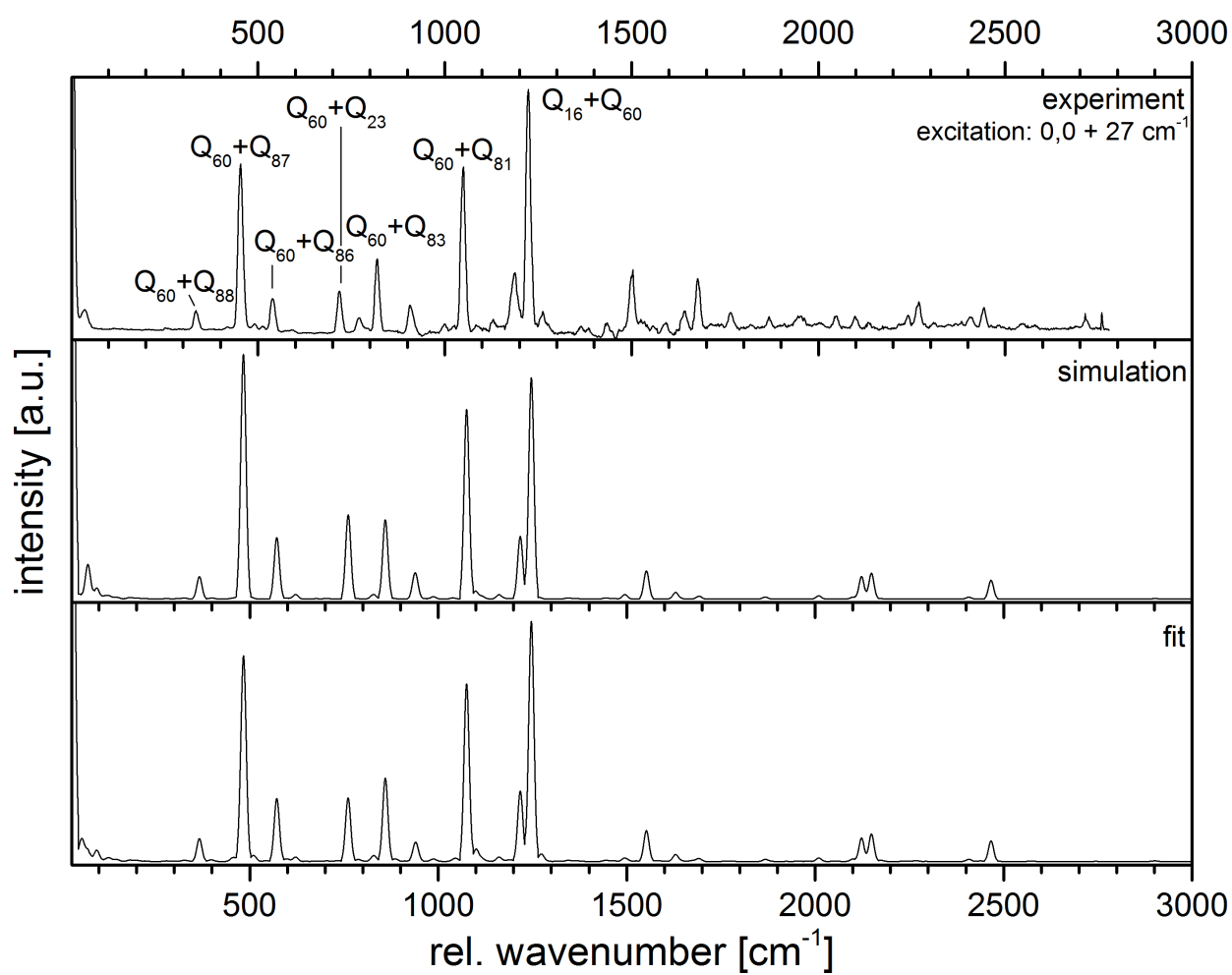


**Figure S2** Fluorescence emission spectrum of the 2-TN dimer upon excitation of the electronic origin at  $0,0 + 27 \text{ cm}^{-1}$ .

# Danksagung

Diese Arbeit wäre nicht entstanden, wenn mir nicht viele Menschen immer wieder beige-standen und mich unterstützt hätten. Ich möchte daher die Gelegenheit nutzen, diesen Menschen hier zu danken.

Zunächst möchte ich Prof. Dr. Michael Schmitt danken, der mir überhaupt erst die Möglichkeit gegeben hat zu promovieren. Auch mit Rat und Tat stand er mir stets zur Seite und war mir so eine große Hilfe.

Auch meinen Kollegen im Arbeitskreis möchte ich für die gemeinsame Zeit danken. Daher, vielen Dank Josefin und Martin Wilke, Michael Schneider, Mirko Lindic und Christian Henrichs für die schöne Zeit.

Besonders bedanken möchte ich mich bei Benjamin Stuhlmann, der meinen Weg seit meiner Master-Arbeit begleitet und mich die ganzen Jahre unterstützt hat.

Auch Alexander Wohler hat sich über die Jahre ein gesondertes Dankeschön verdient, da er immer und jederzeit bereit war zu helfen und einfach alles Korrektur gelesen hat, was man ihm vorgelegt hat.

Nicht zuletzt möchte ich mich auch bei Andreia Lotzwick bedanken, die mir und allen anderen jederzeit den Rücken frei gehalten hat, und immer ein offenes Ohr für unsere Probleme und Sorgen hatte.

Unterstützung habe ich selbstverständlich nicht nur von meinen Arbeitskollegen erhalten, sonder auch von meiner Familie.

Meiner Mutter Christiane und meiner Schwester Anna möchte ich danke sagen, dafür dass sie immer an mich geglaubt und mich immer aufs Neue motiviert haben.

Meinem Opa Peter und meinen Tanten Regina und Steffi danke ich für die Unterstützung die es mir ermöglicht hat, mein Studium ohne große Sorgen bewältigen zu können.

Auch meine Großeltern Karl und Maria Gmerek möchte ich hier danken, auch wenn sie dies leider nicht mehr erleben können.

Der letzte Dank gehört Anne Gräßle. Sie hat mir über viele Jahre zur Seite gestanden, mich unterstützt wo sie konnte und mir immer wieder neue Motivation gegeben. Sie hat meine Sorgen geteilt und mich aufgebaut wenn es nötig war.

Für alle die, die hier namentlich nicht erwähnt wurden: Ich habe euch zwar vielleicht vergessen, bin euch aber trotzdem dankbar.



# Bibliography

- [1] D. L. Nelson and M. M. Cox. *Principles of biochemistry*. W. H. Freeman and Company, 2005.
- [2] G. H. Krause; E. Weis. Chlorophyll fluorescence and photosynthesis: The basics. *Annu. Rev. Plant Physiol. Plant Mol. Biol.*, 42:313–349, 1991.
- [3] P. Atkins. *Physikalische Chemie*. Wiley-VCH Verlag GmbH, 3. edition, 2001.
- [4] Felix Gmerek; Benjamin Stuhlmann; Leonard Alvarez-Valtierre; David W. Pratt; Michael Schmitt. Electronic spectra of 2- and 3-tolunitrile in the gas phase ii: Geometry changes from franck-condon fits of fluorescence emission spectra. *Journal of Chemical Physics*, 144, 2016.
- [5] M. Fujii; M. Yamauchi; K. Takazawa; M. Ito. Electronic spectra of o-, m- and p-tolunitrile-substituent effect on internal rotation of the methyl group. *Spectrochimica Acta Part A*, 50:1421–1433, 1994.
- [6] P. Nagabalasubramanian; S. Periandy; and S. Mohan. *Spectrochim. Acta, Part A*, 74:1280–1287, 2009.
- [7] A. Nagao; A. Kanno; and M. Takayanagi. *J. Mol. Struct.*, 929:43–47, 2009.
- [8] H. Nakai and M. Kawai. *J. Chem. Phys.*, 113:2168–2174, 2000.
- [9] A. I. Jaman; S. Maiti; and R. N. Nandi. *J. Mol. Spec.*, 192:148–151, 2011.
- [10] A. I. Jaman; P. H. Kumar; and P. R. Bangal. *Journal of Atomic, Molecular, and Optical Physics*, pages 480396–1–480396–8, 2011.
- [11] C. H. Park; G. W. Lee; and S. K. Lee. *Bull. Korean Chem. Soc.*, 27:881–885, 2006.
- [12] C. H. Park and S. K. Lee. *Bull. Korean Chem. Soc.*, 27:1377–1380, 2006.
- [13] K. Suzuki; S. i. Ishiuchi; M. Sakai; and M. Fujii. *J. Electron Spectrosc. Relat. Phenom.*, 142:215–221, 2005.
- [14] N.E. Schore and P.C. Vollhardt. *Organic Chemistry, structure and function*. NY: W.H. Freeman and Company, 5th ed edition, 2007.

- [15] Benjmin Chu. *Molecular Forces*. Interscience Publishers, 1967.
- [16] Robert Brause. *Franck-Condon-Analyse an Heteroaromaten und Clustern*. PhD thesis, Heinrich-Heine-Universität Düsseldorf, 2006.
- [17] M. Busker; T. Häber; M. Nispel; K. Kleineremanns. Isomerenselektive ir-spektroskopie von benzol-acetylen-clustern: Vergleich mit der struktur des benzol-acetylen-cokristalls. *Angewandte Chemie*, 120:10248–10251, 2008.
- [18] M. Böning; B. Stuhlmann; G. Engler; K. Kleineremanns. Isomer-selective vibrational spectroscopy of jet-cooled phenol-acetylene aggregates. *The Journal of Physical Chemistry A*, 117:3214–3220, 2013.
- [19] M. Böning, B. Stuhlmann, G. Engler, M. Busker, T. Häber, A. Tekin, G. Jansen, and K. Kleineremanns. Towards a spectroscopic and theoretical identification of the isolated building blocks of the benzeneacetylene cocrystal. *CHEMPHYSICHEM*, 14:837–846, 2013.
- [20] G. Berden; W. L. Meerts; M. Schmitt; K. Kleineremanns. High resolution uv spectroscopy of phenol and the hydrogen bonded phenol-water cluster. *The Journal of Chemical Physics*, 104, 1995.
- [21] Felix Gmerek; Benjamin Stuhlmann; Elvedina Pehlivanovic; Michael Schmitt. Franck condon spectra of the 2-tolunitrile dimer and the binary 2-tolunitrilewater cluster in the gas phase. *Journal of Molecular Structure*, 1143:265–273, 2017.
- [22] M. Schmitt; M. Böhm; C. Ratzler; S. Siegert; M. van Beek; W. L. Meerts. Electronic excitation in the benzonitrile dimer: The intermolecular structure in the s0 and s1 state determined by rotationally resolved electronic spectroscopy. *Journal of Molecular Structure*, 795:234–241, 2006.
- [23] F. A. Balmer; P. Ottiger; S. Leutwyler. Excitonic splitting, delocalization, and vibronic quenching in the benzonitrile dimer. *Journal of Physical Chemistry*, 118:11253–11261, 2014.
- [24] O. Kajimoto T. Kobayashi, K. Honma and S. Tsuchiya. *J. Chem. Phys.*, 86:1111–1117, 1987.
- [25] M. Takayagani and I. Hanazaki. *J. Opt. Soc. Am. B*, 7:1898–1904, 1990.
- [26] W. L. Meerts K. Remmers and I. Ozier. *J. Chem. Phys.*, 112:10890–10894, 2000.
- [27] M. Schmitt I. Kalkman, C. Vu and W. L. Meerts. *ChemPhysChem*, 9:1788–1797, 2008.

- [28] S. Leutwyler S. Kopec, P. Ottiger and H. Köppel. *J. Chem. Phys.*, 142:084308–1–084308, 2015.
- [29] N. Seurre; K. L. Barbu-Debus; F. Lahmani; A. Zehnacker-Rentien and J. Sepiol. *Chem. Phys.*, 295:21–33, 2003.
- [30] K. Sakota and H. Sekiya. *J. Phys. Chem. A*, 109:2718–2721, 1995.
- [31] F. Talbot A.Müller and S. Leutwyler. *J. Chem. Phys.*, 116:2836–2847, 2002.
- [32] A. Held and D. W. Pratt. *J. Chem. Phys.*, 96:4869–4876, 1992.
- [33] Julio de Paula Peter Atkins. *Atkins' Physical Chemistry*. OUP Oxford, 2014.
- [34] Jose Arturo Ruiz-Santoyo; Josefin Wilke; Martin Wilke; John T. Yi; David W. Pratt; Michael Schmitt; Leonardo Alvarez-Valtierra. Electronic spectra of 2- and 3-tolunitrile in the gas phase. i. a study of methyl group internal rotation via rovibronically resolved spectroscopy. *The Journal of Chemical Physics*, 144, 2016.
- [35] A. S. Davydov. *Theory of molecular excitons*. Mc Graw-Hill, 1962.
- [36] Wolfgang Demtröder. *Laserspektroskopie - Grundlagen und Techniken*. Springer-Verlag, 5. edition, 2007.
- [37] Robert J. Le Roy. Where is the intensity maximum in a pure rotational spectrum? *Journal of Molecular Spectroscopy*, 192:237–238, 1998.
- [38] M. Schmitt; U. Henrichs; H. Müller; K. Kleinermanns. *J. Chem. Phys.*, 103:9918–9928, 1995.
- [39] W. Roth; C. Jacoby; A. Westphal; M. Schmitt. *J. Phys. Chem. A*, 102:3048–3059, 1998.
- [40] Daniel Krügler and Michael Schmitt. *Documentation of the program FCfit*. Heinrich-Heine-Universität, Institut für Physikalische Chemie I, 40225 Düsseldorf, Germany, November.
- [41] Spectra-Physics. *Quanta-Ray INDI Pulsed Nd:YAG LASER*, November 2000.
- [42] Lambda Physik GmbH. *Dye Laser FL 3001/2 Instruction Manual*, April 1987.



# List of Figures

1.1	Basic structure of different chlorophyll-types. Table 1.1 shows which substituents form which chlorophyll. . . . .	3
1.2	Structures of the investigated monomers. . . . .	5
1.3	Structure of the 2-TN dimer. <sup>[21]</sup> . . . . .	7
1.4	Structure of the 2-TN-water cluster. <sup>[21]</sup> . . . . .	9
1.5	Schematic drawing of the angle $\theta$ between two transition dipole moments. .	10
1.6	Orientation of the transition dipole moments . . . . .	10
1.7	Transition dipole moments and aggregation. . . . .	11
2.1	Examples for pictures at neighbouring positions of the grating . . . . .	14
2.2	Example for the overlapping Bands in neighbouring pictures. . . . .	15
2.3	Linespectra obtained from the pictures in fig. 2.1 . . . . .	16
2.4	Scheme of an energy diagram . . . . .	17
3.1	Experimental set up. . . . .	23
3.2	Scheme of the sample chamber . . . . .	25